The effect of pH and the solids composition on the settling and self-weight consolidation of mud

H.C.M. Hendriks

Master of Science Thesis

TU Delft

Boskalis

NUS National University of Singapore

Cover page:

Visualisation of the 'Marker Wadden'.

Concept design by Boskalis, accessed from www.rtvbodegraven.nl

The effect of pH and the solids composition on the settling and self-weight consolidation of mud

By:

H.C.M. (Erik) Hendriks

in partial fulfilment of the requirements for the degree of

Master of Science

in Hydraulic Engineering and Water Resources Management

at the Delft University of Technology

and

the National University of Singapore

to be defended publicly on 10-03-2016

Thesis committee:

Prof. dr. ir. J.C. Winterwerp	TU Delft
Dr. ir. W. Jacobs	Boskalis
M. Barciela Rial MSc.	TU Delft
M.E. Ibanez Sanz MSc.	TU Delft/Deltares
Dr. ir. L.A. van Paassen	TU Delft
Dr. Yuan Jing	National University of Singapore
Dr. Chew Soon Hoe	National University of Singapore

An electronic version of this thesis is available at http://repository.tudelft.nl/.

TU Delft Delft University of Technology Boskalis NUS National University of Singapore

Summary

A demand to use mud as fill material for land reclamations has emerged over the past years. Such reclamations start with pumping a muddy suspension into an area enclosed by dikes. The particles in suspension then settle to form a mud layer, so that the supernatant can be removed. This filling process may be repeated several times to completely fill the reclamation area. In 2016, an example of such a reclamation will be constructed in the Markermeer, the Netherlands. To make this work, it is essential to know the timescale of deposition and the properties of the formed soft mud layer.

Formation of mud layers takes place in two steps. First, particles settle from a mud suspension and secondly, self-weight consolidation of a soft mud layer occurs. The goal of this thesis is to gain more understanding of factors influencing these two steps. More specifically, factors which are studied are the composition of the solid particles and the chemical composition of the water, together forming the mud mixture.

Natural mud consists of different particles. Of these different particles, the clay particles are affected by the chemical composition of the water. This is because clay particles have a large specific surface area and surface charge, causing electrostatic interactions between them. The specific surface area and surface charge also mainly determine the plasticity of mud/soil.

Under certain circumstances, clay particles flocculate, thereby forming flocs. Flocs settle more rapid than the individual particles, eventually forming a bed. Because these flocs contain large amounts of water, the formed beds are also very soft. The amount of water contained in the flocs is directly influenced by the size of the flocs (Winterwerp and van Kesteren, 2004) and the rate at which flocculation occurs (Mietta, 2010). The water content of the flocs also influences the settling and self-weight consolidation and thus, flocculation influences the formation of soft mud layers.

From colloid chemistry, it is known that differences in the acidity of the water may influence the rate at which clay particles flocculate. To assess the impact of varying acidity on the settling and self-weight consolidation of mud, settling column experiments were set up in which the pH of the water was systematically varied. This was done for two artificial mud samples, i.e. a kaolinite and bentonite clay powder, and a natural clay sample, taken from the Markermeer. For the natural clay sample, the initial concentration was also varied.

From the experiments, it can be concluded that there is an influence of pH on the settling and self-weight consolidation of mud, but mainly for samples with high to extremely high plasticities. For the kaolinite, a low plasticity mud, the effect of pH is rather limited. Hence, the influence of pH on the settling and self-weight consolidation of mud decreases with decreasing plasticity. This can be understood from a soil mechanical point of view: the factors determining the plasticity, namely the specific surface and surface charge, also directly determine the amount of electrostatic interactions

between the clay particles. If the electrostatic interactions between clay particles in itself are small, their behaviour is also not noticeably altered by varying the suspension pH.

For the natural sediment sample, containing large amounts of calcium carbonate, addition of hydrochloric acid is neutralized due to dissolution of calcium carbonate. However, the dissolution of calcium carbonate also leads to a release of Ca^{2+} ions, which also has a profound impact on flocculation. Because of the large neutralizing capacity of both the fresh water and the natural mud sample, no large changes in acidity are expected in the Markermeer environment, in spite of the presence of pyrite in the Markermeer bed. This confirms findings by Saaltink et al. (2016). The mineralogy of the present clay minerals exerts a much larger influence on the settling and self-weight consolidation process than suspension pH, which is reflected by large differences in gelling concentration and consolidated volumes between the three different mud samples.

Self-weight consolidation marks the transition between fluid and soil mechanics. In fluid mechanics it is common to use the concentration or density to characterize mud layers. However, it is the relative water content of a suspension or mud layer, rather than the absolute water content (cf. density), that determines its settling and self-weight consolidation behaviour. This relative water content is given by the Liquidity Index, that is obtained by normalizing the water content of a suspension or muddy layer by its Atterberg Limits. Using the Liquidity Index enables us to compare different types of mud.

The gelling concentration, a state parameter which is often used in cohesive transport modelling, is also related to a material property of mud, namely the Plasticity Index. A power law relation is proposed relating the gelling concentration to the Plasticity Index. Hence, a first estimate of the gelling concentration for different mud samples can be computed based on the Atterberg Limits of a mud sample.

The undrained shear strengths of the consolidated samples, obtained through a shear vane test, are related to the respective average Liquidity Indices of these beds. For the natural clay, the Liquidity Index of the settled beds appeared to give a good indication of the undrained shear strength, and shows a fair resemblance with results obtained by Locat and Demers (1988) and Houston and Mitchell (1969).

Summarizing: The suspension pH influences the settling and self-weight consolidation of mud, in particular for mud with high to extremely high plasticities. This can be attributed to the surface charge and specific surface area of the clay particles. Furthermore, it is found that the Atterberg limits are valuable material parameters, also from a fluid mechanical point of view. These Atterberg Limits can serve as a tool to predict the settling and self-weight consolidation of soft muddy layers.

Acknowledgements

This thesis marks the completion of my Master of Science at the TU Delft and the National University of Singapore. Looking back on the past 11 months during which I worked on this thesis, I wish to express my gratitude to a number of people.

First of all, I want to thank my graduation committee. Of course for answering my numerous questions, providing feedback during meetings and encouraging me to keep on improving my work. Your feedback helped me greatly in synthesizing the results and writing this report. Apart from that I wish to thank you for several other aspects: Han, thank you for introducing me into the fascinating world of mud and being my guide through it. Working with you has been, and still is, a privilege. Walter, thank you for keeping me on track, encouraging me to think about the bigger picture and the story I wanted to tell with my thesis. Leon, thank you for your commitment. Your vast knowledge on soil mechanics, but also your curiosity and willingness to learn have been a great inspiration. Maria and Maria, thank you both for your helpfulness, whether it involved setting up experiments, carefully reading my report, or scheduling meetings, you were both more than willing to help, accommodating also my last-minute meeting requests. Please know it is greatly appreciated.

For the laboratory work I did, I would like to thank both the staff at the Boskalis Dolman laboratory and Miguel de Lucas from the Deltares FCL laboratory. Thijs van Kessel is gratefully acknowledged for clarifying some of the chemistry-related topics in my work.

I want to thank my colleagues and fellow graduate students at Hydronamic for the pleasant working atmosphere and the interest they showed in my work. For the serious discussions, but also for the laughs we've had over the past 11 months.

I would like to thank my friends for the support, not only during the past 11 months, but also during my entire studies in Delft.

Finally, I would like to thank my family. For enabling me to pursue this Master's and showing great interest in my journeys and my work, but above all for being the awesome family I can always rely on. Finally, and most important: my parents. For their unconditional support, wisdom and for keeping my feet on the ground.

Erik Hendriks

Delft, March 2016

Table of Contents

1. Introduction

A brief introduction into the research topic is given in this chapter. It provides an overview of the background and relevance of the research, specifying which gaps in knowledge need to be filled and how this research contributes to that. Next to that, the methodology of the research is outlined and the formal research questions are posed. Finally a short overview of the report and its structure is given.

1.1 Background

Over the past years, an increasing demand to build with mud has emerged. This poses a challenge, as the engineering properties of mud are less favourable than sand (van 't Hoff and Nooy van der Kolff, 2012). One of the main applications of mud over the past years was to use dredged mud as a hydraulic fill material in land reclamations. Examples of such reclamations can be found in Asia, and also in port areas in Australia and Europe (Boyle et al., 2010, Nooy van der Kolff et al., 2010).

The availability of fill material is the key issue for many reclamations in Asia: whereas sand is scarce in many locations, mud is abundant (Lee et al., 1987, Terashi and Katagiri, 2005). In port areas the incentive to use dredged mud as a building material is often environmentally motivated: dredged mud is reused after it has been dredged from the port basins and fairways. By reusing the dredged material as fill material, it can be prevented that the dredged mud is disposed at sea which could have an adverse environmental impact.

Also in the Netherlands, plans are made to execute large reclamations using mud. A prime example is the Marker Wadden project, a large-scale reclamation which will be constructed in the Markermeer from 2016 onwards.

Using mud for reclamations is, in itself, not a new technique. Generally speaking, such a reclamation starts with pumping a muddy suspension into an area enclosed by dikes. The solid particles then settle from the suspension to form a mud layer, which will then consolidate due to its

own weight. This process is schematically shown in Figure 1.1. Once self-weight consolidation has taken place, the supernatant can be removed and the reclamation area is filled with a muddy suspension again. This filling process has to be repeated several times to completely fill the reclamation area.

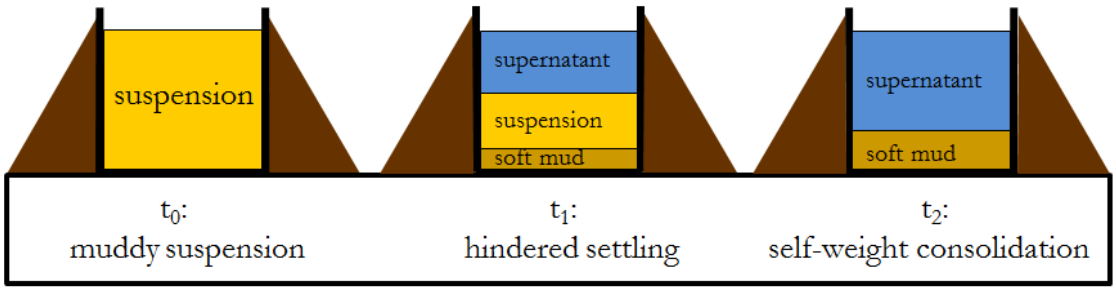

Figure 1.1: Schematic overview of reclamation process using mud. Particles settle from the suspension from $t=t_0$ onwards. After the settling phase, self-weight consolidation takes place ($t=t_2$). The result of self-weight consolidation is a soft mud layer.

To properly design and construct such a reclamation, it is essential to know the timescale of deposition and the properties of the formed mud layer. However, a large variability exists in the engineering properties of mud and its behaviour during settling and consolidation. The factors determining this behaviour are still rather poorly understood.

This research is situated at the interface of the fields of fluid and soil mechanics. Whereas fluid mechanics is mostly concerned with the settling of mud and how settled beds interact with the fluid motion, soil mechanics mainly concerns soils: consolidated beds that, over the course of (many) years, have gained enough strength to become a soil. The interface of these two fields is schematically shown in Figure 1.2.

The main difference between these two fields is the amount of water that is present, when compared to the amount of solids. In fluid mechanics, the amount of water is relatively large compared to the amount of solids, whereas for soil mechanics, it is the other way round. This leads to vastly different orders of magnitude for the undrained shear strengths involved: soft mud layers exhibit strengths of only several Pascals, whereas in geotechnical engineering the undrained shear strength normally is in the order of kilo- or even megaPascals.

Despite the differences, these domains share an important common ground. Often, a significant part of the solid particles are clay particles which determine, for both the fluid and soil mechanical point of view, the material behaviour of mud suspensions or soils.

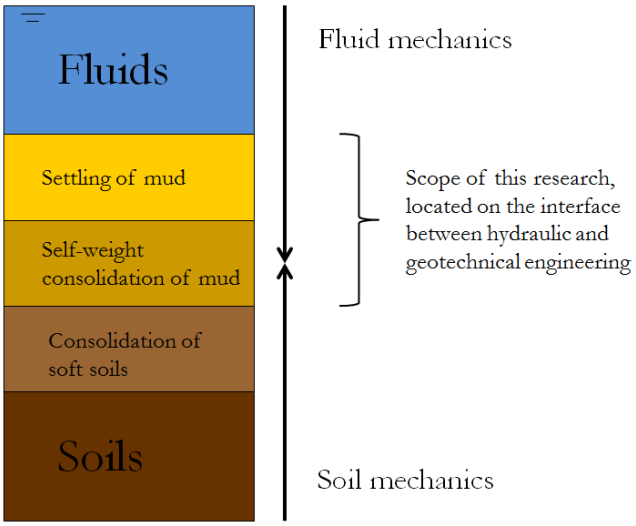

Figure 1.2: Interface of fluid and soil mechanics, with indication of the current research scope

1.2 Problem definition

Although there is an increasing interest in building with mud, the versatile nature of the material makes it difficult to understand the processes governing its material behaviour. This versatility is reflected in its formal definition:

Mud is a mixture of clay, silt, sand, organic material, water and sometimes gas. Besides, contaminants and organisms may also be present in mud (Winterwerp and van Kesteren, 2004).

For these mixtures, the cohesive properties of the clay fraction, dominate the overall behaviour (Toorman and Berlamont, 2015). These cohesive properties are a result of the electrostatic interactions between clay particles. In turn, the electrostatic interactions between the clay particles are influenced by the chemical conditions.

Numerous researchers have studied the behaviour of suspensions and soils containing clay. In the field of fluid mechanics, it focused mainly on the effects of flocculation on sedimentation and erosion patterns of mud (i.e. Kandiah (1974)). In soil mechanics it mainly focused on the consolidation and strength development of (soft) soils (see Terzaghi et al. (1996)).

However, research focusing on the interface of these two research disciplines, i.e. the self-weight consolidation of mud, is rather limited. Been (1980) and Merckelbach (2000) studied the consolidation and strength evolution of soft mud layers but did not systematically research the mechanisms influencing the settling and self-weight consolidation process. A possible mechanism influencing this process is the flocculation of clay particles while they are in suspension, because flocculation has a large impact on the settling of mud (Mehta, 2014).

From colloid chemistry, it is known that the rate at which clay particles flocculate depends on the pH and ionic strength of the water, in combination with the clay particle properties (Mietta et al., 2009). However, it has not yet been studied to what extent the composition of the solid particles and the pH of the suspension influence the settling and self-weight consolidation of mud. This would require incorporating chemistry as one of the relevant research disciplines, leading to a broader research scope. This is schematically shown in in Figure 1.3.

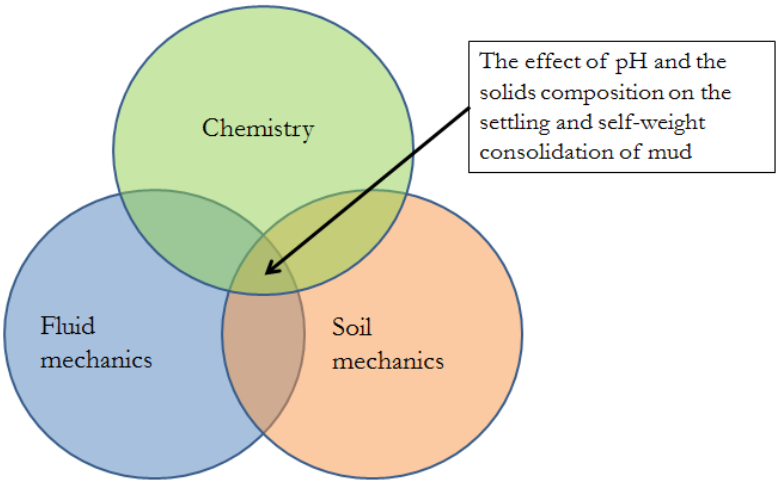

Figure 1.3: Schematic figure indicating the fields of chemistry, geotechnical engineering and morphology. This research is situated at the point where these three different disciplines intersect.

1.3 Research objective

Formation of mud layers takes place in two steps. First, particles settle from of a mud suspension and secondly, self-weight consolidation of a soft mud layer occurs (see also Figure 1.1). The goal of this thesis is to gain more understanding of factors influencing these two steps. Factors that are studied in this research are the composition of the solid particles and the chemical composition of the water, together forming the mud mixture.

The main relevance of this research lies in combining knowledge from the fields of chemistry, soil mechanics and fluid mechanics. The Markermeer is used as a case study, because of the relevance for the Marker Wadden project. However, the aim is to make the found knowledge more generally applicable.

1.4 Research questions

1.4.1 Main research question

Based on the research objective, and related to the background in which this research is situated, the following main research question is posed:

How are the settling and self-weight consolidation behaviour of mud influenced by its solids composition and the suspension pH?

1.4.2 Sub-questions

The main research question is too broad (and complex) to be understandable on its own. Therefore, it has to be broken down into different sub questions. These are presented below:

- What is the influence of the suspension pH on the settling and self-weight consolidation of mud?
- What is the influence of the solids composition on the settling and self-weight consolidation of mud?
- Which parameters can qualitatively describe the settling, self-weight consolidation and the strength development of mud?

1.5 Methodology

To investigate the influence of suspension pH and the composition of solids on the settling and self-weight consolidation behaviour of mud, the following methodology is proposed. This can be roughly divided into (1) a desk study and (2) an experimental study.

1. Desk study

- Literature review on the flocculation of clay particles, focused on the influence of pH and ionic strength on the flocculation of clay.
- Investigate how parameters from soil mechanics can be linked to parameters from fluid mechanics, and vice versa.
- Background study on Acid Sulphate Soils, mainly focusing on their occurrence and impact. This is included because Acid Sulphate Soils contain pyrite, and thereby have the potential to acidify due to natural processes.

2. Experimental study

To assess the impact of varying acidity on the settling and self-weight consolidation of mud, settling column experiments were set up in which the pH of the water was systematically varied. Two artificial mud samples, i.e. a kaolinite and bentonite clay powder, and a natural clay sample, taken from the Markermeer. These three clay samples all serve a specific purpose:

- The Markermeer clay is included because the Markermeer is regarded as an interesting location because of the 'Marker Wadden' project.
- The artificial mud samples are tested to make the obtained knowledge more generally applicable. The kaolinite and bentonite are regarded as extremes in terms of plasticity, the kaolinite has a low plasticity while the bentonite has an extremely high plasticity.

By including the three different clay types, the influence of the solids composition on the settling and self-weight consolidation, and its interaction with the water pH, can also be studied.

1.6 Report outline

In Chapter 2, the theoretical background on mud and the related processes is presented. Chapter 2 also elaborates on the various engineering domains from which the knowledge of mud dynamics stems, such as colloid chemistry (Section 2.3) and soil mechanics (Section 2.5). Chapter 3 gives an overview of the performed experiments and the experimental procedure of these experiments. Chapter 4 presents the results of these experiments, which are discussed and analysed in Chapter 5. In Chapter 6, the major findings and conclusions are summarized, accompanied by recommendations for future work and how to use the obtained knowledge in daily practice.

2. Theoretical background

This chapter presents an overview of relevant theory. To begin with, an overview of used terminology is given and characteristics of mud are discussed. In later paragraphs, the physical processes determining the settling and self-weight consolidation of mud are discussed. The settling and self-weight consolidation process, and how to describe it is also discussed. Next to that, a crossover is made between the fields of fluid and soil mechanics. Geochemistry and aquatic chemistry and how they can possibly impact mud is also discussed.

2.1 Terminology

A wide variety of terms exist related to mud and soils. To clarify matters, a short overview is given of the relevant terms and definitions. The following general definitions exist in the field of fluid mechanics:

- Sediment: Particulate matter that is carried by water or wind and deposited on the surface of the land or the seabed.
- Cohesive sediment: Sediment containing a significant proportion of clay, the electromagnetic properties of which cause the sediment to bind together (CIRIA, 1996).
- Mud: Mud is defined as a mixture of clay, silt, sand, organic material, water and sometimes gas. Besides, contaminants and organisms may also be present in mud (Winterwerp and van Kesteren, 2004). For these mixtures, the cohesive properties of the clay fraction, enhanced by the properties of the organic matter, dominate the overall behaviour (Toorman and Berlamont, 2015).

The terms mud and cohesive sediment are interchanged frequently. However, in daily language "mud" often refers to the deposited state of mud particles. In this state mud can occur as a fluid-like or soil-like entity (Toorman and Berlamont, 2015). When a deposit is called mud, it generally contains a large amount of water and therefore, it has a rather low bulk density.

In soil mechanics, the terms slurry and soil are the most commonly used terms. Their definitions read:

- Slurry: A fluid mixture of a solids mixed in a liquid (usually water).
- Soil: a natural body comprised of solids (minerals and organic matter), liquid, and gases that occurs on the land surface (Soil Survey Staff, 1975).

These two definitions, contrary to mud, mainly describe the density of a mixture of solids and liquid. For instance, a mixture consisting only of sand and water can be called a slurry, but such a mixture cannot be called mud as it does not contain clay particles. The main conclusion is that caution should be exercised when encountering these different terms. In the following, the terms mud and soil are most frequently used.

2.2 Mud properties

The introduction to mud properties given in this section, is largely based on the book by Winterwerp and van Kesteren (2004).

As was noted before, mud is a very diverse material. Next to that, its composition of mud and thus its behaviour varies in space and time and is mainly governed by the availability of its constituents, meteo-hydrodynamic conditions, biological factors and history. Clay particles and organic material, in relation to the chemical properties of the liquid phase, such as water or pore water, determine the cohesive behaviour of mud.

In the following sections, the granular, mineral and organic composition of mud mixtures is discussed. Next, the mechanisms behind the cohesive behaviour of the mixture are discussed, as well as their implications.

2.2.1 Granular composition

Mud is composed of granular material, which settles in water through gravity. The solid phase of mud is characterised by its particle size distribution. Many classifications occur, such as the US, British and Dutch standards. The Dutch standards, NEN-EN-ISO 14688-1 (NEN, 2013), for particle size distributions are followed in this study: these are presented in Table 2.1. It is noted that classifications vary per country.

Table 2.1: Particle size classification (NEN, 2013)

Grain size fraction	Grain size D [μm]
Gravel	>2000
Sand	63-2000
Silt	2-63
Clay	<2

All size classifications distinguish between clay, silt, sand and gravel fractions. The gravel fraction is absent in mud, or very small, so it will not be considered in the remainder of the research. It is important to realise that fraction names refer to size only, and do not consider the mineral composition of the particles. Therefore, all fractions can contain mineral and organic solids.

In addition to Table 2.1, another commonly used fraction definition is the mud fraction , designating particles smaller than 63 μm. Hence, the term mud is almost as versatile as the material it describes. The particle size classifications listed in Table 2.1 are also plotted in Figure 2.1, together with the definition of mud.

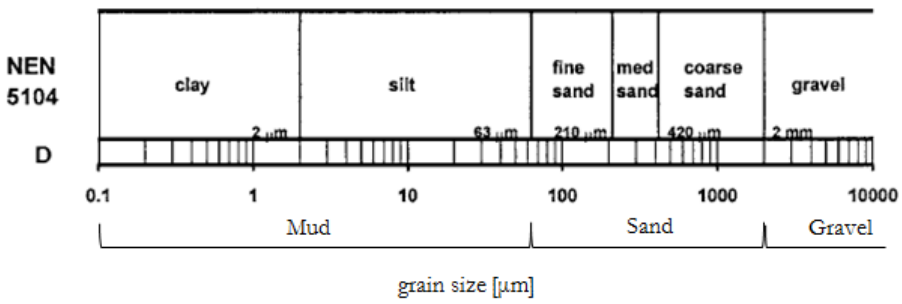

Figure 2.1: Particle size classifications in the Dutch standard. Adapted from Winterwerp and van Kesteren (2004).

Within the clay fraction, a separate sub-fraction worth mentioning is the colloidal fraction. Due to Brownian motion, this fraction does not settle in water, and the size of these particles is in the order of 0.1 μm or less. This colloidal fraction is mainly important for the behaviour of clay minerals in the water column, such as the formation of aggregates and flocs, which will be discussed below.

2.2.2 Mineral composition

Sediments consist of silicate and non-silicate minerals. Silicates, which may range in their composition and structure, often form a major component of the mineral solids fraction. The most common silicate groups are quartz, feldspar and clay minerals. Non-silicate materials are precipitates of salts, oxides and hydroxides, depending on the chemical conditions.

The clay fraction (D<2 μm) in the sediment is mainly composed of clay minerals. The most common clay minerals are kaolinite, illite, montmorillonite, and chlorite. In the silt fraction

(2<D<63 μm), quartz, feldspar and carbonates are dominant, although clay minerals may still be present. In the sand fraction (D>63 μm), clay minerals are practically absent. An example of a mineralogical fraction analysis is shown in Figure 2.2, illustrating the description given above.

Clay minerals generate cohesion (see also Section 2.2.4). Their disc-like shape yields a very high specific surface area and an electrical charge distribution, which interacts with the ambient water (dipoles). As a rule of thumb, sediment mixtures are regarded as cohesive if the clay content ξ_{cl} is larger than 7% (in weight).

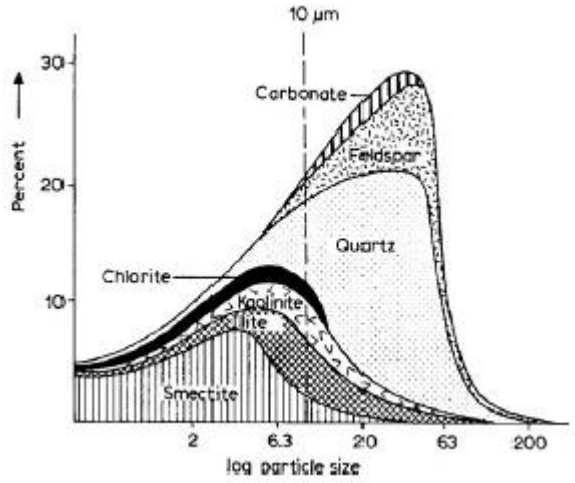

Figure 2.2: Example of mineralogical fraction analysis for Mississippi alluvial mud (Weaver, 1989)

The non-silicate minerals in mud generally concern salts, oxides and hydroxide precipitations. The non-silicate mineral groups and some examples of these minerals are presented in Table 2.2. The occurrence of these non-silicate minerals depends mainly on the local chemical conditions: availability of oxygen and specific metals, and their reduced state.

Table 2.2: Non silicate minerals found in mud. Based on Winterwerp and van Kesteren (2004)

Non-silicate mineral group	Example of mineral and composition
Carbonates	Calcite ($CaCO_3$)
Sulphates	Gypsum ($CaSO_4$ $2H_2O$)
Sulphides	Pyrite (FeS_2)
Phosphates	Vivianite ($Fe_3(PO_4)_2$ $8H_2O$)
Oxides	Hematite (Fe_2O_3)
Hydroxides	Goethite (FeO(OH))

2.2.3 Organic composition

Organic matter can have considerate effects on the formation of mud flocs and the stability of the bed. It primarily consists of organic polymers. In mud, it mainly exists of particulate organic matter (D>0.45 μm) and dissolved organic matter (D<0.45 μm).Organic matter can originate from outside

a sedimentation area, or be generated within the sediment by means of biological processes. Although the organic components in mud mixtures are not the main point of interest in this study, it is essential to also consider them, as they may significantly influence the behaviour of mud.

2.2.4 Cohesive behaviour

The most characteristic property of clay particles is that they can form flocs when the particles are brought in contact with a fluid, like water. A floc is defined as: An agglomeration of a large number of primary clay mineral particles cohering by attractive electrochemical forces, biochemical bonding or binding (Mehta, 2014). These flocs are characterised by very open structures formed by many, in the order of 10^3-10^4, clay particles. Because of their open structure, they contain large amounts of water (80-95% of their volume). In marine environments, almost all cohesive sediment that is found is flocculated.

In case sand and/or silt particles are not in mutual contact, and when the pore water not only contains water but also clay, a clay-water matrix may occur. Such a matrix only occurs at a (cohesive) strength, which is large enough to keep sand and silt particles in suspension (Jacobs, 2011).

It was argued by Winterwerp and van Kesteren (2004) that mud can only exhibit cohesive properties when the actual porosity of the sand-silt skeleton is larger than the maximum porosity for which sand and silt particles still have mutual contact. This is sketched in Figure 2.3, in which the left panel shows the sand-silt particles without the presence of clay, and the right panel includes clay, which forms the clay-water matrix that was referred to above.

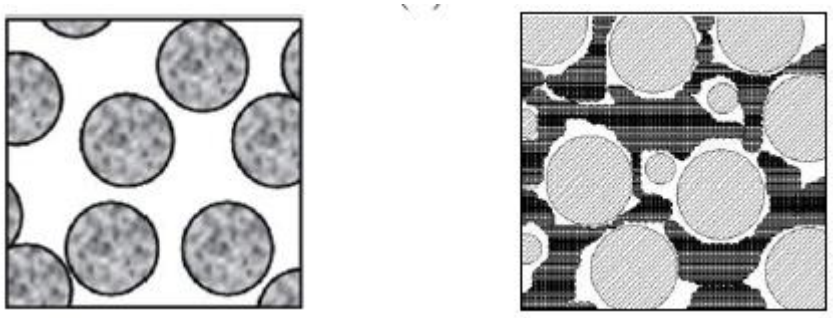

Figure 2.3: Schematized packing densities for a sand-silt mixture, without (left panel) and with (right panel) clay particles (Jacobs, 2011).

In addition, the presence of organic matter, the amount of clay particles – their mineralogy – and the chemical properties of the liquid phase determine the cohesive behaviour of mud. To understand why these factors influence cohesive behaviour a more fundamental perspective is required. Therefore, the principles of colloid chemistry are introduced in the following paragraph.

2.3 Colloid chemistry

Aggregation of small dispersed particles in liquid media is the domain of colloid chemistry, which is not only relevant for mud dynamics, but also plays a role in sanitary engineering and the chemical industry. Firstly an introduction into colloid chemistry is given, and afterwards, the consequences for mud dynamics are discussed.

2.3.1 Definition of colloids

Colloids are microscopically dispersed particles, which are suspended throughout another substance. If the solid particles are dispersed in water and exhibit a weak (or completely absent) affinity with the water, they are termed hydrophobic colloids (Verwey et al., 1948). A hydrophobic colloid is said to be stable if, during the period of observation, it is slow in changing its state of dispersion (Stumm and Morgan, 1996). Clay particles, when suspended in demineralized water, are generally stable. The particles do not form flocs, but are suspended in the solution: a prime example of a stable colloidal dispersion (Van Olphen, 1977).

Hydrophobic colloids may be coagulated or flocculated by comparatively small amounts of electrolyte added to the system, and the effective amounts depend characteristically on the valence type and the nature of the electrolyte. When a hydrophobic sol is coagulated, the at first apparently homogeneous liquid becomes turbid and distinctly non-homogeneous (Verwey et al., 1948).

2.3.2 Clay particles and the double diffuse layer

The initial stability of clay particles, and thus the absence of flocculation, is due to their surface charge, which is negative across their faces and edges. When placed in a solution, cations from the solution are attracted to the clay surfaces to maintain electrical neutrality. Because of this attraction of cations to the surface, the concentration of cations will be greater at the clay surface than it is in the bulk solution. However, due to this cation concentration gradient, cations will also tend to diffuse away from the clay surface towards the bulk solution. These oppositely oriented effects result in an equilibrium situation in which the zone around the clay layer has some finite, but diffuse, thickness where the electrical potential decreases with distance away from the clay surface. This layer, encompassing both the negatively-charged clay surface, and the positively-charged diffuse cation zone next to it, is called the diffuse double layer (Van Olphen, 1977). Conceptually, clay particles and the double diffuse layer can be represented as sketched in Figure 2.4.

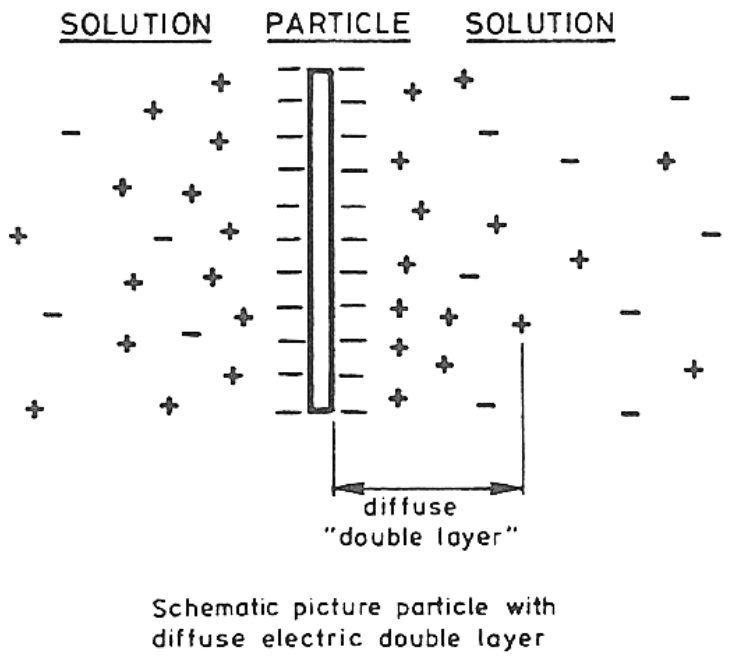

Figure 2.4: Conceptual sketch of clay particle with negative surface charge and diffuse double layer (Winterwerp, 2014).

It can now be understood why clay particles remain stable when dispersed in a solution with a very low (or absent) ionic strength. When clay particles come closer to one another, they repel one another due to the electrostatic repulsion between their respective double layers. Hence, the particles do not aggregate but stay in suspension. However, the presence of electrolytes drastically changes this picture.

2.3.3 The effect of electrolytes

When the ionic strength of the ambient solution increases, the double layer is compressed, which, in turn, leads to the aggregation of the clay particles. In other words, the colloidal dispersion becomes unstable. The effect of an increase in ionic strength on the thickness of the double layer can be understood as follows: with an increasing ionic strength, more cations are present in the bulk solution, thereby decreasing the gradient of the cation concentration. Hence, there is a lesser tendency for the cations in the double layer to diffuse away from the clay surfaces, and the double layer is compressed. With a thinner double layer, the clay particles can move closer to one another before being repelled, thereby enabling van der Waals forces to promote flocculation.

The van der Waals forces act between all units of matter and thus, also cause attraction between colloidal particles (Mitchell and Soga, 2005). The van der Waals forces are electromagnetic, and are inversely related to inter-particle distances (d), scaling with d^{-3} or d^{-4}. If the double layer is compressed, the particles may move closer before they repel one another. With decreasing inter-particle distance the van der Waals forces increase, and may even overcome the electrostatic repulsion generated by the double layer. If that is the case, flocculation will occur. Though, it must

be said that van der Waals are the weakest intermolecular forces, and the flocs generated by the process described above are generally small and are easy to break up.

Not only the presence of electrolytes has an impact on flocculation, but mainly the type of electrolyte that is present. The Hardy-Schulze rule states that the flocculation value of electrolytes is predominantly determined by their valence, when their charge opposes that of the particle under consideration. According to the DLVO model (i.e. Verwey et al. (1948)) the critical coagulation concentration of ions in suspension of opposite sign to the charge on the colloid, is proportional to the inverse power of the valence of the ion, and this power is 6 (Sposito, 1989).

The above explanation holds if the electrolytes in the ambient solution are indifferent (or inert), implying they do not engage in any sort of specific reaction with the colloid or its surface (Van Olphen, 1977).

2.3.4 Influence of H^+ and OH^-

Besides the influence of indifferent electrolytes, which compress the double layer, another mechanism is to be considered, being the reactivity of the clay edges with H^+ or OH^-. Hence, the flocculation behaviour of clay is also influenced by the pH of the ambient solution. The underlying processes have been reported, for instance, by Mitchell and Soga (2005). A remark must be made though, that the following is true for kaolinite suspensions, and not all clay types are necessarily similar to kaolinite (to the contrary, some are substantially different!).

The edge surfaces of the kaolinite particle can interact with the potential-determining H^+ and OH^- ions in solution, like an oxide surface, but the basal surfaces are considered to be (largely) unreactive in this respect. The surface potential at the edge surface is a function of the pH value of the suspension fluid. This means that at low pH values, which are below the isoelectric point of the edge surface of kaolinite, the edges of the clay particles become positively charged, and Coulombic attraction is promoted between the edges and the negatively charged faces, leading to edge-face aggregation.

For montmorillonite, another clay mineral, Tombacz and Szekeres (2004) concluded that its colloidal behaviour is influenced simultaneously by the pH and indifferent electrolyte content of the aqueous medium. Besides, they noted that the role of the ambient solution pH is twofold. Firstly, the H^+ ions have the affinity to neutralize the permanent negative charges of the clay particle faces and secondly, they reverse the sign of the particle edge charge.

2.3.5 Modes of aggregation and floc properties

In the previous paragraphs, several concepts from the field of colloid chemistry were discussed. Linking these concepts to environments that are encountered in marine and freshwater circumstances is done later in this research. However, by interpreting these concepts, an

understanding of differences in flocculation behaviour may be developed. As will be discussed in Section 2.5, differences in flocculation behaviour also impact the settling and self-weight consolidation of mud. To begin with, this paragraph elaborates on how differences in ionic strength and pH, or a combination of both, lead to changes in flocculation behaviour.

Four modes of aggregation can be distinguished. The four modes are listed according to the numbered states in Figure 2.5:

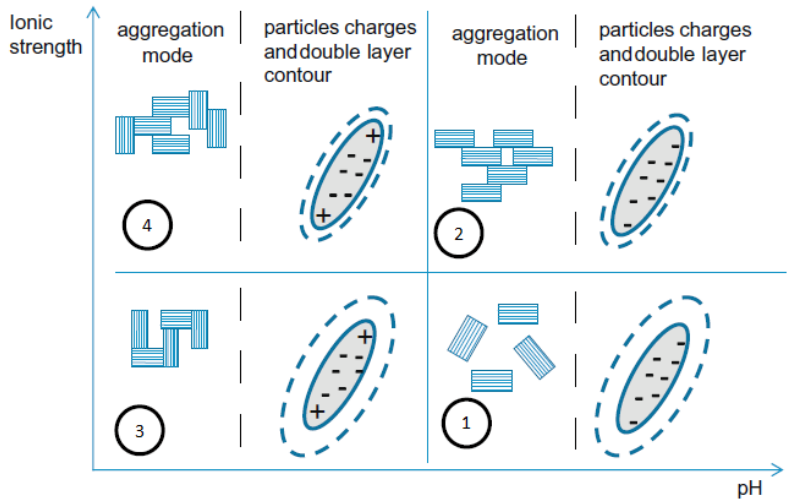

Figure 2.5: Sketch of preferred modes of aggregation of kaolinite (Mietta et al., 2009).

1. *Low ionic strength and high pH*

The double layer is thick and the clay particle edges negatively charged. Due to the electrostatic repulsion of their double diffuse layers, particles are unlikely to aggregate, and the suspension is stable (Mietta et al., 2009).

2. *High ionic strength and high pH*

When the ionic strength is increased, but the pH is still high (well above the isoelectric point of the clay surface edges) the double layer is compressed, and the van der Waals forces may overcome the electrostatic repulsion, causing the clay particles to flocculate in a face-face fashion.

3. *Low ionic strength and low pH*

Beyond the isoelectric point of the edges, pH*, the edges become positively charged, promoting Coulombic attraction between the particles. This pH is estimated to be $5 \leq pH \leq 7$ by, for instance, Rand and Melton (1977). Moreover, multiple researchers (Kaya et al., 2006, Nasser and James, 2008, Mietta et al., 2009) noted that flocs at low pH form faster and they are expected to be more porous than at high pH. Because of the Coulombic attraction and relatively thick double layers, the

flocs formed under these circumstances are thought to be the strongest with edge-face aggregation being the preferred mode of aggregation.

4. *High ionic strength and low pH*

If, next to a low pH, also an increase in ionic strength takes place, two simultaneous processes play a role. The double layer is compressed due to higher ionic concentration in the ambient solution, and the particle edges become positively charged. This leads to both edge-face and face-face aggregation.

Two remarks are made about these 4 different modes. Firstly, ionic strength and pH are related quantities, as H^+ ions also contribute to the ionic strength of a solution. Secondly, the above story holds for indifferent electrolytes, which are assumed not to react with the particles, and only contribute to the compression of the double layer.

Although the concepts introduced in this section are highly idealized and most data regarding them were acquired through lab tests, they have proven to be useful tools in describing flocculation phenomena, which will be elaborated upon in the following paragraph.

2.4 Flocculation

In the previous section, the fundamentals of floc formation and the factors influencing it were discussed. This paragraph will elaborate more on the specifics of mud flocs and their formation. To begin with, the concept of self-similar fractals is also introduced in this paragraph.

2.4.1 Self-similarity and the fractal approach

To accurately describe the structure of flocs, which come in a wide range of sizes, the conceptual model of self-similar flocs is introduced. Krone (1963) postulated a hierarchy in flocs, starting from clay particles, on to flocculi, which eventually form full flocs. He noted that clay particles, which are the primary particles for flocs, form aggregates due to their cohesive character. In turn, these aggregates can combine to form larger aggregates. This process repeats itself, until eventually, full-size flocs are formed (Merckelbach, 2000). These orders of aggregation, as they are called, are idealized in Figure 2.6.

The order of aggregation concept is consistent with the postulate that properties of clay mineral flocs can be approximately described in terms of self-similarity (Mehta, 2014). Kranenburg (1994) proposed to treat mud flocs and beds as self-similar fractal structures, meaning they obey power-law behaviour at all scales. Kranenburg (1994) already noted that it would be naïve to expect that cohesive sediment, with its large variability in composition and properties, would form exactly self-similar aggregates. However, several properties of cohesive sediment can actually be described by

power-law relations, such as aggregate density, permeability and viscosity. Hence, as a first approximation, it seems just to treat mud flocs as self-similar fractals.

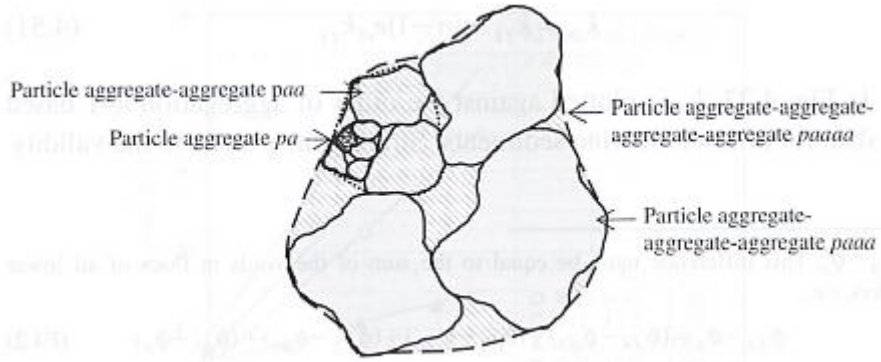

Figure 2.6: The main aggregate is made up of one-order lower aggregates, each consisting of aggregates which are, in turn, one order lower, and so on. After Mehta (2014), adapted from Krone (1963)

Self-similar fractals can be described by using the fractal dimension n_f, which is defined as (Mehta, 2014):

$$n_f = \frac{\log(n)}{log\left(\frac{D_f}{D_p}\right)} \tag{2.1}$$

n = number of particles [-]

D_f = floc diameter [μm]

D_p = primary particle diameter (coagulated clay particles) [μm]

The fractal dimension ranges between $1 \leq n_f \leq 3$. Very tenuous or stringy aggregates have a n_f which approaches 1 (Merckelbach, 2000). In the case of massive, Euclidean particles n_f is equal to 3. Mud flocs generally have a fractal dimension between 1.4 (very fragile flocs) to 2.2 (strong estuarine flocs) (Winterwerp and van Kesteren, 2004).

As can be seen later on, the fractal dimension is a convenient parameter to describe several properties of mud, both during the (hindered) settling and consolidation phases.

2.4.2 Floc growth

Flocculation is the result of the simultaneous processes of aggregation and breakup. Aggregation, or floc growth, occurs when colliding particles cohere and increase in mass. Breakup, or disaggregation, is due to a shear stress exerted on the floc by flow and collisions (Mehta, 2014). Equilibrium is attained when these processes balance each other. The required time to reach

equilibrium is called the flocculation time. This flocculation time is an important concept, as flocs may not reach equilibrium conditions, both in natural or in laboratory environments (Winterwerp, 1998).

The aggregation of flocs depends on the frequency with which the particles collide, and the efficiency with which they cohere after the collisions. Hunt (1980) identified three mechanisms leading to inter-particle collision. These mechanisms are:

- Turbulent shear stress
- Brownian motion
- Differential settling

Research has shown that in coastal and estuarine environments, aggregation will mainly be caused by the turbulent shear stress (O'Melia, 1980, van Leussen, 1994, Stolzenbach and Elimelech, 1994).

Breakup depends on shear rate, as well as inter-particle collisions. Generally speaking: if the shear forces on the flocs become too large, they break up into smaller flocs (Mehta, 2014).

In Section 2.3.5 it was noted that differences in ionic strength and pH cause different flocculation times, and also differences in floc size and floc density. However, the ionic strength or the pH of a solution does, in itself, not influence the general flow properties. Hence, they do not influence the mechanisms underlying collision frequency. So, to impact the flocculation process they must, in some way, have an effect on the collision efficiency, as already noted by Mietta (2010). Serra and Casamitjana (1997) suggest that the collision efficiency (of latex particles, to be precise) solely depends on the short range interactions between the particles. These short range interactions are, indeed, governed by the physicochemical properties of the suspension fluid.

Timescales

The flocculation time, which was mentioned before, depends on the size of the initial flocs, physicochemical properties of the suspension fluid, sediment concentration and the shear rate. It is defined as the time it takes for a population of flocs to reach dynamic equilibrium. During dynamic equilibrium aggregation and breakup balance each other, and the floc size distribution remains constant in time (Mietta et al., 2009).

2.4.3 Floc size

The upper limit for floc size is taken at approximately the Kolmogorov length scale (Winterwerp, 1998), which is the smallest length scale known in turbulence. It is the length scale at which the energy of the turbulent eddies is dissipated into heat by viscosity, and is inversely related to the shear rate G.As discussed before, turbulence has a twofold influence on flocs: it causes both floc aggregation and breakup.

Dyer (1989) compiled data from different sources, relating floc diameter to both suspended sediment concentration and shear stress, for aggregation by shear stress only. The results are shown in Figure 2.7. Dyer used the shear stress as a surrogate for the shear rate G. Floc size is found to increase with shear stress, reaching a maximum at approximately 0.1 Pa, then decreasing with shear stress as breakup will start to dominate aggregation. An analogous explanation holds for sediment concentration: floc size is first found to increase with sediment concentration, but then again decreases (Mehta, 2014).

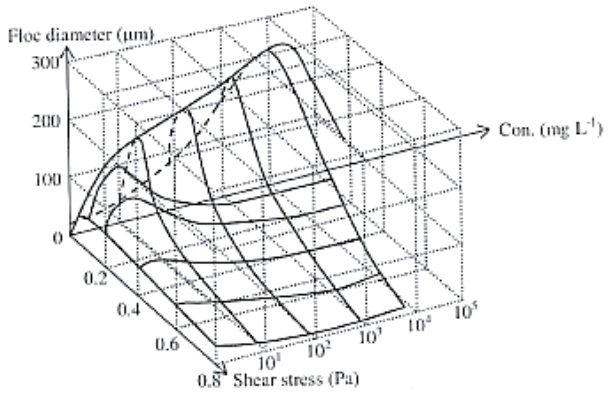

Figure 2.7: Results from Dyer (Dyer, 1989), showing the relationship between floc diameter, sediment concentration and shear stress

The influence of physicochemical properties on floc growth and size was studied by Mietta et al. (2009), who studied the development of the mean floc size (as a function of time) at a shear rate of $G = 35\ s^{-1}$, whilst varying the physicochemical conditions of the suspension fluid. Results found for mean floc size, for low sediment concentrations ($O(\varphi)= 10^{-5}$), are presented in Figure 2.8.

In Figure 2.8, the aforementioned Kolmogorov length scale is plotted as a dashed line. All found equilibrium floc sizes are smaller than this length scale. Both the pH of the solution and the valence of the cations have a considerable influence on the equilibrium floc size. Furthermore, the equilibrium floc size increases with decreasing shear rate.

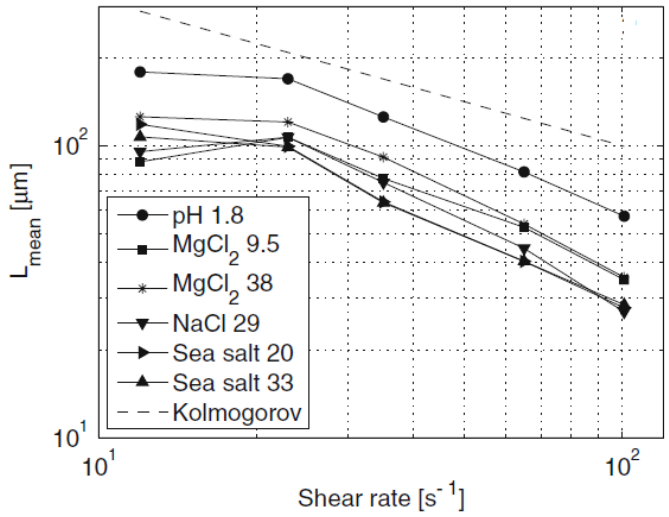

Figure 2.8: Mean floc size as a function of shear rate for suspensions with different chemical properties. Mud was sampled from the Lower Western Scheldt. Salt concentrations are expressed in ppt (Mietta et al., 2009).

Now the theoretical concepts of colloid chemistry and flocculation have been laid out, the following section elaborates on how they affect the settling and consolidation of mud.

2.5 Settling and self-weight consolidation

Under 'natural' circumstances, erosion and sedimentation of sediments, which may be non-cohesive or cohesive, are two ongoing processes. For this research, erosion is of lesser importance as the main interest is how mud settles and consolidates in relatively calm circumstances.

In the previous paragraphs it was elaborated that mud comes in flocs, thereby trapping silt (and possibly sand) particles in a clay-water matrix. The water content of these flocs is particularly high and typically varies between 80-95% of the total volume. These flocs are fundamentally different from sand and silt particles, which can be considered as massive, Euclidean particles. To begin with, settling of an individual mud floc is considered. Afterwards, this will be expanded to the hindered settling of mud flocs.

2.5.1 Settling of a single mud floc

The settling of a single particle was firstly described by Stokes, who developed a schematised model for settling particles in a viscous fluid. The Stokes' law for an Euclidean particle settling in a viscous fluid reads:

$$w_s = \frac{(\rho_s - \rho_w) g D^2}{18\mu} \tag{2.2}$$

To arrive at this formulation, Stokes presumed that the gravity working on a particle is at equilibrium with the drag force, working in opposite direction. For massive particles, this

formulation holds. However, mud flocs are certainly not massive particles, as they mainly consist of water: therefore Stokes' law does not apply to mud flocs.

To account for variations in floc size and floc density, Winterwerp (Winterwerp, 2002) proposed the following formula for the settling of an individual mud floc in still water:

$$w_{s,0} = \frac{\alpha}{18\beta}\frac{(\rho_s - \rho_w)g}{\mu} D_p^{3-n_f} \frac{D_f^{n_f-1}}{1 + 0.15Re_f^{0.687}} \tag{2.3}$$

In this formulation, α and β are shape factors of the flocs, D_p is the diameter of primary mud particles, n_f is the fractal dimension of mud flocs, and Re_f is the particle Reynolds number. The formula for settling mud flocs is analogous to the formulation proposed by Stokes, and for massive, spherical particles ($n_f = 3$, $\alpha = 1$ and $\beta = 1$) it converges to Stokes' law.

Logically, settling mud flocs do not come alone. With increasing sediment concentration, mud flocs will start to hinder each other in their settling, due to several effects. This hindered settling phase occurs for concentrations of several grams/litre onwards.

2.5.2 Hindered settling

Individual flocs will start to hinder each other in their settling behaviour for concentrations larger than 2-3 g/l. It is caused by the influence of neighbouring particles on the settling velocity of an individual particle within a suspension. Winterwerp (2002) has suggested the following hindered settling formulation:

$$w_s = w_{s,0}\frac{(1-\phi)^m(1-\phi_p)}{1+2.5\phi} \tag{2.4}$$

Where:

w_s = effective settling velocity [m/s]
$w_{s,0}$ = individual mud floc settling velocity [m/s]
φ = volumetric concentration: c/c_{gel} [-]
φ_p = volumetric concentration of primary particles: c/ϱ_s [-]

Winterwerp (2002) reasoned that, as each floc within a suspension can be considered to settle in the remainder of the suspension, three main hindering effects ought to be distinguished, being:

1. Return flow and wake formation caused by the settling particles, which will affect the settling velocity of neighbouring particles, decreasing their effective settling velocity by a factor (1-φ). This effect is large because of the high water content of the mud flocs, thereby yielding a large volumetric concentration for relatively low sediment concentrations.

2. A changed viscosity in which the particles settle, which can be modelled based on the classical Einstein formula: $\mu_{eff} = \mu_{mol}(1 + 2.5\phi)$.

3. The buoyancy effect, which scales with $(1-\varphi_p)$, where φ_p is the volumetric concentration of primary particles.

Dankers and Winterwerp (2007) suggested adding the exponent to the return flow term, to account for non-linear effects. This means that hydrodynamic effects generated by the settling particle (for example acceleration and deceleration of flow, and the curvature of streamlines) are incorporated. Mostly, the exponent m is taken equal to 2.

The effective settling velocity during hindered settling can be measured through a simple settling column experiment, by tracking the suspension-water interface over time.

2.5.3 Gelling concentration

In the previous paragraph, the term gelling concentration was introduced in defining the volumetric concentration φ. Its formal definition reads: 'the concentration for which a network structure exists, i.e. when flocs are in direct contact with each other' (Winterwerp and van Kesteren, 2004). By definition, the volumetric concentration φ is equal to 1 at the gelling concentration.

Because the flocs are very open and contain a lot of water, the gelling concentration is already reached for relatively low sediment concentrations. Gelling concentrations reported as low as 50 g/l (Buscall et al., 1988) exist. However, there is a large spread in reported gelling concentrations, with reported values ranging up to 280 g/l (Sills, 1998). This large spread in gelling concentrations is discussed later on, in Section 5.4.3. Dankers (2006) proposed two different methods to measure the gelling concentration for mud mixtures:

- The first method is by determining the height of the settling curve for which a clear deflection is observed. The gelling concentration can then be calculated as the product of the initial concentration and the ratio of the measured height versus the column height.
- The second method is by setting up two settling columns with varying initial concentrations. By doing so, two solutions for Equation (2.4) are obtained, from which the two unknowns $w_{s,0}$ and c_{gel} can be solved.

When expressed in parameters relating to the floc size and structure, the gelling concentration is defined as (Winterwerp and van Kesteren, 2004):

$$c_{gel} = \rho_s \left(\frac{D_p}{D_f}\right)^{3-n_f} \tag{2.5}$$

Again, the fractal dimension n_f and the floc diameter D_f are the variables which are subject to variation when the flocculation behaviour is augmented. Mietta et al. (2009) found that with a decrease in pH, thereby also increasing the ionic strength, or solely an increase in ionic strength, the floc diameter D_f increases. With increasing floc size, Maggi (2005) found that the fractal dimension n_f also decreases:

$$n_f \approx \left(\frac{D_f}{D_p}\right)^{-0.1} \tag{2.6}$$

Combining equations (2.5) and (2.6) it is hypothesized that with decreasing pH or increasing ionic strength, a decrease in the gelling concentration c_{gel} ought to be observed. If the gelling concentration is reached, hence a space-filling network of mud flocs has developed, we no longer speak of hindered settling, but this is called consolidation.

2.5.4 Self-weight consolidation

After sediment is laid down by sedimentation, it passes from being a fluid supported suspension, to a loose structure until it becomes a soft soil, the strength of which then gradually increases under additional load. Compression of a soil is called consolidation. During consolidation, porosity decreases and less space is available for pore water. Eventually, pore water is expelled from the soil (Verruijt and van Baars, 2007).

In the case of consolidating mud beds, consolidation is caused by the self-weight of the soil and, while the bed is soft, is accompanied by large strains (Been and Sills, 1981). To understand which material properties influence self-weight consolidation, it is useful to closely examine the Gibson formula (Gibson et al., 1967), which is one of the most common self-weight consolidation formulas. It reads:

$$\frac{\partial e}{\partial t} + (1+e)^2 \left(\frac{\rho_s - \rho_w}{\rho_w}\right) \frac{d}{dz}\left(\frac{k}{(1+e)^2}\right) + \frac{(1+e)^2}{g\rho_w} \frac{\partial}{\partial z}\left(\frac{k}{1+e}\frac{\partial \sigma'}{\partial z}\right) = 0 \tag{2.7}$$

Where:

t = time [s]

e = void ratio [-]

ρ_s = density of solids [kg/m^3]

ρ_w = density of water [kg/m^3]

k = permeability [m/s]

σ' = effective stress in vertical direction [N/m²]

Without going into the derivation of this equation, it can be inferred from this equation that self-weight consolidation is a function of void ratio, permeability and effective stress, where the latter two are both a function of void ratio. Expressions for σ' (e) and k(e) are needed to solve this equation, which will also be elaborated upon further. The third term in the equation above is also known as the coefficient of consolidation c_v, which, for small strains, reduces to the consolidation coefficient as originally defined by Terzaghi (Winterwerp and van Kesteren, 2004).

Three distinct phases can be distinguished in the self-weight consolidation process. These are indicated in Figure 2.9. HS indicates the Hindered Settling phase, C-I indicates first-phase (I) Consolidation. C-II indicates Consolidation, second phase (II).

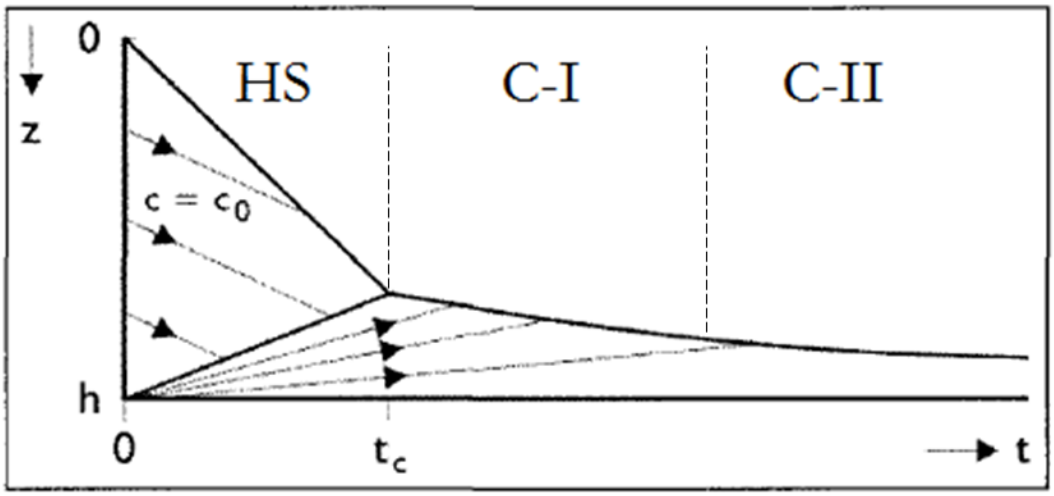

Figure 2.9: Indication of three different stages in self-weight consolidation. Adapted from Winterwerp and van Kesteren (2004).

Figure 2.9 shows a characteristic settling curve: the height of the sediment-water interface as a function of time. The three distinguished phases are discussed further below.

Hindered Settling phase (HS)

Hindered settling, which was discussed in Section 2.5.2. Mud flocs settle, and a steady decline of the sediment-water interface is observed. The interface will move downward at a more or less constant pace, until the gelling concentration is reached. The time at which this occurs is indicated in Figure 2.9 by the time of contraction t_c.

Consolidation - Phase I (C-I)

During the first consolidation phase, which was first described by Kynch (1952), the Gibson equation is simplified by assuming that effective stresses are negligible during the first phase of consolidation. Gibson's equation can then be simplified to:

$$\frac{\partial e}{\partial t} + (1 + e^2)\left(\frac{\rho_s - \rho_w}{\rho_w}\right)\frac{\partial}{\partial z}\left(\frac{k}{(1+e)^2}\right) = 0 \tag{2.8}$$

This simplification can be applied under the assumption that the small stresses that do develop, are counteracted by the water that is flowing upwards. As can be seen from this equation, the change of void ratio in time is governed by the permeability of the bed, which determines the outflow of water. Therefore, this phase is also called the permeability regime. As may be expected, the permeability of the bed also depends on the void ratio e.

Consolidation - Phase II (C-II)

Due to ongoing deposition of mud flocs, a surcharge is formed, initiating the second phase of consolidation. During this phase, effective stresses, defined as $\sigma' = \sigma - p$, will also start to play a role in the self-consolidation of the bed. Hence, Equation (2.7) needs to be solved in its full form.

To solve the differential equations for both phases, expressions for k(e) and σ' (e) need to be specified as well. In this research, the concept of fractal theory is utilized to describe the self-weight consolidation process.

2.5.5 Fractal theory applied to self-weight consolidation

The self-similarity of flocs, and the fractal approach following it from it as posed by Kranenburg (1994), was discussed in Section 2.4.1. By using this concept, material functions for the self-weight consolidation of sediment water mixtures, containing small amounts of sand, were derived by Merckelbach (2000) and Merckelbach and Kranenburg (2004). They assumed that the bed structure is built of a network of flocs consisting of clay and water, enclosing silt particles in the clay-water matrix. If the sand content in the mixture is below a threshold value (Section 2.2.4), sand particles merely fill space in the matrix, without affecting the network structure or properties.

If the mass balance of settling and self-weight consolidation is written in the form of an advection-diffusion equation, the constitutive equation for the fractal approach to modelling self-weight consolidation reads:

$$\frac{\partial \phi_s}{\partial t} - \frac{\partial}{\partial z}\left[w_{s,0} f\left(\phi_s, c_{gel}\right) + \Delta_\rho k \phi_s^2\right] - \frac{\partial}{\partial z}\left[\Gamma_t + \Gamma_c\right]\frac{\partial \phi_s}{\partial z} = 0 \tag{2.9}$$

The terms k (permeability) and Γ_c (coefficient of consolidation) are elaborated upon in the following paragraph.

2.5.6 How flocculation influences the settling and consolidation process

The settling phase, during which flocculation takes place, is succeeded by the consolidation phase. It seems evident that changes in flocculation behaviour, during the hindered settling phase, will also influence the self-weight consolidation behaviour of mud.

When the acidity and/or ionic strength of the ambient solution increase, the mean floc size L_{mean} also increases, as shown, for instance in Figure 2.8. These results were found for kaolinite suspensions by various researchers (Mietta et al., 2009, Kaya et al., 2006, Nasser and James, 2008). If the mean floc size is taken as a representative for the floc population, it is posed that D_f, the floc diameter, will increase. Owing to the fact that the fractal dimension of the flocs, n_f is smaller than 3 (as discussed in Section 2.4.1), this increase in size will lead to a smaller density as the floc size increases.

Next to that, if the fractal dimension also decreases with increasing floc size according to Equation (2.6), this would result in an even greater increase in relative water content W. As this water has to be accommodated in the flocs, the pores in the flocs itself will increase, resulting in an increased void ratio e for the flocs. It is hypothesized that the change in these floc parameters have the following effect.

<u>During the settling phase</u>

If only a single mud floc is considered, a larger floc size means it will settle faster. However, as the gelling concentration decreases, φ will be influenced and thus, the effective settling velocity w_s will decrease at an earlier stage.

The gelling concentration c_{gel} decreases, as it depends inversely on both the floc diameter D_f and the fractal dimension n_f, see Equation (2.5). This can be understood by realising that with more porous flocs, it takes a lower suspended sediment concentration to form a space-filling network. Subsequently, with a decreased gelling concentration, the permeability regime is reached for higher volumes of the soft mud layer.

It is unclear to what extent restructuring of the flocs will occur upon reaching the gelling concentration and subsequent initial consolidation.

<u>During the permeability regime</u>

During the initial consolidation phase, the permeability determines the rate at which water can flow out of the bed. To arrive at a formulation for the permeability, the reasoning of Kranenburg (1994) is followed.

When the gelling concentration is reached, the volumetric concentration φ equals unity. The size D_f of the aggregates then scales as:

$$D_f \sim D_p \phi_p^{\frac{1}{n_f-3}} \tag{2.10}$$

If the flow through the pores is modelled as (laminar) Poiseuille flow, this gives:

$$k \sim l^2 \tag{2.11}$$

Where l stands for a typical size of such a pore. The assumption of scale invariance implies that the diameter of the largest pores, hence l, scales with D_f. Combining Equations (2.10) and (2.11) leads to the following relationship:

$$k \sim {D_p}^2 \phi_p^{\frac{2}{n_f-3}} \tag{2.12}$$

Hence, the permeability of the bed is inversely proportional to the fractal dimension n_f

This proportionality was parametrised and fitted to experimental data by Merckelbach (2000), yielding the following result:

$$k = K_k \left(\frac{\phi_p^m}{1 - \phi_p^{sa}} \right)^{-\frac{2}{3-n_f}} \tag{2.13}$$

It is noted that also the amount of sand in the mixture is accounted for, as Kranenburg derived the formula for a purely clay-water matrix (Merckelbach and Kranenburg, 2004).

As the outflow of water in the permeability regime is governed by the permeability only, the parameters K_k and n_f in Equation (2.13) can be estimated by fitting Equation (2.14) with mud-water interface measurements as was done by, for instance, De Lucas Pardo (2014). By setting up experiments with various acidity and/or ionic strength, it can be determined how these chemical properties influence the coefficient K_k and/or the fractal dimension n_f.

$$h(t) - \zeta_s = \left(\frac{2-n}{1-n} \zeta_m \right)^{\frac{1-n}{2-n}} \left((n-2) K_k \frac{\rho_s - \rho_w}{\rho_w} \right)^{\frac{1}{2-n}} t^{\frac{1}{2-n}} \tag{2.14}$$

Phase II:

During this phase, both the permeability and the effective stress play a role. To determine a material function for the effective stress, a similar approach is followed as was done for the permeability. This leads to:

$$h_\infty = \zeta_s + \frac{n}{n-1}\frac{K_p}{g(\rho_s-\rho_w)}\left(\frac{g(\rho_s-\rho_w)}{K_p}\zeta_m\right)^{\frac{n-1}{n}} \tag{2.15}$$

By measuring the final bed height, and through the fractal dimension that was obtained by fitting Equation (2.14), the effective stress parameter K_p can be obtained. Together with the permeability parameter K_k and the fractal dimension n_f, the coefficient of consolidation c_v can be determined:

$$\Gamma_c = c_v = \frac{2}{3-n_f}\frac{K_k K_p}{g\rho_w} \tag{2.16}$$

This coefficient of consolidation is a measure for the rate at which consolidation proceeds.

2.6 Geotechnical considerations

Whereas the settling of mud belongs to the domain of fluid mechanics, once the deposited sediments have fully consolidated and have become a soil, the domain of soil mechanics is reached. The self-weight consolidation of mud overlaps both of these domains. Therefore, it may prove valuable to investigate which common ground is shared by the fields of morphology and geotechnical engineering.

In Section 2.5, settling and consolidation were discussed. Consolidation occurs when pressure acting on a saturated soil increases due to overburden either by placement of sediment or application of an external load. As a result, water is expelled and particles are forced to be closer to each other. Self-weight consolidation, which was discussed in Section 2.5.4, does not require overburden as compression occurs due to the soil's own weight (Mehta, 2014). Once a soft bed/slurry has consolidated and effective stresses start to develop, the slurry will pass on from a slurry to a soil (eventually). However, it is important to realize that this process may even take several years.

Two concepts from geotechnical engineering will be considered in the following sections. These concepts are:

- The undrained shear strength (Section 2.6.1)
- The Atterberg limits (Section 2.6.2)

Section 2.6.3 will then discuss the research that has related these concepts. To conclude the geotechnical considerations, it is finally discussed how the results in this research in this research are linked to the existing theory.

2.6.1 Undrained shear strength

The undrained shear strength of a soil is a measure for the resistance a soil yields against deformation, or in other words: the maximum allowable shear stress applied on a soil sample before failure takes place (van Paassen, 2004). The undrained shear strength is a soil property, but depends on depth, as it depends on the water content of a soil or slurry. It is one of the key engineering parameters in geotechnical engineering.

A common way to measure the undrained shear strength of a soil is through a shear vane test. A possible procedure is to insert the shear vane into a soil sample and thereafter, to rotate it at a constant rate (See Merckelbach (2000) for more details on shear vane testing). This is the procedure that will be followed in this research, as previous researchers have measured the undrained shear strength of cohesive soil samples accordingly (Merckelbach, 2000, Jacobs, 2011). The stress response of a sample to such a test is qualitatively sketched in Figure 2.10. In this picture, the remoulded shear strength c_v corresponds to the undrained shear strength.

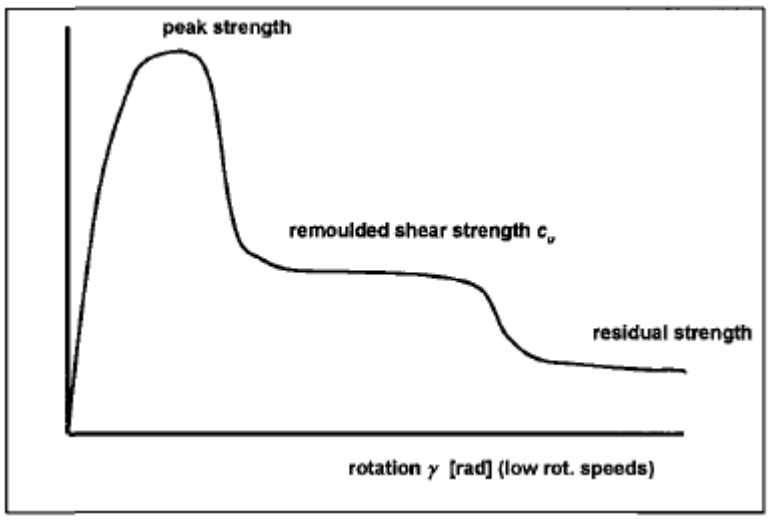

Figure 2.10: Qualitative sketch of stress response of soil sample to shear vane test. After Winterwerp and van Kesteren (2004)

2.6.2 The Atterberg Limits

In geotechnical engineering, the cohesive properties of a soil are commonly characterised by the Atterberg Limits (Winterwerp and van Kesteren, 2004). The Atterberg limits consist of two limits, which are formally described below:

- Liquid Limit (LL): the water content at which a soil passes from the plastic to liquid state. This transition point is comparable to the water content at an undrained shear strength of 1.7 kPa (Bora and Sharma, 2003).
- Plastic Limit (PL): the water content at which a soil passes from the solid to the plastic state. This transition point is comparable to the water content at an undrained shear strength of 170 kPa (Bora and Sharma, 2003).

A schematic overview of these definitions is given in Figure 2.11.

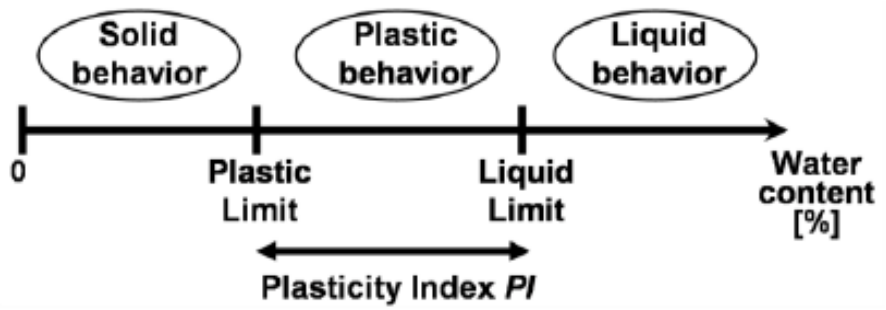

Figure 2.11: Schematic overview of the Atterberg limits. The difference between the plastic and liquid limit is known as the plasticity index PI (Jacobs, 2011)

The Atterberg Limits reflect the ability of a soil to hold a certain amount of water and to still behave as a soil, or a plastic substance. The Plastic and Liquid Limit are utilized to define two indices, which in turn can be used to characterise soils and mud layers. Firstly, the Plasticity Index is discussed:

- Plasticity index (PI): the difference between the liquid and plastic limit. This, as well as the liquid and plastic limit, is expressed as a water content percentage.

$$PI = LL - PL\ [\%] \tag{2.17}$$

The Plasticity Index of a soil or mud depends on the activity (A) and the clay size fraction (Skempton and Northey, 1952). Hence, the Plasticity Index can also be defined as:

$$PI = A * (\xi_{cl} - \xi_{cl,0}) \tag{2.18}$$

The activity of clay depends on several factors. The most important factors are:

- The specific surface area of the clay particles
- The surface charge (or CEC) of the clay particles
- The pore fluid composition

The greater the activity, the more important the influence of the clay fraction on soil properties and the more susceptible the activity becomes to changes in factors such as the type of exchangeable cations and pore fluid composition (Mitchell and Soga, 2005).

The second index that is discussed is the Liquidity Index:

- Liquidity index (LI): the normalized water content is called the Liquidity Index (LI), which is defined as:

$$LI = \frac{W - PL}{PI} \tag{2.19}$$

The Liquidity Index is useful for expressing and comparing the consistencies of different clays. It normalizes the water content relative to the range of water content over which a soil is plastic (Mitchell and Soga, 2005). The Liquidity Index is a common parameter in geotechnical engineering, which expresses the relative water content of a soil (or slurry). The Liquidity Index is generally applied for consolidated soils, for which the water content W lies between the Plastic Limit and the Liquid Limit (PL<W<LL), resulting in a Liquidity index which is between 0 and 1. Natural mud mixtures generally exhibit a water content which is larger than the Liquid Limit (W>LL), which requires extrapolating LI to values >2 (Jacobs, 2011).

Winterwerp and van Kesteren (2004) argue that this extrapolation may lead to inaccuracies, because the Atterberg Limits will then be used to describe mixtures beyond the application area these limits were originally derived for. However, the interesting property of the Atterberg Limits is that they describe the ability of soils (also depending on the physico-chemical conditions of the solution) to contain water and still retain their strength. It is exactly this property that makes them useful for describing mud properties as well.

2.6.3 Undrained shear strength as a function of relative water content

Several researchers, for instance Locat and Demers (1988) and Jacobs (2011), have empirically determined relations between the undrained shear strength of slurries/soils and their relative water content (with LI>1). The relative water content is determined by normalizing the water content by the Atterberg Limits. As their approaches differed, they will be discussed separately:

Locat and Demers (1988) determined the remoulded strength of sensitive clays for various samples, and plotted these as a function of the respective Liquidity indices of these clays. A relation between the remoulded strength and the Liquidity index was then obtained by fitting a curve through their results. This results in the expression:

$$c_u = \left(\frac{19.8}{LI}\right)^{2.44} \tag{2.20}$$

with c_u expressed in N/m^2.

In this research, the average Liquidity Index of the beds is computed through the average void ratio of the bed. This is then normalized by means of the Atterberg Limits, which are rewritten as void ratios. For the derivation of Equation (2.21), see Appendix B.1.

$$LI = \frac{\bar{e} - e_{PL}}{e_{LL} - e_{PL}} \tag{2.21}$$

Jacobs (2011) tested artificially generated clay samples, whose properties can be controlled better than natural samples. In this research, normalization through the Atterberg limits occurred in a slightly different manner, as this was done by expressing the water content as a relative water content W_{rel}, which is defined as:

$$W_{rel} = \frac{W}{PI} \tag{2.22}$$

With this definition, an expression for the undrained shear strength of pure clay-water mixtures was also found:

$$c_{u,clw} = 2770 * {W_{rel}}^{-2.5} \tag{2.23}$$

with c_u expressed in N/m^2. Both Equation (2.20) and (2.23) will be compared to experimental findings in Chapters 4 and 5.

2.7 Geochemistry & aquatic chemistry

Mud, as was noted before, is a heterogeneous by nature. It consists of silicates, organic matter and non-silicates, all three encompassing a larger set of materials. The non-silicate materials, and the different groups they are divided in, were presented in Table 2.2. The most important feature of these non-silicate materials is the fact that they can react, thereby inducing changes in the chemical composition of the solution and of the sediment itself.

As discussed in Section 2.3, changes in ionic strength or pH of the ambient water lead to a change in the flocculation behaviour of clay. Hence, it leads to a different settling behaviour, and presumably, also to differences in consolidation behaviour. To be more precise, the latter is exactly the focal point of this study. Therefore, it is useful to briefly investigate the chemical processes that exist in the interaction between mud and water, but also air.

2.7.1 Sediment-solution interactions

Mud, and the fluid it is in, are both chemically active, meaning interactions between the solid and liquid phase exist. The mud, or its constituents, can exert an influence on the liquid it resides in, and vice versa.

As it is out of the scope of this research to closely examine the chemical implications of sediment-solution interactions, only some general principles are described. The driving force for chemical reactions is the Gibbs free energy of reaction (Stumm and Morgan, 1996).

Generally speaking, reactions can proceed by themselves if they are exergonic, that is if they release energy. From a thermodynamic point of view, chemical elements strive to attain a state with the lowest amount of free energy. The forward and reverse reactions are competing with each other and differ in reaction rates. These rates depend on the concentration and therefore change with time of the reaction: the reverse rate gradually increases and becomes equal to the rate of the forward reaction, establishing the chemical equilibrium. If a reaction is irreversible, it mostly will run faster than equilibrium reactions.

This research will not consider reactions taking place because of biological processes.

2.7.2 Addition of inorganic chemicals to sediment

As will be discussed in Sections 3.5 and 3.6, variations in the pH of the suspension liquid are applied with inorganic chemicals, i.e. hydrochloric acid (HCl) or sodium hydroxide (NaOH). Besides affecting the double diffuse layer of the clay particles (as discussed in Section 2.3.4), effects on the other constituents of the clay must be given thoughtful consideration. A first indication of which processes are initiated upon adding inorganic chemicals, is given by Mitchell and Soga (Mitchell and Soga, 2005):

"Exposure of soil materials to some inorganic chemicals can initiate a variety of processes that cause reactions and alterations of the particles and other constituents of the soil mass. Among these reactions are:

- Acids dissolve carbonates, iron oxides, and the alumina octahedral layers of clay minerals. The use of hydrochloric acid for identification of carbonate minerals by observation of a rapid effervescence reaction is standard practice.
- Bases can break down silicate minerals. The creation of a high pH environment (pH of 12.4 or greater) is essential to the effectiveness of lime [CaO or $Ca(OH)_2$] stabilization of clays. If sulphates are present, highly expansive minerals may form, as well.
- Oxidation of sulphides, especially pyrite, leads to formation of sulfuric acid that, in turn, can break down some rock minerals and generate gas."

2.7.3 Chemical parameters

Two common parameters to express the chemical properties of a liquid are:

- pH: the -log of the H^+ concentration in a solution
- EC: the electrical conductivity of a solution

Acids and bases are salts. So, when adding either one of them to change the pH of a solution, the ionic strength is also influenced. Hence, one cannot distinguish the effect of varying acidity without keeping the ionic strength constant.

The electrical conductivity of a solution is a measure of the ability of a solution to conduct electricity and is expressed in Siemens per meter. It is noted that the electrical conductivity is not necessarily the same as the ionic strength. However, the EC can be expressed as an ionic strength, assuming that the dissolved ions are all a specific molecule. For low ionic strengths, the relation between electrical conductivity is more or less linear, for higher ionic strengths it becomes nonlinear.

3. Materials and methods

Parameters describing the settling and self-weight consolidation of mud were obtained from theory, as presented in the previous chapter. These parameters are determined experimentally, thereby enabling us to answer the posed research questions. First, this chapter presents an overview of the performed experiments. Next, the materials used for these experiments are discussed. Finally, the experimental setup and procedures are described. The results of these experiments follow in Chapter 4.

Laboratory tests are carried out both at the Boskalis Dolman laboratory in Papendrecht and at the Deltares Fysisch Chemisch Laboratory (FCL) in Delft.

3.1 Overview of experiments

Three different experiments are carried out. These are listed in Table 3.1, together with the parameters measured during these experiments and the method according to which the parameters are measured. The details of the three experiments listed in Table 3.1 are discussed in Sections 3.5, 3.6 and 3.7, respectively.

Table 3.1: Overview of performed experiments

Experiment	Measured parameters	Method according to:
Small settling columns (1 L)	w_s, c_{gel} n_f, K_k, K_p	Dankers and Winterwerp (2007) Merckelbach and Kranenburg (2004)
Large settling columns (2 L)	w_s,$w_{s,0}$, c_{gel} n_f, K_k, K_p	Dankers and Winterwerp (2007) Merckelbach and Kranenburg (2004)
Undrained shear strength	τ_p, c_u	Winterwerp and van Kesteren (2004)

3.2 Materials – clay

Three clay types were used in the experiments: two clay powders and one natural clay. Comparing the results of the aforementioned experiments, for the three different clayey materials, is essential in understanding which properties of the clay influence the settling and self-weight consolidation of mud. In the following paragraphs, the three clay types are described both qualitatively and quantitatively.

3.2.1 Collection and qualitative description

For each of the clays used, a short qualitative description is given, as well as remarks on the collection of the clay.

Kaolinite

Commercially available Kaolinite, which is a clear white, fine-grained powder. Kaolinite is a 1:1 clay mineral generally known for its relatively low activity and hence, its low plasticity. The kaolinite as applied is purchased at Keramikos – Keramisch Centrum Nederland, which is a reseller of Fuchs Keramische Massen (Sibelco Germany).

Bentonite

Commercially available Bentonite, which is a yellow-greenish, fine-grained powder. Bentonite is generally applied in foundry moulding sands, but also in civil engineering practice, because of its ability to form strong gels with water, even at relatively low solids concentrations. Bentonite is a 2:1 clay mineral generally known for its very high activity and hence, its (in most cases) high plasticity. The bentonite as applied is purchased at Keramikos – Keramisch Centrum Nederland, which is a reseller of Fuchs Keramische Massen (Sibelco Germany).

Markermeer clay

The Markermeer clay is a natural clay sample collected in the Markermeer in the Netherlands (Coordinates WGS84: 52.3795, 5.0209). A map of the location where it was excavated can be found in Appendix C.1 (Figure C.3). The Markermeer clay is a sticky, relatively soft clay. It contains shells, and has a dark grey colour, which is almost black.

The clay sample was collected on 24-06-2014 by Boskalis, several meters below the lake bed, from a clay layer which is also known as the Zuiderzee deposit. After collection, it was transported to Delft, where it has been stored in a cold storage cell at Deltares. For the experiments at the Boskalis Dolman laboratory, the clay was transported to Papendrecht, where it was stored in a refrigerator at 6 ºC.

The clay has been collected as a part of the Marker Wadden research project, jointly undertaken by TU Delft and Utrecht University. This research project is officially known as: "Smart Ecosystems: Regime shifts from mud systems to dynamic wetlands". It will be referred to as the Marker Wadden research in the remainder of the report. The clay sample itself is referred to as the MM-IJ2 sample hereafter, to be consistent with the Marker Wadden research coding.

3.2.2 Overview of determined material properties

Table 3.2 lists the determined properties for the three clay types used, with the corresponding method. The material properties that were obtained from other sources are also listed, together with the relevant source.

Table 3.2: Material properties and corresponding methods and sources

Determined properties	Method
Particle size distribution	Malvern Mastersizer with Hydro 2000MU measuring cell
Cation Exchange Capacity	Methylene Blue Adsorption test (Verhoef, 1992)
Liquid Limit	ASTM D4318
Plastic Limit	ASTM D4318
Water content	ASTM D2216-10
Obtained properties	Source
Particle density	Sibelco Germany
Mineralogy	Sibelco Germany and Marker Wadden research report (Barciela Rial, 2015)
Chemical composition	Sibelco Germany and Marker Wadden research report (Barciela Rial, 2015)

3.2.3 Kaolinite

The quantitative properties of the used Kaolinite are discussed in this section, except for the Atterberg Limits. Most results are listed in Table 3.3, except for the chemical composition of the clay powder, which is listed in Table 3.4.

Particle size distribution (psd)

The particle size distribution of the Kaolinite was both supplied by the manufacturer and determined experimentally (see Appendix C.1). The particle size distribution of the Kaolinite is characterized by the clay-sized fraction and sand-sized fraction, as they were introduced in Table 2.1. The psd as obtained with the Malvern Mastersizer seems to underestimate the clay-sized fraction, which is in agreement with the research of Jacobs (2011). The implication is that the details supplied by the manufacturer regarding the clay-sized fraction are followed in the remainder of the research. A possible explanation lies in the fact that a Malvern Mastersizer measures a volumetric fraction, whereas the manufacturer supplied an estimate of the mass fraction.

Calculating the clay fraction based on the obtained plasticity index, with a standard activity for kaolinite (A=0.7) led to an estimate of ξ_{cl}=28 %.

Table 3.3: Properties of the Kaolinite clay powder

Property	Experimental	Manufacturer
Particle size		
Fraction <2 μm [%]	~6	21
Fraction >63 μm [%]	~1	<0.5
Particle density [kg/m³]	N/A	2650
Water content [%]	0.1	<1.0
Cation Exchange Capacity [meq/100 gr]	2.95 ± 0.03	N/A

Particle density, mineralogy and chemical composition

According to the manufacturer, the Kaolinite powder predominantly contained the Kaolinite mineral; hence, only the chemical composition of the material was supplied (Table 3.4). Regarding the chemical composition, it is found that the chemical composition of the kaolinite used is comparable to the kaolinite clay used by Mietta et al. (2009) and can be regarded as a rather pure clay powder, in spite of the presence of small amounts of iron and potassium. Although of its relatively small clay fraction (by size), the chemical composition shows that this is definitely kaolinite, which is a clay mineral. This paradox is inherent to the definition of clay, which denotes both a size fraction and mineralogy. Hence, the kaolinite is addressed as a clay powder in the remainder of this report.

Table 3.4: Chemical composition of the Kaolinite clay powder

Chemical composition	Weight percentage [%]
SiO_2	51.1
Al_2O_3	33.9
Fe_2O_3	0.4
TiO_2	<0.4
Na_2O	<0.1
K_2O	<2.4
Loss on ignition (L.O.I.)	11.0

Cation Exchange Capacity

The cation exchange capacity of the tested Kaolinite is on the lower side of the spectrum for Kaolinite, for which the Cation Exchange Capacity typically ranges between 3-15 meq/100g according to literature (Mitchell and Soga, 2005). The measured value of 2.95 meq/100 grams implies that the surface charge of the Kaolinite is very small, as the CEC is a measure of the total surface charge.

3.2.4 Bentonite

The quantitative properties of the used Bentonite are discussed in this section, except for the Atterberg Limits. Most results are listed in Table 3.5, except for the chemical composition of the clay powder, which is listed in Table 3.6.

Particle size distribution (psd)

For the bentonite, only a >63μm fraction was supplied by the manufacturer, and the only estimate of the <2 μm fraction is the experimentally obtained result. This fraction is likely to be an underestimation of the actual <2 μm fraction. (Malvern procedure; small particles are obscured) This should be borne in mind when interpreting the results. Calculating the clay fraction based on the obtained plasticity index, with a standard activity for bentonite (A=7) led to an estimate of ξ_{cl}=31 %.

Table 3.5: Properties of the Bentonite clay powder

Property	Experimental	Manufacturer
Particle size		
Fraction <2 μm [%]	~11	N/A
Fraction >63 μm [%]	~5	<7
Particle density [kg/m^3]	N/A	2650
Water content [%]	11.1	10 ± 2
Cation Exchange Capacity [meq/100 gr]	78 ± 2	>68
Mineralogical composition		
Montmorillonite [%]	N/A	>65
Quartz [%]	N/A	<10
Other minerals [%]	N/A	<25

Particle density, mineralogy and chemical composition

The particle density, mineralogy and chemical composition of the Bentonite powder were provided by the manufacturer. Although quartz and other minerals are also present, the bentonite powder consists mostly of montmorillonite, which belongs to the smectite type minerals. Verhoef (1992) distinguished the three terms as follows:

- Bentonite is a soil (or rock) which originates from volcanic ash
- Montmorillonite is the principal clay mineral in bentonite soils
- Smectite is the clay mineral group to which montmorillonite belongs

The chemical composition of the Bentonite is shown in Table 3.6.

Table 3.6: Chemical composition of the Bentonite clay powder

Chemical composition	Weight percentage [%]
SiO_2	54.6
Al_2O_3	16.9
Fe_2O_3	5.1
TiO_2	0.5
CaO	3.1
MgO	4.2
Na_2O	3.1
K_2O	1.7
Loss on ignition (L.O.I.)	9.3

Cation Exchange Capacity (CEC)

For the Bentonite, the CEC was determined to be 78 ± 2 meq/100gr, which is a value corresponding to values found in literature for sodium bentonites.

3.2.5 Markermeer clay

The Markermeer clay exhibits a more complex composition compared to the clay powders used. Next to various clay and sand minerals, it also contains shells, organic matter and non-silicates. Unless stated otherwise, the data on the Markermeer clay was determined by Barciela Rial (2015), as part of the Marker Wadden research project.

Particle size distribution

The particle size distribution of the Markermeer clay can be seen in Figure 3.1. Several aspects of this psd are worth noting:

- Ultrasonic treatment of the mud has a profound impact on the obtained particle size distribution. Due to the ultrasonic treatment, clay flocs are broken down, and the larger flocs, which would be regarded as particles with a large diameter are broken up into their smaller constituents. Hence, it leads to the psd being shifted to the left as can be observed in Figure 3.1.
- The obtained psd suggests that only 6-7% of the sample can be regarded as clay (<2 μm), and hence, the sample is on the border between cohesive or non-cohesive sediment. From both qualitative observations and Atterberg limit testing it can be deduced that the clay sample is definitely cohesive. It is likely that the clay-sized fraction is underestimated, which is not illogical as the psd was obtained with a Malvern Mastersizer.
- A separate measurement on the clay sample was performed at the Boskalis Dolman laboratory, which involved the determination of the mud fraction(<63 μm) by means of the Dutch standardised RAW test (CROW, 2000). For further details see Appendix C.1. This value is plotted as a dot in Figure 3.1, and yields a higher mass percentage for the mud

fraction. In the following, the mass fraction (ξ_{mud}=90.2%) obtained by the RAW test is used in calculations.

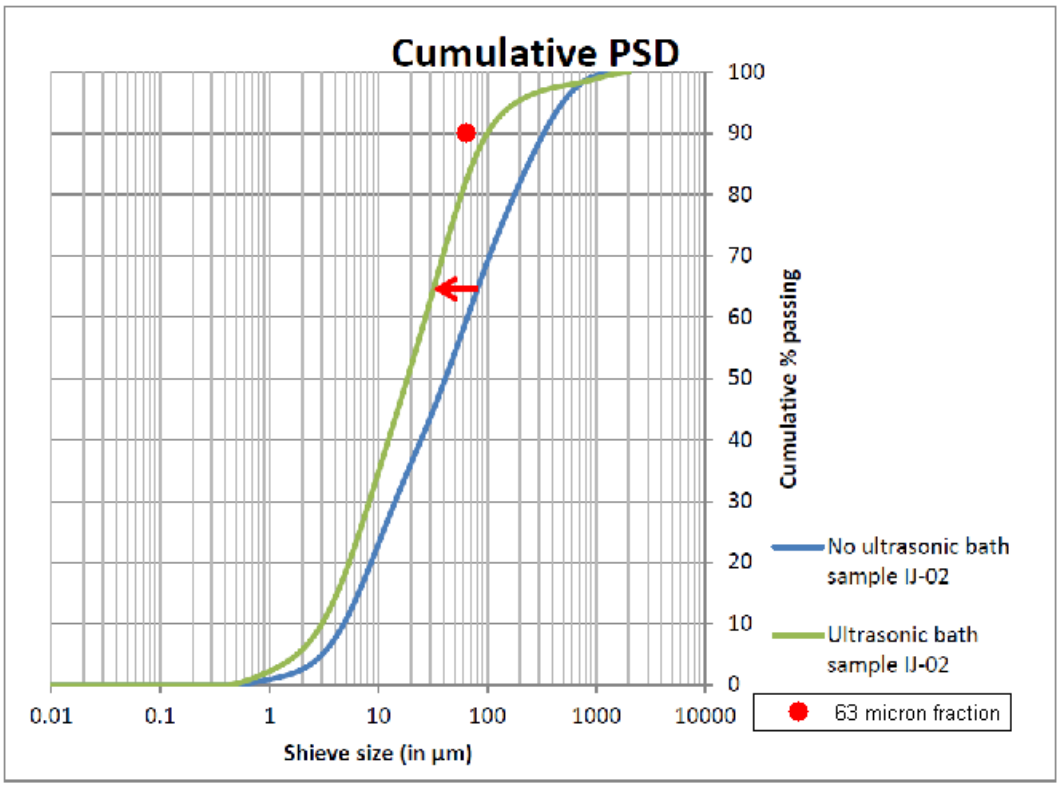

Figure 3.1: Particle size distribution for Markermeer clay. The red arrow indicates the effect of ultrasonic treatment on the determined psd

Mineralogy and chemical composition

The chemical and mineralogical composition of the Markermeer clay were obtained through XRD analyses; results can be found in Table 3.7 and Table 3.8 respectively.

Table 3.7: Chemical composition of Markermeer clay (Barciela Rial, 2015)

Mineral	Theoretical Formula	Weight percentage [%]
Non-phyllosilicates		
Silicates		
Quartz	SiO_2	36.5
Plagioclase	$(Ca,Na)(Si,Al)_4)O_8$	6.6
Alkali feldspar	$(K.Na)Si_3AlO_8$	1.9
Carbonates		
Calcite	$CaCO_3$	9.1
Dolomite	$CaMg(CO_3)_2$	1.3
Ankerite (Fe0.2)	$CaFe_{0.2}Mg_{0.8}(CO_3)_2$	0.1
Ankerite (Fe0.54)	$CaFe_{0.54}Mg_{0.46}(CO_3)_2$	0.2
Ankerite (Fe0.68)	$CaFe_{0.68}Mg_{0.32}(CO_3)_2$	0.2
Oxides/Hydroxides		
Hematite	Fe_2O_3	0.3
Rutile	TiO_2	0.2
Anatase	TiO_2	0.3
Sulphides		
Pyrite	FeS_2	0.6
Total non-phyllosilicates		57.3
Phyllosilicates		
2:1 Al Phyllosilicates	$K(Al,Mg,Fe)_2(Si,Al)_4O_{10}[(OH)_2,(H_2O)]$	35.6
Kaolinite	$Al_2Si_2O_5(OH)_4$	2.2
Chlorite	$(Mg,Fe)_5Al(Si_3Al)O_{10}(OH)_8$	4.9
Total phyllosilicates		42.7

Next to the large percentage of clay minerals that are present (42.7%), also a fair amount of quartz is present (36.5%). For the non-silicates, the carbonates appear to be the most abundant group in the sample, whereas the amounts of oxides and sulphides, i.e. pyrite, is rather limited.

As for the clay minerals, the most abundant clay minerals are Illite and Smectite (Table 3.8). Hence, it is to be expected that this clay type has a fairly large activity and plasticity.

Table 3.8: Clay mineralogy of Markermeer clay

Mineral	Weight percentage [%]
Illite/Smectite mixed layer (I/S ratio: 0.65/0.35)	31
Illite	29
Kaolinite	10
Smectite	24
Chlorite	6

Cation Exchange Capacity

The CEC was also determined for the Markermeer clay. To obtain this measurement, the clay was dried and ground into a powder, which was then sieved with a <63 μm sieve. Afterwards, one portion of the powder was treated with hydrogen peroxide to remove the present organic matter. This was done to get a first indication of whether the CEC is affected by the presence of organic matter. As can be seen from Table 3.9, the presence of organic matter led to a slight increase in the CEC.

Table 3.9: Cation Exchange Capacity for Markermeer clay

Sample name	CEC (meq/100 gr)
MMIJ2-untreated	13.5 ± 1.5
MMIJ2-treated	11.3 ± 1.1

3.2.6 Sample preparation

The clay samples are prepared using different procedures. Two different approaches are considered:

- Settling column tests

The water content of the various clays is determined; afterwards the amount of clay needed to make a solution with specified concentration (in g/l) is weighed and mixed with water with a specific pH and/or ionic strength. The mixture is then put in a settling column to equilibrate. The procedure that is followed after the initial mixing is outlined in Sections 3.4, 3.5 and 3.6.

- Atterberg Limits

The Liquid Limit of the Markermeer clay could readily be determined, for determination of the Plastic Limit it was dried for several hours. To the contrary, the clay powders needed to be mixed with demineralized water with specified amounts of acid, base or salt added. The mixtures were prepared at a higher water content than the expected Liquid Limit. After preparing the clay mixture, it was stored in a refrigerator (6 ºC) for a week (van Paassen, personal communication, 2015). Afterwards, the Liquid Limit and the Plastic Limit were determined for various pore water compositions.

3.3 Materials – water and chemicals

The properties of the used water and chemicals are presented in this section.

3.3.1 Water

Two types of water are used for the experiments:

- Tap water
- Demineralized water

Tap water contains a variety of dissolved ions, has a specific pH value and its properties vary with its corresponding catchment area, and the treatment it received. With regard to the flocculation of clay, using tap water has the main advantage it induces flocculation, because of the dissolved ions that are present in the tap water. However, the main drawback of using tap water is that one cannot control the amount of dissolved ions that are present. Next to that, the properties of the tap water may also vary with time, making it less reliable for experiments.

In demineralized water, as its name suggests, the majority of the dissolved ions have been removed. Because of this property, one can control the pH and the ionic strength of the water, simply by adding specific amounts of salt, acid or base. A drawback is the absence of flocculation for mixtures of clay and demineralized water, because the clay particles are stable (in a colloidal sense, see Section 2.3.2). Besides, surface water always contains dissolved ions, therefore the applicability of experiments performed with demineralized water needs to be considered carefully.

For the majority of the experiments at Boskalis Dolman (see Section 3.5), tap water was used. The rationale behind this was to make sure that the clay particles would flocculate. During the experiments it became clear that through the addition of either acid, base or salt (or a combination of these) flocculation would readily occur, even when demineralized water is used for the experiments. Using demineralized water has the advantage that its constituents, and mainly the dissolved ions in the water, can be (largely) controlled, as opposed to tap water, which always contains a variety of dissolved ions. Specifications of the tap water, as supplied by Oasen drinking water company, can be found in Appendix C.1.4. Because of the drawbacks associated with the use of tap water, mostly the presence of various dissolved ions, demineralized water was used during the final experiment carried out at the Boskalis Dolman laboratory.

At the Deltares FCL laboratory (see Section 3.6), only demineralized water was used.

3.3.2 Chemicals

The chemicals that are used in the experiments at Boskalis Dolman are listed in Table 3.10. Both the used acid and base are salts, with a valence of 1, thus a salt with an identical valence should be used to keep the ionic strength constant during the experiments. This stems from the fact that, as

discussed in Section 2.3.3, the valence of the electrolytes in the suspension influence the flocculation behaviour of clay.

Table 3.10: Chemicals used in Boskalis Dolman laboratory experiments

Type	Specification and supplier
Acid	Chloric acid 1M 1.02 g/ml pH=0 - BOOM laboratory equipment
Base	Sodium hydroxide pellets, dissolved in demineralized water pH=14 - Merck
Salt	Sodium chloride, extra pure - BOOM laboratory equipment

The chemicals used in the Deltares FCL laboratory are listed in Table 3.11.

Table 3.11: Chemicals used in Deltares FCL laboratory experiments

Type	Specification and supplier
Acid	Chloric acid 1N standard solution pH=0 – Acros Organics
Base	Sodium hydroxide pellets, dissolved in demineralized water pH=14 - Merck
Salt	Sodium chloride, Baker analysed – JT Baker

3.3.3 Chemical parameters

As discussed in Section 1.4, the pH and electrical conductivity (EC) of the suspension liquid are the parameters that are subject to variation in this research. The EC is used as a measure of the ionic strength of the solution. These two properties are measured with the devices listed in Table 3.12.

Table 3.12: Chemical properties of suspension liquid and measuring devices

Property	Boskalis Dolman laboratory	Deltares FCL laboratory
pH	HACH HQ30d with PHC 101 probe	HACH HQ30d with PHC 101 probe
EC	WTW LF318	HACH HQ30d with CDC probe

3.4 Laboratory experiments – general considerations

To measure the properties as outlined in Section 3.1, settling column experiments were set up. General considerations regarding the experiments are addressed in this section. Next, the different experiments are discussed, in separate sections.

Several important concepts that should be kept in mind when executing the experiments are:

- Chemical equilibrium between the ambient solution and the used clay should be achieved – or at least enough time should be taken to try and establish equilibrium.
- The mud should be stirred long enough to promote flocculation, however stirring should be done gently to prevent floc breakup. The proposed mixing period is one hour, based on findings by Mietta et al. (2009).

3.4.1 Chemical equilibrium

In order to avoid testing artefacts, a steady chemical state should be achieved for the various clays. A first estimate is taken from de Wit (1992), who performed experiments on Kaolinite powder, and found that for a 15 L suspension to achieve a steady chemical state, the clay needed to be in a container (whilst being mixed daily) for 3 weeks. Based on these findings, it was decided to let the mud equilibrate for 1 week in the 1 L settling columns, and for 2 weeks in the 2 L settling columns. These values are smaller than the 3 weeks proposed by de Wit (1992), but so are the volumes. Hence, these periods are seen as adequate, although measurements of the suspension pH and EC will be taken to verify this assumption.

3.4.2 Mixing the sediment

As the shear rate in the settling columns itself is practically zero, mixing is done prior to the experiments, as it is evident that mixing is needed to promote flocculation (Section 2.4.2). Several mixing methods were described by Safar et al. (2015). Two of these methods are schematically shown in Figure 3.2.

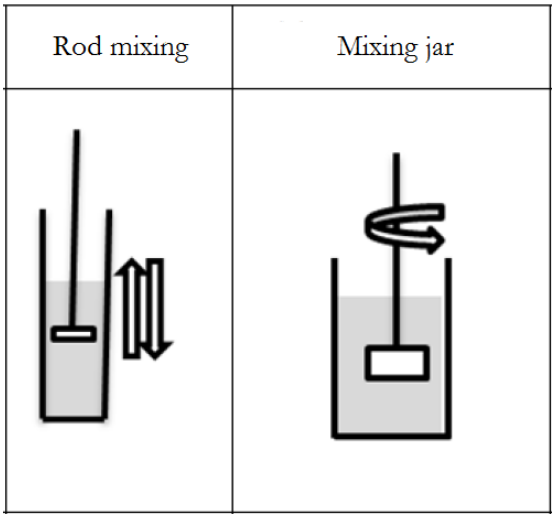

Figure 3.2: Sediment mixing methods. Adapted version of sketch Safar et al. (2015).

It is proposed to mix the sediment in a mixing jar before starting with the settling column measurements, because using a mixing jar allows to mix the sediment for prolonged periods of time. If this is not possible, using a mixing rod to mix the sediment is seen as the alternative procedure. Because both methods are used, they are both discussed below.

1. Rod mixing

A plastic rod is inserted into the column through the opening, and is moved up and down slowly. The shear rate for this method can be estimated by:

$$G \cong \frac{h}{\Delta t}\frac{r^2}{(R-r)(R^2-r^2)} \tag{3.1}$$

h = settling column height [mm]

R = diameter of settling column [mm]

r = diameter of mixing rod plate [mm]

Δt = time from top to bottom of settling column [s]

The original formula by Safar et al. (2015) contained a du/dz term instead of the shear rate G. Based on the units of du/dz and G, that are both [s^{-1}], it is chosen to express the shear rate as G.

2. Mixing jar

This method is regarded as the most reliable mixing method. In a mixing jar, the shear rate is estimated through the formula suggested by Serra et al. (2008):

$$\log G = -0.856 + 1.37 \log S_p \tag{3.2}$$

S_p is the impeller rotation speed in rotations per minute. The shear rate obtained by using the formula is consistent with Bouyer et al. (2005) and is therefore assumed to be valid for a mixing jar with the following dimensions: 95 mm inner diameter and 110 mm for the height of the fluid. The suspension is stirred using a single rectangular paddle. The paddle is 25 mm high and 75 mm in diameter and is placed 10 mm above the bottom of the jar. As the mixing jars used in this research are comparable, Equation (3.2) will be used to calculate the shear rate in the mixing jars.

The used stirring rate may well influence the experimental results. For instance, a too high shear rate will result in a decrease of the Kolmogorov length scale (Section 2.4.2), thereby limiting the floc size. On the other hand, imposing a shear rate which is too low could have adverse effects as well: sedimentation of the clay particles which are being mixed can occur, and a longer mixing time is required to arrive at equilibrium floc sizes. Next to that, pouring the sediment from the mixing jars into a settling column may also affect the results. This was done gently, but floc breakup is regarded inevitable.

3.5 Lab experiment I – Small settling columns

The first series of experiments were performed at the Boskalis Dolman laboratory during the period June-October 2015. The main goal of these experiments was to develop an understanding of the material behaviour, by comparing the settling and consolidation behaviour of three clayey materials, for three different pH values each. The clays used were (1) Kaolinite (2) Bentonite and (3) Markermeer clay. Next to investigating the settling and consolidation behaviour, undrained

shear measurements were taken at the end of the last experimental run. The undrained shear strength measurements are discussed in Section 3.7.

3.5.1 Experimental setup

Experiment I consisted of several experimental runs. Each run consisted of 3 settling columns per clay type, with a target pH of 3, 7 or 10, respectively. The settling columns used have a capacity of 1L, a height of 34 cm and a diameter of approximately 5 cm.

The initial concentration c_0 was set to 40 g/l. This concentration was not varied during various experimental runs, and was chosen in such a way that it:

- Is below the expected gelling concentration.
- Is high enough so settled beds with sufficient height for undrained shear strength measurements will develop

The settling columns were placed in a room with a temperature ranging between 20-24 ºC. The water temperature ranged between 20 to 22 ºC.

During the preliminary experiments measurements were done visually, but during the experiments that followed, a camera (GoPro Hero 4 Black) was used to take pictures of the settling columns. This camera was set to take a picture every minute for the entire duration of the experiment, which could be analysed after the experiment. The main advantage of this method is the high temporal resolution of the measurements, and that the process, which is rather lengthy, could also be tracked during non-working hours. A picture of this setup is shown in Figure 3.3.

Figure 3.3: Experimental setup at the Boskalis Dolman Laboratory

3.5.2 Experimental procedure

After determining the water content of the several clays, these were mixed with a solution of water (either tap water or demineralized) , with added HCl or NaOH to obtain the intended pH value. Upon buffering of the acid or base, additional HCl (pH=0) or NaOH (pH=14) was added to restore the intended pH value.

After 5 days, the pH and the EC of the suspension were measured. If necessary, adjustments were made by adding either the acid or base mentioned above. During this step, sodium chloride was added. Again, the sediment was shortly mixed.

Measurements of the pH and EC were taken for at least 4 moments in the experiment. These are list in Table 3.13.

Table 3.13: Measurements of pH and EC during Experiment I

Measurement	Moment
1	t=-7 days: mixing of sediment and solution
2	t=-2 days: adjusting pH and EC for buffering of acid or base.
3	t=0: before start of experiment
4	End of the experiment

Before the start of the experiment, the sediment was mixed for a specified period and with a

specific shear rate G. Next, the suspension was gently poured into the settling columns and the mixture was homogenized over the vertical by shortly stirring with the mixing rod.

3.5.3 Typical result

The GoPro photographs are manually processed to determine the height of the sediment-water interface. Plotting the obtained interface height as a function of time gives the settling curve.. Typical settling curves for Experiment I are drawn in Figure 3.4, for the three types of clay.

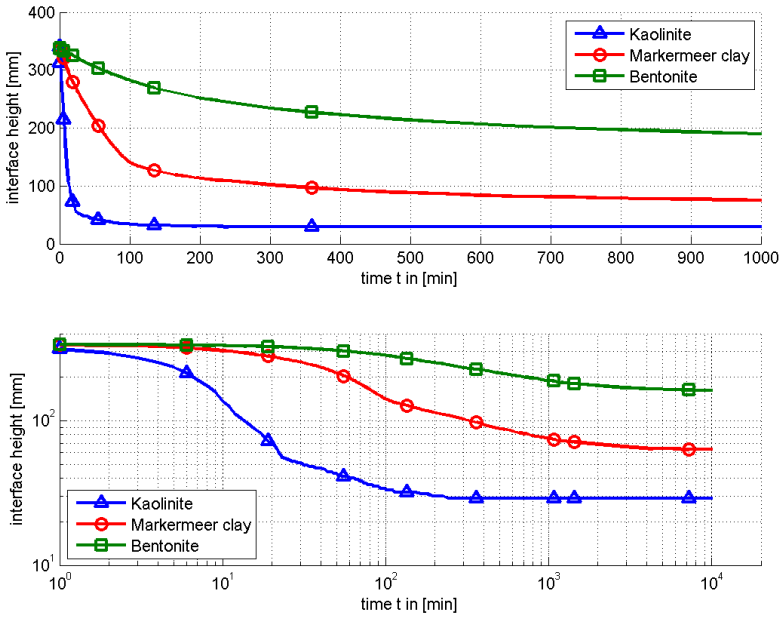

Figure 3.4: Height of water-suspension interface as a function of time for Kaolinite, Markermeer clay and Bentonite on linear and double logarithmic scale

The time range as plotted is 1000 minutes, whereas the entire experiment took approximately one week. This is done to show the hindered settling phase, that takes place during the first 100-200 minutes of the experiment for Kaolinite and Markermeer clay. For Bentonite, such a phase appeared not to be present, because no deflection could be observed in the settling curve, either plotted on a linear or log-log scale.

3.6 Lab experiment II – Large settling columns

The second series of experiments were performed at the Deltares FCL laboratory. This experiment had two main goals: (1) to obtain an estimate for the gelling concentration for various pH values and (2) to test consolidated samples with a shear vane at the end of the experiments. The consolidation process was also monitored.

3.6.1 Experimental setup

During these experiments, 2L settling columns were used. These columns are wider and taller than the columns used in experiment I, as the 2L columns are 8 centimetres in diameter and

approximately 40 cm high. 9 columns are set up, for which the initial concentration c_0 is systematically varied, and also the pH is varied for the various columns. The settling columns were placed in a room where the temperature ranged from 20-23 ºC. The water temperature ranged from 21 to 22 ºC. See Table 3.14 for the other experimental settings.

Whilst the pH was varied by adding chloric acid or sodium hydroxide, the ionic strength was kept constant by adding sodium chloride. Varying initial concentrations led to the need to add different amounts of chloric acid or sodium hydroxide to achieve a comparable pH value. The processes involved are discussed in Section 5.1.

The water-bed interface was monitored with a Canon EOS 400D camera. During the first 2 days, a picture was taken every two minutes. For the next phase, the frequency was decreased to once every 30 minutes.

Table 3.14: Experimental settings - Experiment II

Column code	c_0 [g/l]	pH [-]
		intended
MMIJ2-LSC1	30	3
MMIJ2-LSC2	30	7
MMIJ2-LSC3	30	10
MMIJ2-LSC4	40	3
MMIJ2-LSC5	40	7
MMIJ2-LSC6	40	10
MMIJ2-LSC7	50	3
MMIJ2-LSC8	50	7
MMIJ2-LSC9	50	10

The nine columns, as they were set up, are shown in Figure 3.5.

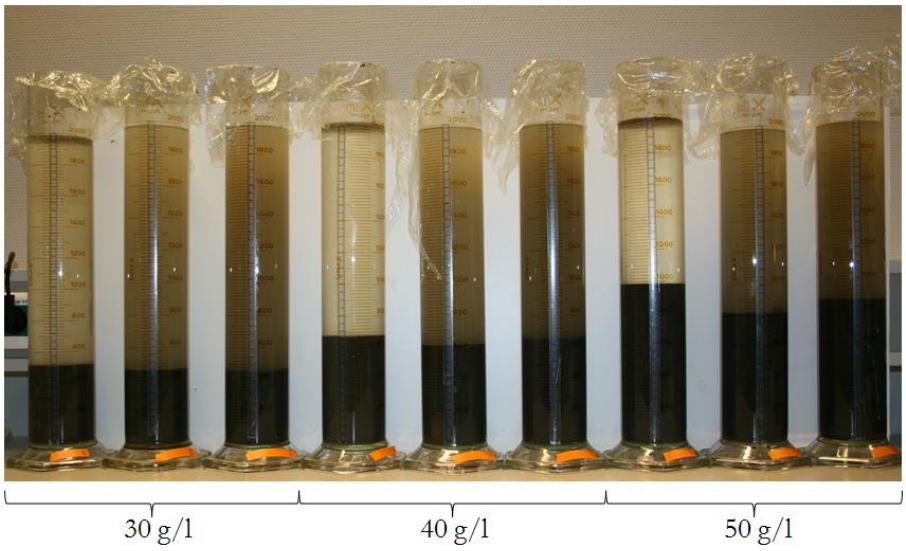

Figure 3.5: Experimental setup of Experiment II, with 9 settling columns. The acidity per subset increases from left to right, pH=3 for the left column, pH=7 for the middle column and pH=10 for the right column.

3.6.2 Experimental procedure

The experimental procedure for Experiment II is discussed below.

Estimating the gelling concentration

To properly set up the settling column experiment, first the gelling concentration should be estimated to assure that the initial concentration is below this critical concentration (as no settling phase is present when $c_{initial}>c_{gel}$). If the initial concentration is beyond the gelling concentration, two problems will occur:

- As the volumetric concentration φ is 1 (by definition), no flocculation and thus no floc growth will occur. If the effect of flocculation on the total settled bed height is to be determined, it is crucial that during experiments such a phase is actually present.
- If, for the settling columns, one of the initial concentrations used is larger than the gelling concentration, an erroneous estimate for the gelling concentration will be obtained.

The gelling concentration of the Markermeer clay for either the acidic or alkaline solution, as these are thought to be the extreme conditions, is determined by performing small jar tests. The jars are placed in a mixing jar setup (VELP Scientifica JLT6), mixed for two hours at a shear rate of $G = 30\ s^{-1}$. This shear rate was based on the findings of De Lucas Pardo (2014) and Mietta (2010). After mixing the sediment for two hours at this shear rate, it was mixed with a mixing rod, before tracking the interface measurement.

This resulted in an estimate of the gelling concentration $c_{gel} \approx 85$ g/l for the acidic solution and 102 g/l for the alkaline solution. As can concluded from Table 3.14, the initial concentrations were chosen such that they were smaller than the gelling concentration.

Measuring the pH and EC

Measurements of the pH and EC were taken for at least 4 moments in the experiment. These are:

Table 3.15: Measurements of pH and EC during Experiment II

Measurement	Moment
1	t=-14 days: mixing of sediment and solution
2	t=-2 days: adjusting pH and EC for buffering of acid or base.
3	t=0: before start of experiment
4	End of the experiment

Mixing the sediment

Mixing the sediment was done with a mixing rod. This was mainly done as using the mixing jar had some practical issues. For instance, 2L of suspension needed to be mixed per column while only 1L jars were available, hence there was not sufficient capacity.

Data collection and processing

Photographs taken with the EOS 400D camera are processed using a Fortran script, which automatically discerns the water-suspension (and later on the water-bed) interface and gives as output the pixel number at which this interface is located for the specific picture. The pixel number is then converted to an interface height, which is used for further analysis.

3.6.3 Typical result

Plotting the obtained interface height as a function of time gives the settling curve, which can be used for further analysis. A typical settling curve for Experiment II is drawn in Figure 3.6. The time range as plotted is only 2000 minutes, whereas the entire experiment took more than one month. This is done to show the hindered settling phase, that takes place during the first 200 minutes of the experiment (approximately).

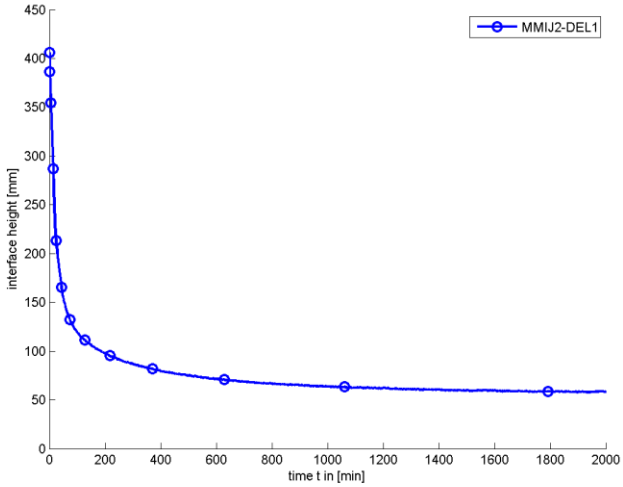

Figure 3.6: Height of sediment-water interface as a function of time for column MMIJ2-LSC1.

3.7 Undrained shear strength

At the end of both the small and large settling column tests, the undrained shear strength of the samples was determined. The samples are tested in-situ, which is considered necessary, since removing the samples from their columns is likely to completely disturb them.

3.7.1 Experimental setup

After consolidation of the clay samples, the samples are left in their columns. Because of the expected very low undrained shear strengths of the material, the measuring device needs to have a high accuracy, i.e. it has to be able to measure stresses of N/m^2 rather than kN/m^2. Next to that, the settling columns are 340 to 420 mm high, so an elongated vane has to be used, which can be lowered into the sample, which is at the bottom of the column.

These two requirements led to using a rheometer, equipped with a shear vane, which is mounted to an extendable rod. The vertical position of the vane can be adjusted by lowering or raising the position of the rheometer as a whole. A sketch of the setup can be seen in Figure 3.7.

The shear vane used is a FL100 type vane: a six-bladed vane with a diameter D of 22 mm and a height h of 16mm. The rheometers and vane used are listed in Table 3.16.

The rheometer is used to rotate the shear vane at a constant rate. The torque needed to rotate the vane, because of the resistance of the soil it is rotated in, is recorded. Combining the measured torque with the shear vane geometry then yields a stress. When this stress is plotted as a function of angular rotation, the undrained shear strength is a part of the obtained curve. The rate of rotation should be low, because of the low undrained shear strength of the samples.

Table 3.16: Rheometers used to determine the undrained shear strength

Laboratory	Rheometer type	Vane
Boskalis Dolman	Haake Viscotester VT550	FL100
Deltares FCL	Haake M1500	FL100

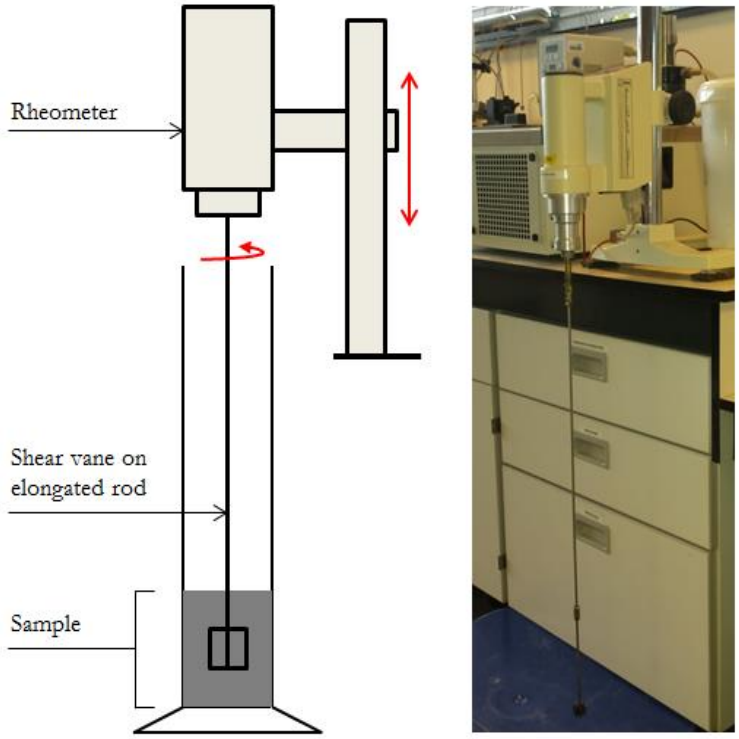

Figure 3.7: Sketch of measurement setup of rheometer (left panel). Photograph of rheometer at BKD laboratory equipped with shear vane on extendable rod, without sample (right panel).

3.7.2 Experimental procedure

Before the samples were tested, the final bed heights were noted and the supernatant was siphoned out of the settling column. A film of water remained on top of the bed as this could not be removed without disturbing the settled bed.

The height inside the bed, to which the vane was lowered, was calculated according to the final bed height. The vane was set to a height, such that its middle line was aligned with half the height of the settled bed. This is sketched in Figure 3.8. For a proper measurement an undisturbed volume is required, approximately 3 times the vane diameter and 1.5-2.0 times the vane height.

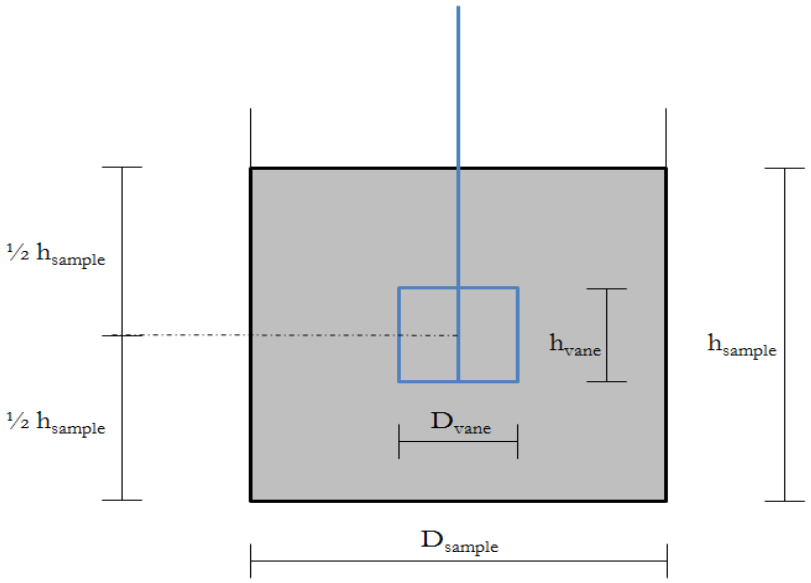

Figure 3.8: Dimensions of shear vane and sample. The shear vane is drawn in blue. Alignment of vane in sample is also sketched, with the centre line of the vane aligned with the centre line of the sample.

The sample requirements for shear vane testing are summarised in Table 3.17, using the dimensions defined in Figure 3.8.

Table 3.17: Shear vane testing requirements

Shear vane test requirement
$D_{sample} > 1.5\text{-}2.0*D_{vane}$
$h_{sample} > 3.0*h_{vane}$

When the sample and the rheometer are prepared, the vane is lowered into the bed carefully. When this is done, the rotation rate and the duration of the test are set. The vane is rotated at a low constant rate, and is rotated for a minimum of two full rotations.

3.7.3 Typical result

The output of the rheometer is a measured shear stress, which can be characterised by a peak strength τ_p and a remoulded (or undrained shear) strength c_u, as they were conceptually shown in Figure 2.10. A typical shear stress recording, produced by a shear vane measurement, is displayed in Figure 3.9 During the initial 15-30 degrees of the test, a peak strength is reached, which depends on soil fabric, but also on the testing procedure (Merckelbach, 2000). Afterwards, the recorded shear stress gradually decreases until it reaches an average value. This is the remolded strength, which is calculated as the average recorded shear stress from 360 to 720 degrees. Sample is the MMIJ2-LSC5 sample (see also Table 3.14).

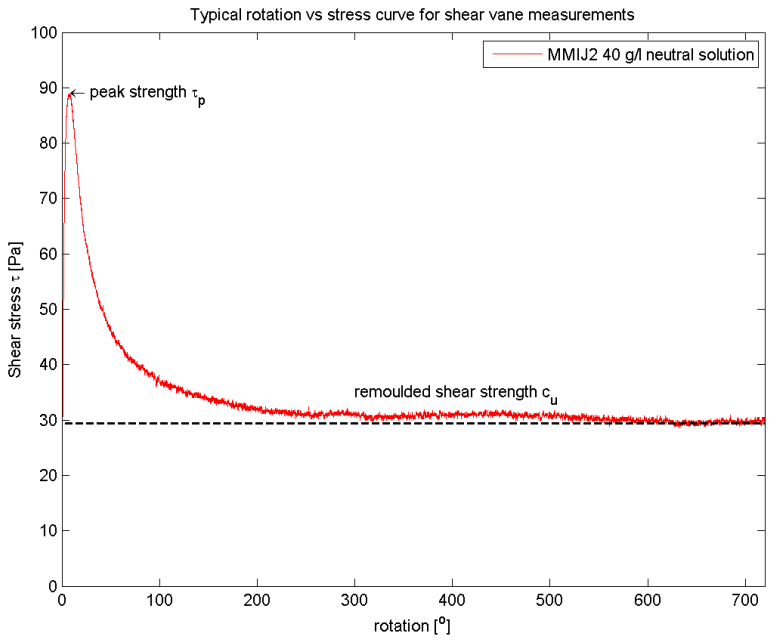

Figure 3.9: Typical shear stress measurement curve for measured samples. The rotation-stress curve shown in this figure is for the MMIJ2-LSC5 sample.

4. Experimental results

In this chapter, the results of the laboratory experiments are presented. First, the determined Atterberg Limits of the three clays are presented. Next, the results of the small settling column (SSC), large settling column (LSC) and undrained shear strength experiments are presented. These are grouped into the three aspects of mechanical behaviour defined in Section 1.4.2, being: settling, consolidation and undrained shear strength.

4.1 Atterberg Limits

The Atterberg Limits are determined for the kaolinite, bentonite and Markermeer clay. The purpose of determining these limits is to normalize the results of the various clays by means of the Atterberg Limits, which is common practice in the field of geotechnical engineering.

The two clay powders were both tested with various pore water compositions. The pore water compositions are discussed later in this paragraph. The Markermeer clay was only tested with its natural pore water, as this water content was already close to the Liquid Limit.

4.1.1 Plasticity chart

The Atterberg Limits of all three clayey materials are plotted in a plasticity chart. The plasticity chart shows the relation between the Liquid Limit of a soil and its Plasticity Index. For the various used clays, the results are displayed in Figure 4.1. Besides the obtained results for these clays, two linear trends are plotted as well. The A-line (solid) distinguishes between inorganic clays and sediments rich in organic matter and silt, whereas the B-line (dashed) envelops sediments found in the natural environment (Winterwerp and van Kesteren, 2004).

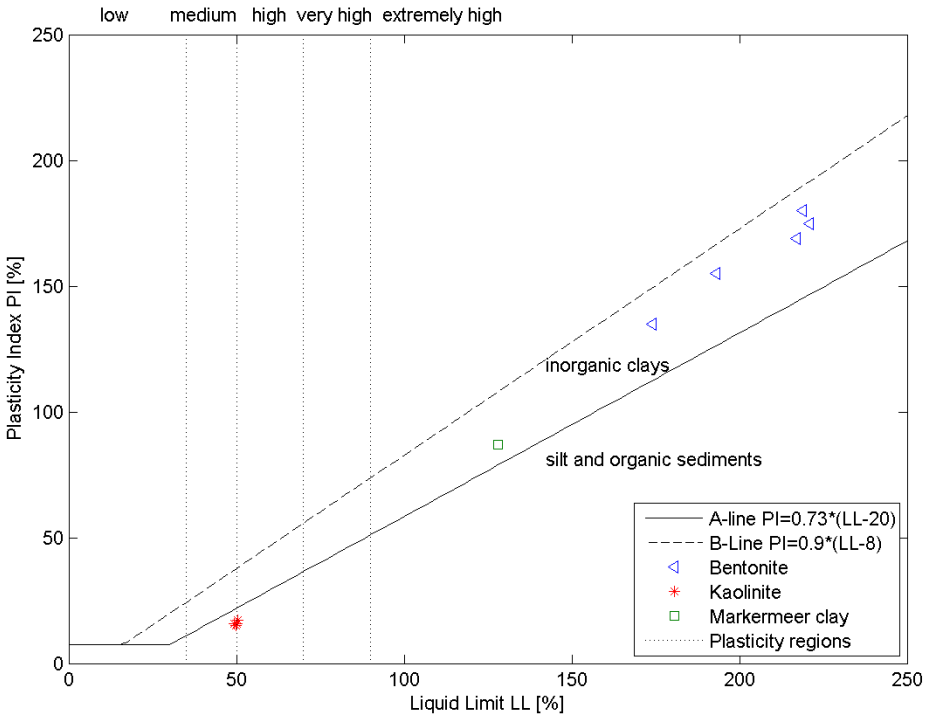

Figure 4.1: Plasticity chart with determined Atterberg limits for Kaolinite, Bentonite and Markermeer clay

From Figure 4.1, the following observations can be made:

- The kaolinite used in the experiments is classified as a silt with a medium plasticity. Compared to the other clays, the plasticity of the kaolinite is rather low. This is in line with the low Cation Exchange Capacity, as discussed in Section 3.2.3.
- The Markermeer clay can be classified as a clay with an extremely high plasticity. Taking into account that the Markermeer clay consists only for 40% of clay minerals (Table 3.7), this high plasticity is even more remarkable.
- The Bentonite clay is classified as a clay with an extremely high plasticity. The spread in the obtained results is due to variations of the pore water for which the Atterberg Limits were determined.

4.1.2 Atterberg limits of Bentonite

The Atterberg Limits of the bentonite clay powder were determined for 5 varying pore water compositions which are listed in the legend of Figure 4.2. Solutions were prepared with demineralized water which was brought to a pH of 3 (acid), 10 (alkaline) or was modified by adding sodium chloride. The Plastic Limit for all 5 samples varied between 38-48%, which is relatively small compared to the larger variations measured for the Liquid Limit.

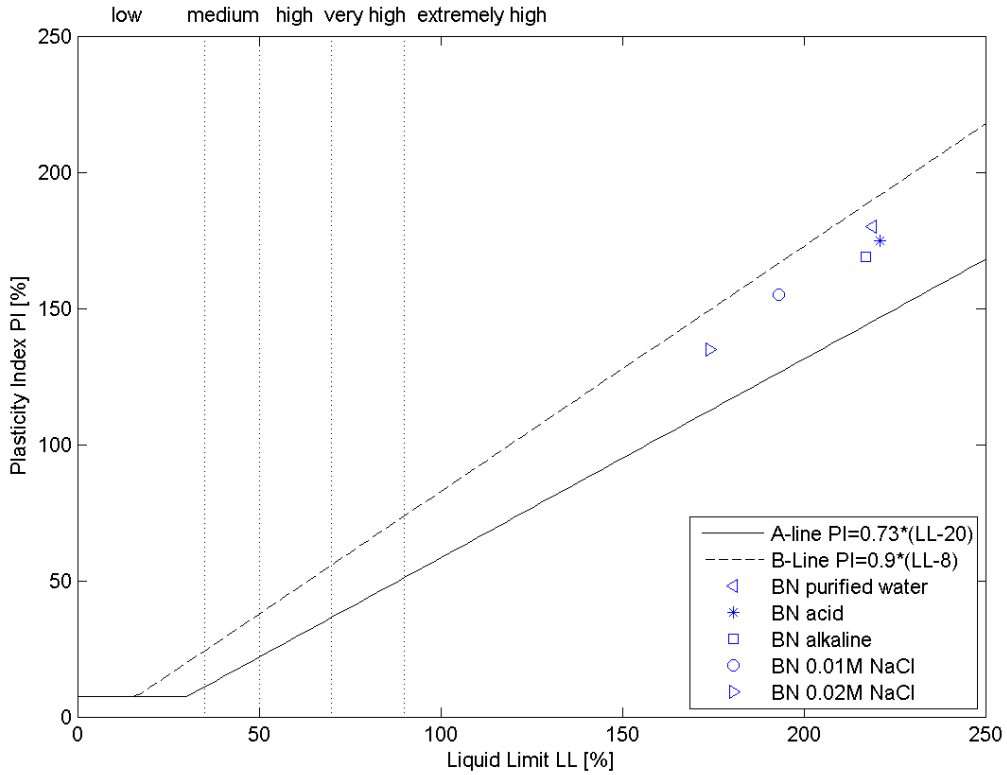

Figure 4.2: Plasticity chart with determined Atterberg Limits for Bentonite for different pore water compositions

The addition of sodium chloride led to a decrease of the Liquid Limit, with an increase in ionic strength leading to a further decrease in Liquid Limit. This decrease is consistent with findings by van Paassen (2004). However, the salt concentration of the pore water used in the current experiments was substantially smaller than the salt concentration in the research of van Paassen (2004) (0.02M as maximum salt concentrations vs. 0.5M as minimum salt concentration in pore water). However, already a large decrease in Liquid Limit was observed for these low ionic strengths.

The addition of acid or base, although these both cause an increase in ionic strength, did not have an effect on the Liquid Limit. However, the ionic concentration of a pH=3 and a pH=10 solution are 10^{-3} and 10^{-4} respectively, which is an order of magnitude smaller than the ionic concentrations of the sodium chloride pore waters used. Next to that, it is believed that the amount of acid and base are buffered by the Bentonite, owing to two factors:

- The Bentonite has a large Cation Exchange Capacity, meaning it has the ability to neutralize considerable amount of added acid or base.
- During the settling column experiments, buffering of added acid was observed for low concentrations of solids. The samples tested for Atterberg Limits have a much higher

solids to water ratio than the settling column experiments, and therefore more buffering will take place.

4.1.3 Atterberg limits of Kaolinite

The Kaolinite was also tested with varying pore water compositions. Again, solutions prepared with demineralized water were either acid (pH=3), alkaline (pH=10) or saline (0.01M NaCl). These different preparations resulted in the values plotted in Figure 4.3.

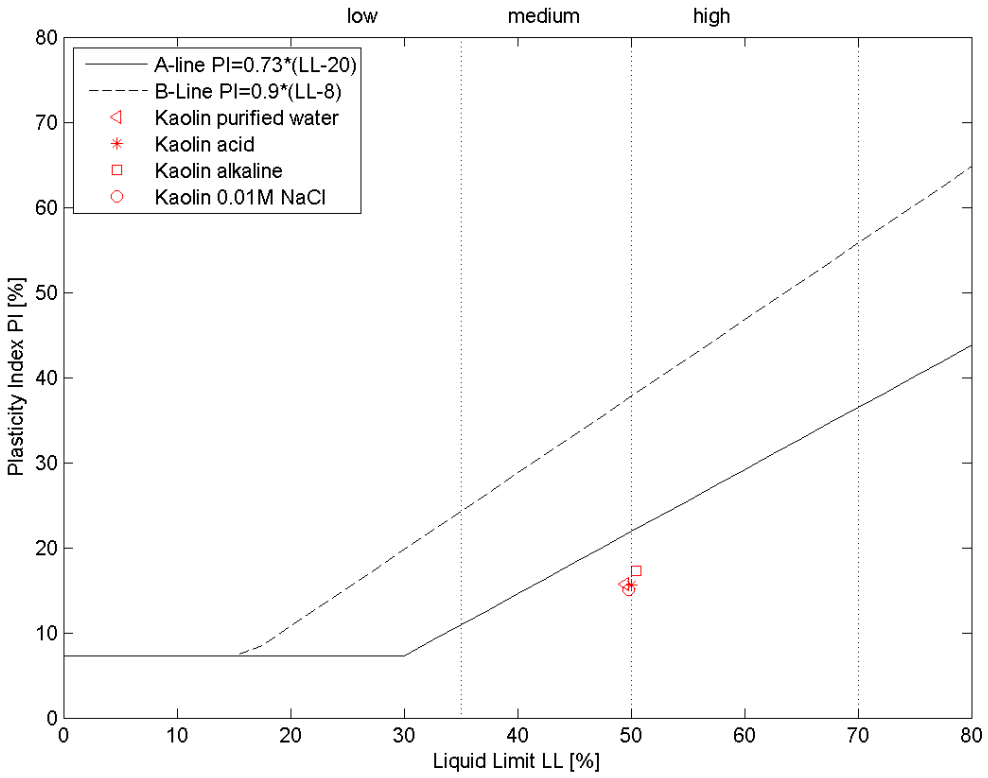

Figure 4.3: Plasticity chart with determined Atterberg Limits for Kaolinite for different pore water compositions

As Figure 4.3 shows, changes in pH or ionic concentration did not yield any significant differences in Atterberg Limits (neither in Plasticity Index nor the Liquid Limit). The Liquid Limit remained fairly constant, around 50% water content, and so did the Plastic Limit. Again, this is consistent with the findings of van Paassen (2004), who found that changes in pore fluid salinity had a relatively small impact on Speswhite, a material that is comparable to the tested kaolinite in terms of plasticity.

4.2 Settling

This section presents the results for the hindered settling phase of the experiments. The output of the small and large settling column experiments (Sections 3.5 and 3.6) are settling curves, the first part of such a curve representing the hindered settling phase. This phase is characterised by means of the effective settling velocity w_s (Section 2.5.2) and the gelling concentration c_{gel} (Section 2.5.3). The results for the Kaolinite clay settling are discussed first, followed by the results for the Bentonite and the Markermeer clay. For all three clayey materials, the qualitative findings are discussed first, followed by the measured effective settling velocities and the determined gelling concentrations.

Figure 4.4 gives an overview of the start and end of the hindered settling phase. The hindered settling phase starts at t=0 and ends at $t=t_c$, the moment at which the gelling concentration is reached.

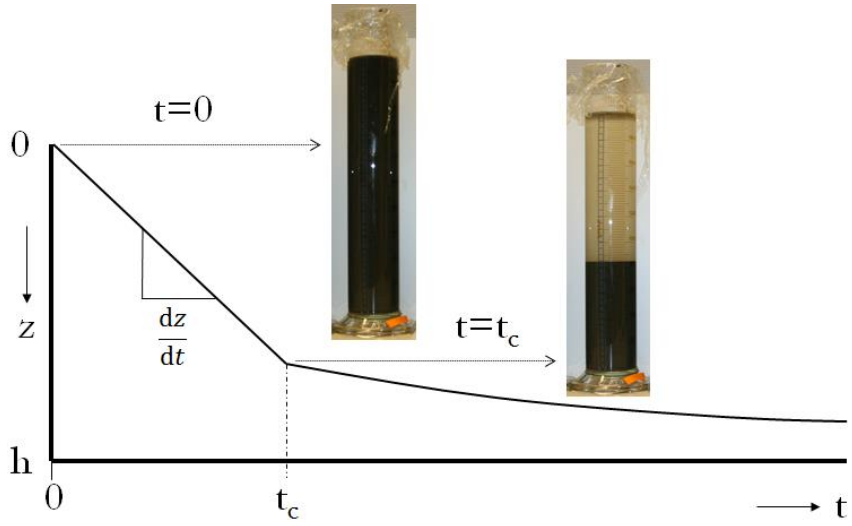

Figure 4.4: Schematized settling curve with indication of start and end of hindered settling phase. The inserted photos correspond with the start of the settling column experiment (t=0) and the point of contraction t_c. A clear water-suspension interface can be seen in the right photograph.

The effective settling velocity is computed by taking the derivative of the initial section of the settlement curve as a function of time, and is indicated as the dz/dt term in Figure 4.4. The initial section is defined as the part of the curve for which the settlement curve follows a (more or less) linear downward trend. The effective settling velocity and the gelling concentration are a means by which the qualitative settling curves can be quantified.

As the main parameter which is varied is the pH, whilst the ionic strength is kept constant, the effective settling velocity is plotted as a function of pH in the remainder of this paragraph.

4.2.1 Kaolinite

Qualitative findings

Qualitative differences were observed in the settling behaviour of the kaolinite for the various pH values. For the four experimental runs (listed in Table 4.1) the acid columns showed similar behaviour. In the acid column, the water-suspension interface became clear within several minutes, with a rather clear supernatant. The neutral columns remained turbid for a longer period of time than the acid column. As a result, the transition from water to suspension was more gradual. A clear water-suspension interface developed after about 15 minutes. The alkaline columns remained turbid for 1-2 hours. After 10 minutes, a water-suspension interface could be identified. However, there was no real clear supernatant at that time. Eventually, turbidity decreased, leading to a more pronounced interface between the suspension and the supernatant.

Effective settling velocity

The measured effective settling velocities for the kaolinite are shown in Figure 4.5. The main observation for the current experiments is that only small differences in settling velocity are measured for the various pH values, in spite of the qualitative differences that are observed.

The initial ionic strength of the suspensions was kept constant for the different experimental runs. The EC of the suspensions was 1.2 mS/cm, which corresponds to an ionic strength of approximately 0.01M NaCl.

In the experiments not only the pH was varied, but also the shear rate at which the mud mixture was mixed in order to promote flocculation. In experiments K-1, K-2 and K-3, all other parameters were kept constant, while the shear rate G was varied. However, it can be concluded from Figure 4.5 that for the kaolinite in the acid suspension, the mixing rate did not influence the effective settling velocity.

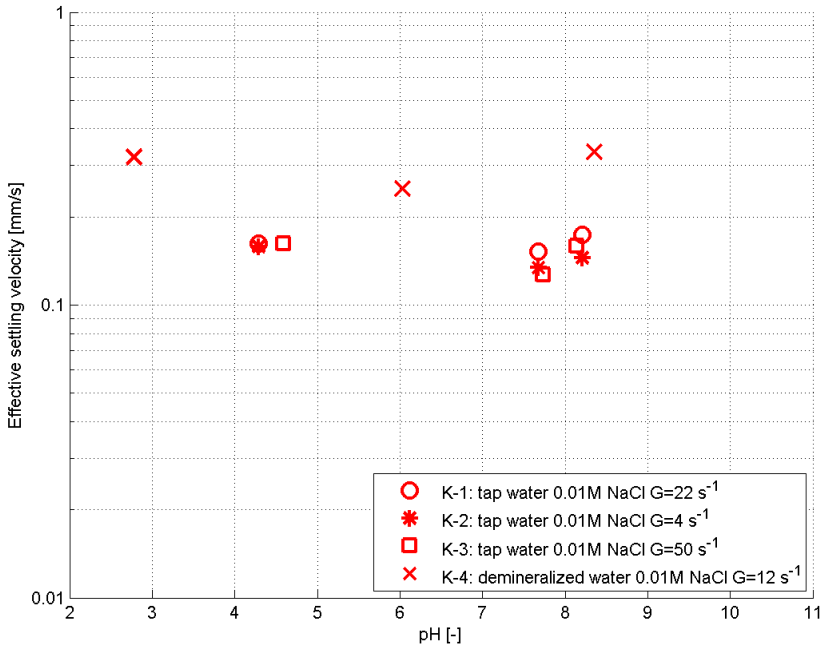

Figure 4.5: Effective settling velocity of Kaolinite as a function of suspension pH

On the contrary, the kaolinite in the neutral and the alkaline solution was affected by the different shear rates; the highest effective settling velocity was measured for G=22 s^{-1}, with G=50 s^{-1} and G=4 s^{-1} leading to lower effective settling velocities. Apparently, the largest flocs, leading to the highest effective settling velocity, are formed at an intermediate shear rate. At the higher shear rate (G=50 s^{-1}), the high shear forces may have broken up the flocs. This is consistent with the theory that flocs scale with the Kolmogorov length scale, which is inversely related to the shear rate. Mixing at a the lowest shear rate (G=4 s^{-1}), may on the other hand have led to flocs that did not fully develop, hence the lower effective settling velocity.

Furthermore, it is remarkable to see that using demineralized water instead of tap water (which were both brought to the same ionic strength in the preparation for the settling experiments) led to a settling velocity which was twice as large for the pH values under consideration. However, the shear rate was also varied, which could have impacted floc formation and thus the settling velocity. The spread in the measured pH values of the suspension (as can be seen in Figure 4.5) for the separate tests will be discussed later on.

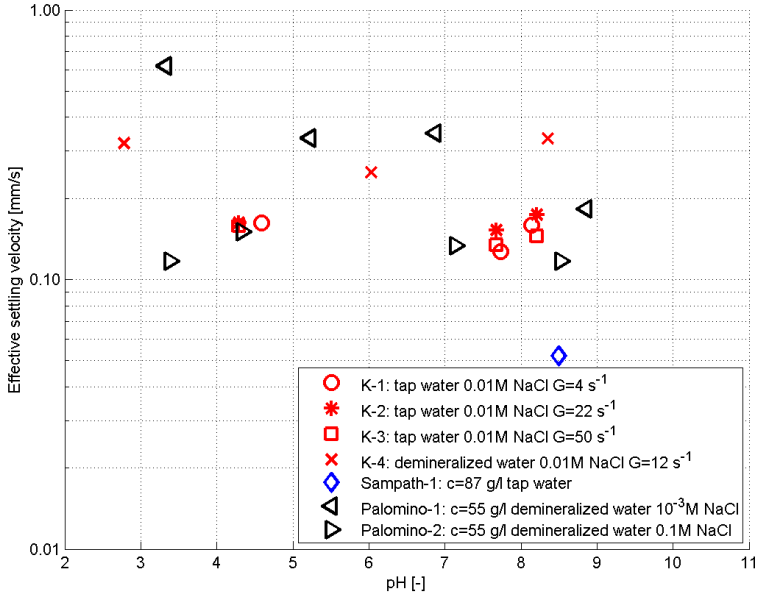

Figure 4.6: Effective settling velocity of Kaolinite as a function of suspension pH with references

Because kaolinite is a material that has been widely studied before, Figure 4.6 shows how results compare to literature. Palomino and Santamarina (2005) and Sampath (2009) also studied the settling of kaolinite, but used slightly different settings than those that were used in this research. The applied settings are listed in Table 4.1.

Table 4.1: Experimental settings for Kaolinite, in comparison with references

Experiment code	c_0 [g/l]	ionic strength [M]	water used [-]	stirring method
K-1	40	0.01 - NaCl	tap water	Rod mixing G=4 s^{-1}
K-2	40	0.01 – NaCl	tap water	Mixing jar G=22 s^{-1}
K-3	40	0.01 – NaCl	tap water	Mixing jar G=50 s^{-1}
K-4	40	0.01 – NaCl	demineralized	Mixing jar G=12 s^{-1}
Sampath-1	87	N/A	tap water	N/A
Palomino-1	55	$3*10^{-3}$ – NaCl	demineralized	N/A
Palomino-2	55	0.1 – NaCl	demineralized	N/A

The fifth entry in Table 4.1 refers to research done by Sampath (2009), but the extent to which the current results are comparable with this work is questionable. The initial concentration for the settling column tests was 87 g/l, which is twice as high as c_0 in the current experiments. This ought to explain the difference in settling velocity. Besides, the ionic strength was not controlled in that research and no details on the mixing procedure were given.

The research of Palomino and Santamarina (2005) is regarded more comprehensive. In this research, the settling behaviour of kaolinite was studied as a function of pH for various ionic strengths. The measured parameters included both the effective settling velocity and sedimented

volume, but also pH and ionic strength were measured. Although their experiments differed from the current experiments (the initial concentration and column width differed) the settling velocities obtained are in the same order of magnitude. For a low ionic strength, $3*10^{-3}$ M NaCl, the settling velocity showed a clear pH dependency as the settling velocity increases with decreasing pH. The pH dependency appeared to be absent for the experiment in which the ionic strength was relatively high (0.1M NaCl).

The ionic strength in the current experiments, $1*10^{-2}$ M NaCl, falls between the two aforementioned ionic strengths. Likewise, the measured settling velocities fall between the settling velocities measured by Palomino and Santamarina (2005), indicating that the ionic strength is one of the main factors controlling the settling rate. To the contrary, no clear pH dependency on the settling velocity could be observed in the performed experiments. This is possibly due to the specific ionic strength used in the current experiments.

Experiments K-1 to K-3 were performed using tap water which may have influenced the results, because of the ions that are already present in the tap water. Using tap water led to the following observations:

- The pH of the suspension liquid appeared to be restored towards equilibrium upon addition of either chloric acid or sodium hydroxide. This was first attributed to the clay itself, but when demineralized water was used no buffering was observed. Hence, this is probably due to the tap water.
- The measured effective settling velocities during experiments K-1 to K-3 were twice as small as those for experiment K-4. It must be noted that also the shear rate G by which the mixture was stirred in Experiment K-4 differed from the other experiments. Therefore, the differences in effective settling velocity cannot solely be attributed to using tap water instead of demineralized water.

Gelling concentration

For the kaolinite, the gelling concentrations were obtained by identifying the interface height for which a significant deflection in the settling curve is visible. From this interface height, an average concentration is calculated. These concentrations are listed in Table 4.2. The found gelling concentrations are quite high, and no clear trend is observed for the gelling concentrations found for either acid, neutral or alkaline suspensions.

Table 4.2: Gelling concentrations found for kaolinite

	acidic [g/l]	neutral [g/l]	alkaline [g/l]
K-1	250	210	260
K-2	240	260	250
K-3	250	260	260
K-4	240	230	170

4.2.2 Bentonite

Qualitative findings

For the bentonite experiments, no hindered settling phase was observed. This is concluded based on two qualitative findings:

- The water-suspension interface moved downward at a very slow rate. In the order of 0.01 mm/s rather than 0.1 mm/s as observed for the kaolinite.
- No large differences in colour of the suspension could be observed, in comparison with both the kaolinite and Markermeer clay settling experiments, where there was a gradient in the colour of the suspension with height.

When the bentonite was mixed with an acid or neutral solution (made with either tap or demineralized water), the pH of the solution rose to 9-10. This can be linked with the high CEC of the clay mineral itself. The EC of the suspensions was either 1.2 mS/cm or 2.5 mS/cm, corresponding to an ionic strength of approximately 0.01M or 0.02M NaCl.

Settling column tests

Two important remarks regarding the bentonite settling column tests can be made: During the preliminary test mixing was done by manually inverting the columns. The samples were mixed, but not at a controlled rate. Next to that, the mud sample only resided in the columns shortly. These two factors give rise to question the validity of the results from the preliminary experiments.

In experiment BN-1, jar mixing was applied and the ionic strength was 0.02M. A summary of the experimental settings is given in Table 4.3.

The measured effective settling velocities differ by an order of magnitude for the two experiments, indicating that the experimental procedure has a large influence on the experimental results. Because the validity of the results from the preliminary tests is questionable, only the results from the BN-1 experiment are discussed.

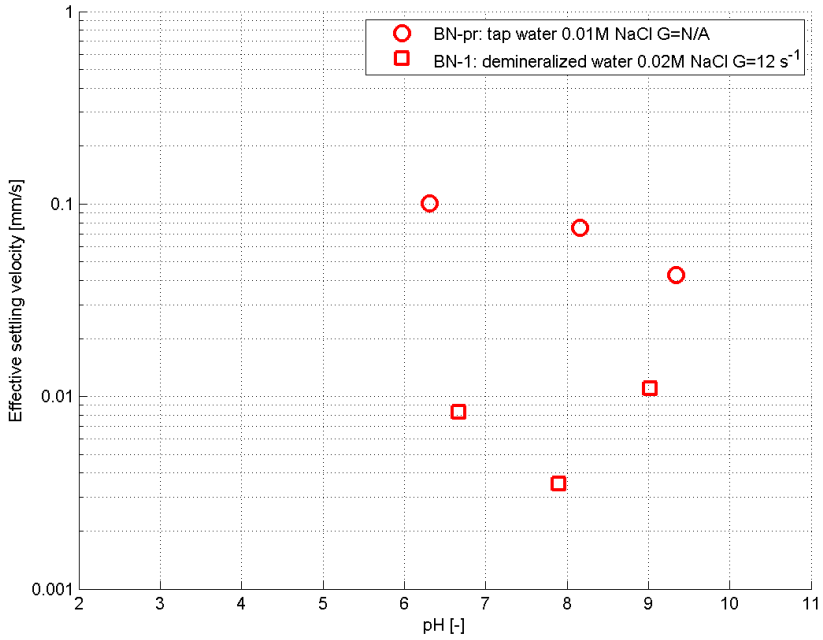

Figure 4.7: Effective settling velocity of bentonite as a function of suspension pH

The concept of effective settling velocity can be questioned for settling velocities which are as low as 0.01 mm/s. With that noted, large differences in the measured effective settling velocities do exist, but there is no general trend related to the suspension pH. It cannot directly be related to flocculation theory, which states that flocs become more porous. If more porous flocs were formed, the effective settling velocity would have shown a decrease with decreasing pH, because the gelling concentration is already low, and in that case it would have decreased further.

Table 4.3: Experimental settings for bentonite

Experiment code	c_0 [g/l]	ionic strength [M]	water used [-]	stirring method
BN-pr	40	0.01 - NaCl	tap water	hand inversion
BN-1	40	0.02 – NaCl	demineralized	Jar mixing G=12 s^{-1}

Gelling concentration

The initial concentration as it was applied in the experiments appears to be close to the gelling concentration of bentonite, or even above the gelling concentration. To verify this qualitative finding, a separate experiment was set up to obtain a proper estimate for the gelling concentration for the Bentonite. In this separate experiment lower initial concentrations (c_0 = 5 and 10 g/l) were used. During this experiment, the suspension had an ionic strength of 0.02M. The estimate for the gelling concentration obtained from this experiment is c_{gel}= 55 g/l. The obtained fit with measured data is shown in Appendix C.3.1(Figure C.12).

This finding confirms the qualitative finding posed earlier: the initial concentration, compared to the gelling concentration, is too high to study the settling behaviour of bentonite.

4.2.3 Markermeer clay

Qualitative findings

For the Markermeer clay, the qualitative findings are described in more detail than was done for the kaolinite and bentonite. Changing the pH of the solution influenced several of the constituents present in the clay and initiated several geochemical processes. The effect of mixing the Markermeer clay with either acid or alkaline water is discussed first.

When the Markermeer clay was mixed with the acid solution (pH=3), buffering occurred, i.e. the pH of the solution rose to 6-7 in several hours. The solution pH is restored to a neutral solution. If the sediment was stirred, i.e. using a mixing jar, this rise in pH occurred even faster. Apparently, a process takes place which 'consumes' the available H^+ ions and that this process also depends on mixing.

A comparable, but much slower process was observed when mixing the Markermeer clay with the alkaline solution (pH=10). The pH was restored to neutral values, pH≈7, but this happened in the order of days. Again, stirring the sediment sped up the process. The buffering of the acid and base, and the processes involved are discussed in more detail in Sections 5.1.2 and 5.2.2.

Regardless of the buffering that took place, the turbidity of the supernatant increased with increasing pH, in a similar fashion as the kaolinite. For all the acid suspensions, a clear water-suspension interface developed after several minutes of the settling column experiment. The supernatant liquid remained turbid throughout the experiment, for several of the alkaline suspensions.

After the clay had been in the columns for several days, a grey layer started to form on the upper sediment layer. According to De Lucas Pardo (2014) this is the oxic layer that is developing on top of the anoxic settled bed. This grey layer was mainly visible for the neutral and alkaline beds, but was not present in the column with the acid pore water.

Apart from the above, two other observations are worth noting for the acid columns:

- Rust developed in several of the acid columns. Red colour, higher in the water column.
- Particulate matter rose to the surface in the acid column. Probably, this is organic matter that adhered to little gas bubbles.

Effective settling velocity

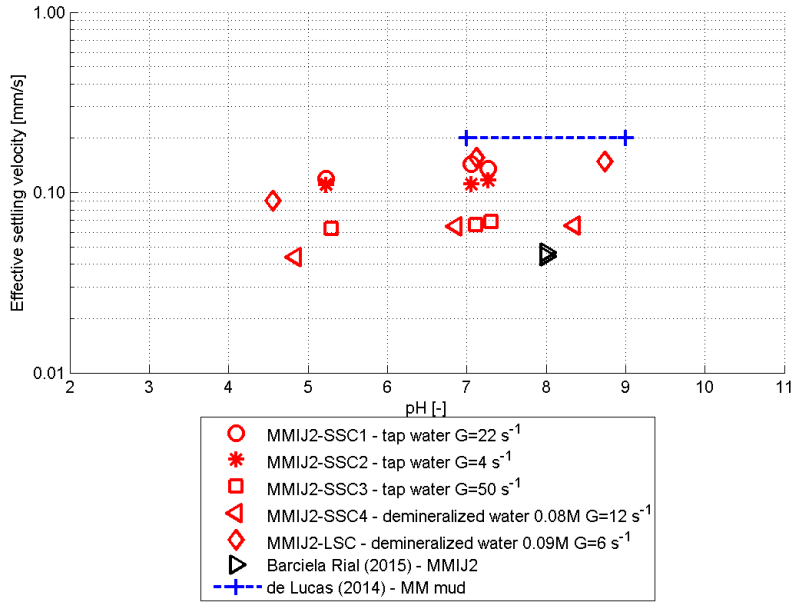

Figure 4.8: Effective settling velocity for Markermeer clay as a function of suspension pH

The measured effective settling velocities are plotted in Figure 4.8. This graph includes both the measured settling velocities of the small settling column experiments (Experiment I), denoted with the '1-4 SSC' suffixes, and the large settling column experiment, denoted with the 'LSC' suffix. The measured settling velocities range from 0.05 mm/s to 0.15 mm/s. Generally speaking, the effective settling velocity for the acid suspensions is smaller than the effective settling velocity for the neutral and alkaline suspensions. The latter two are similar for most experiments.

Because of the buffering of both the acid and base, additional chloric acid and sodium hydroxide were added, thereby increasing the ionic strength of the solution. As reported in Table 4.4, the ionic strength was not kept constant for the first three small settling column experiments. During the fourth small settling column experiment and the large settling column experiment, the ionic strength was kept constant for all columns.

Table 4.4: Experimental settings for Markermeer clay

Experiment code	c_0 [g/l]	ionic strength [M]	water used [-]	stirring method
MMIJ2-SSC1	40	not controlled	tap water	Jar mixing G=22 s^{-1}
MMIJ2-SSC2	40	not controlled	tap water	Rod mixing G=4 s^{-1}
MMIJ2-SSC3	40	not controlled	tap water	Jar mixing G=50 s^{-1}
MMIJ2-SSC4	40	≈0.08 - NaCl	demineralized	Jar mixing G=12 s^{-1}
MMIJ2-LSC	40	≈0.09 - NaCl	demineralized	Rod mixing G=6 s^{-1}

The measured EC's during the MMIJ2-4 experiment were 7.5 ± 0.4 $*10^3$ µS/cm, and during the MMIJ2-LSC experiment these were 9.0 ± 0.1 $*10^3$ µS/cm. From these values, ionic strengths were calculated in terms of sodium chloride molarity.

Gelling concentration

Gelling concentrations for Markermeer clay were determined for both Experiment I and II. For Experiment I, the gelling concentration was calculated from the interface height for which the deflection in the settling curve is observed (see Figure 4.4). For the 2L settling column experiments it was determined by setting up nine columns for which the ionic strength was constant, but pH and initial concentration were varied (see Table 3.14 for further details). This resulted in the following estimates:

Table 4.5: Gelling concentrations found for Markermeer clay

	acidic [g/l]	neutral [g/l]	alkaline [g/l]
MMIJ2-1	109	136	124
MMIJ2-2	109	113	118
MMIJ2-3	97	97	97
MMIJ2-4	109	118	109
MMIJ2-LSC	80	85	88
MMIJ2 - Barciela Rial (2015)	-	82	-

The values found correspond with the hypothesis posed in Section 2.4.2. With decreasing pH, the gelling concentration decreased, leading to an increase in volume of the bed at the start of self-weight consolidation. Barciela Rial (2015) also calculated the gelling concentration for MM-IJ2 clay from settling column experiments and found c_{gel}=82 g/l, using tap water without the addition of additional salts. This shows that the results found for the gelling concentration are reproducible yielding an estimate of the same order of magnitude.

4.3 Consolidation

After the settling phase, the consolidation phase commences. Consolidation of settled muddy beds consists of two phases, the permeability phase (C-I) and the effective stress phase (C-II), as displayed in Figure 4.9. Utilizing fractal theory, these phases can be characterized by the fractal dimension n_f (both Phase I and II) the permeability parameter K_k (Phase I) and the effective stress parameter K_p (Phase II).

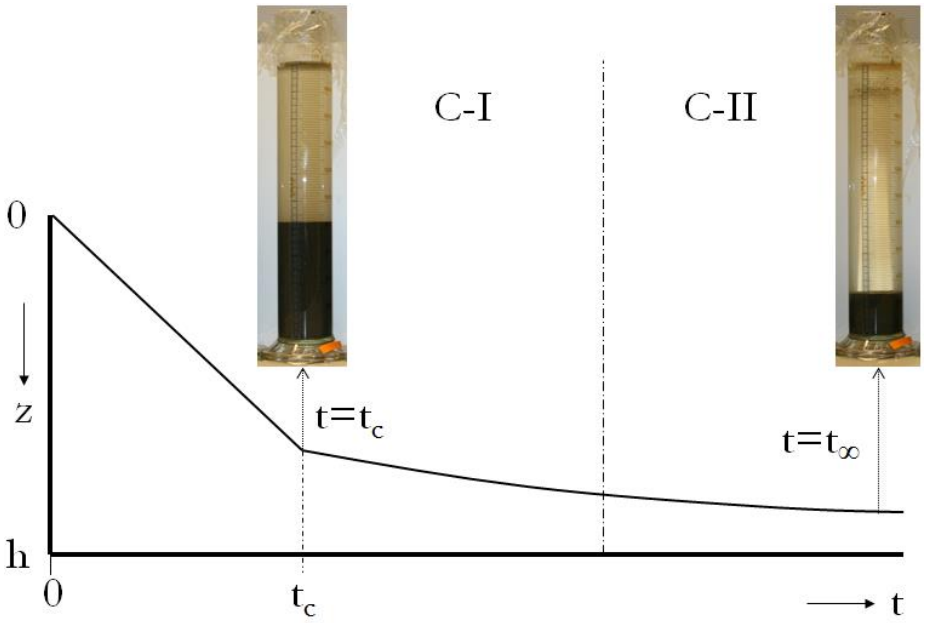

Figure 4.9: Schematized settling curve with indication of start and end of consolidation phases. The inserted photos correspond with the start of the consolidation phase, the point of contraction at t=t_c and the end of the consolidation phase at t=t_∞. The consolidation phase itself is divided into two phases, C-I and C-II. The x-axis is not to scale.

4.3.1 Consolidation phase I

First, the obtained parameters for consolidation phase I are presented. The determined parameters for consolidation phase II are presented in Section 4.3.2.

Curve fitting

The fractal dimension n_f and permeability parameters K_k are determined by fitting Equation (2.14) to the interface measurements. Ideally, this curve is fitted to all interface measurements between the time of contraction (t_c) and the end of the consolidation phase C-I. However, the transitions between the HS, C-I and C-II phases are not so clear.

To determine the starting and ending point of consolidation phase I, the settling curve is plotted on a double logarithmic scale, with Figure 4.10 showing such a curve. A deflection in the settling curve marks the transition from the hindered settling phase to consolidation phase I. A power law relation, i.e. a straight line on a double logarithmic scale, describes the first phase of consolidation after a bed has been formed. Once the interface measurements start to deviate from this power law fit, the permeability phase ends and phase II consolidation commences.

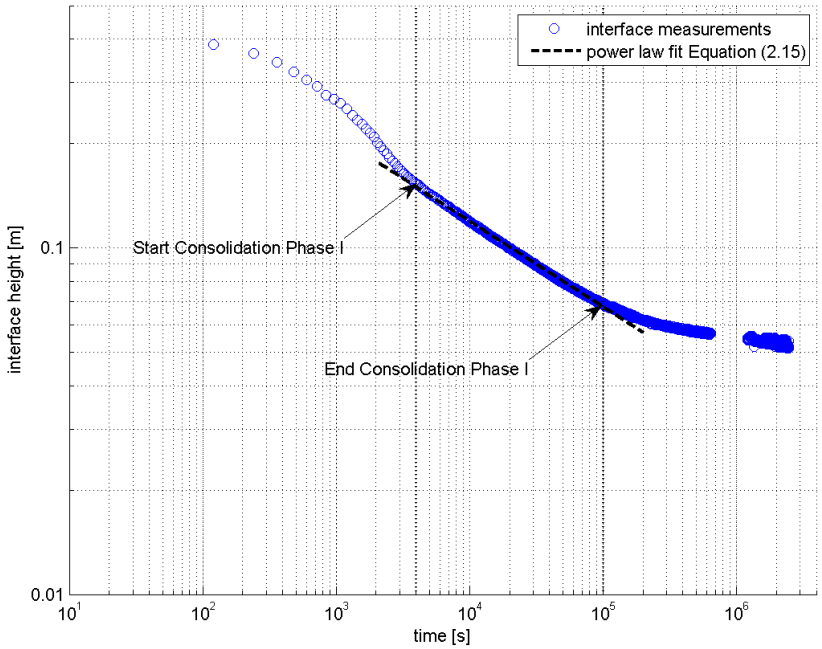

Figure 4.10: Typical result for power law fit on interface measurements for phase C-I

Small settling columns

For the small settling column experiments, the parameters for consolidation phase I are listed in Table 4.6. The parameters obtained for the bentonite and kaolinite clays show a similar pattern. With decreasing pH (hence, increasing acidity), the fractal dimension decreases and the permeability increases. These parameters indicate that with increasing acidity, the formed beds are more porous.

The determined permeability of the bentonite beds is 3 to 4 orders of magnitude smaller than their equivalent kaolinite beds. However, the concentration of the bentonite suspension was already close to (or maybe even above) the gelling concentration at the start of the experiment. Hence, the transition between hindered settling and consolidation phase I cannot be identified clearly. Fitting the power law relation on the interface measurements will probably not encompass the entire C-I phase, simply because the full C-I phase was not present in the dataset. Therefore, the obtained fractal dimension and permeability parameter K_k are lower and higher, respectively.

Table 4.6: Consolidation parameters for large settling columns – kaolinite, bentonite and Markermeer clay

Column code	c_0 [g/l]	pH [-]		K_k [m/s]	n_f [-]
		start	end		
K-1	40	2.83	2.78	2.46E-10	2.59
K-2	40	6.62	6.03	2.68E-11	2.64
K-3	40	9.50	8.35	9.89E-13	2.71
BN-1	40	4.78	6.67	7.60E-14	2.64
BN-2	40	7.46	7.90	2.27E-15	2.66
BN-3	40	9.90	9.02	1.57E-18	2.75
MMIJ2-1	40	4.24	4.84	1.26E-13	2.65
MMIJ2-2	40	7.99	6.86	1.65E-13	2.66
MMIJ2-3	40	10.16	8.35	1.26E-13	2.65

The determined parameters for the natural clay do not show a clear trend, as the K_k is in the order of $1*10^{-13}$ m/s for all three samples, and the fractal dimensions are 2.65 or 2.66. This is remarkable, as the settling velocity of the mud in the acid suspension was much smaller than the settling velocity of the mud in the neutral and alkaline suspensions, respectively. The gelling concentration also decreased with decreasing pH, both hinting at the formation of more porous flocs.

Large settling columns

For the large settling column experiments, the parameters for consolidation phase I are shown in Table 4.7. The K_k values that were found for the columns with acid water were significantly larger than the K_k values found for the neutral and alkaline pore waters. The fractal dimension n_f found for the different settling columns shows a similar, albeit oppositely directed, trend: with decreasing pH the fractal dimension n_f also decreases.

Table 4.7: Consolidation parameters for large settling columns – Markermeer clay

Column code	c_0 [g/l]	pH [-]		K_k [m/s]	n_f [-]
		start	end		
MMIJ2-LSC1	30	4.80	5.06	2.48E-13	2.64
MMIJ2-LSC2	30	7.37	7.60	7.35E-14	2.67
MMIJ2-LSC3	30	9.30	7.98	1.95E-14	2.69
MMIJ2-LSC4	40	4.56	5.00	7.32E-13	2.63
MMIJ2-LSC5	40	7.12	7.62	1.28E-13	2.67
MMIJ2-LSC6	40	8.74	7.82	3.58E-14	2.69
MMIJ2-LSC7	50	4.63	5.02	2.98E-12	2.61
MMIJ2-LSC8	50	7.09	7.56	4.14E-14	2.69
MMIJ2-LSC9	50	8.40	7.84	1.34E-14	2.70

Whereas the results for the neutral and alkaline pore water showed only a small variability between the K_k found for the different initial concentrations, the K_k found for the acid pore water varied from $1.1*10^{-13}$ to $7.46*10^{-13}$, which means a fivefold increase. For the acid columns, the K_k also

appears to increase with increasing initial concentration. The neutral and alkaline suspensions show opposite behaviour, with the fractal dimension increasing and the K_k decreasing with increasing initial concentration.

A decrease in fractal dimension, and a related increase in permeability, was expected based on the theory that flocs form faster and are more porous under acidic conditions. However, the dissolution of calcium carbonate, because of addition of hydrochloric acid, deserves further investigation. This will be discussed in Section 5.2.2.

4.3.2 Consolidation phase II

Curve fitting

With the obtained fractal dimension, the only measured value needed to obtain the effective stress parameter K_p is the final bed height (Merckelbach and Kranenburg (2004), De Lucas Pardo (2014)). This parameter is calculated using Equation (2.15). The final bed height was measured for all columns prior to undrained shear strength testing.

Small settling columns

Measurement of final bed height occurred after t=42 days, for the Kaolinite, or t=34 days for the Bentonite and Markermeer clay. The measured bed heights and determined parameters are listed in Table 4.8:

Table 4.8: Effective stress parameter for consolidated kaolinite, bentonite and Markermeer clay samples - small settling column experiment

Column code	h_∞ [m]	n_f [-]	K_p [Pa]
K-1	0.026	2.59	7.51E+04
K-2	0.023	2.64	1.05E+05
K-3	0.028	2.71	2.65E+06
BN-1	0.090	2.64	2.06E+08
BN-2	0.137	2.66	6.92E+09
BN-3	0.157	2.75	1.66E+13
MMIJ2-1	0.054	2.65	3.14E+07
MMIJ2-2	0.045	2.66	1.21E+07
MMIJ2-3	0.053	2.65	2.70E+07

Large settling columns

Measurement of final bed height occurred after t=42 days (7/10 till 18/11). The measured bed heights and determined parameters are listed in Table 4.9.

Table 4.9: Effective stress parameter for consolidated Markermeer clay samples - large settling column experiment

Column code	h_∞ [m]	n_f [-]	K_p [Pa]
MMIJ2-LSC1	0.051	2.64	2.40E+07
MMIJ2-LSC2	0.043	2.69	2.51E+07
MMIJ2-LSC3	0.046	2.71	9.94E+07
MMIJ2-LSC4	0.060	2.63	1.10E+07
MMIJ2-LSC5	0.053	2.68	2.13E+07
MMIJ2-LSC6	0.056	2.70	6.35E+07
MMIJ2-LSC7	0.08	2.61	7.84E+06
MMIJ2-LSC8	0.064	2.70	6.46E+07
MMIJ2-LSC9	0.069	2.71	1.67E+08

The effective stress parameter K_p tells us something about the ability of the bed to consolidate. Assessing the found results, this implies that the settled beds in the acid environment consolidate less and will develop less strength than the beds settling in the neutral solution. The settled bed that developed in the alkaline environment would, according to this rationale, develop the largest strength. However, comparing these findings with shear vane testing should confirm these found values.

4.3.3 Consolidation coefficient calculated from fractal approach

The coefficient of consolidation c_v is calculated according to formula (2.16). This results in the following values for both the small and large settling column experiments:

Table 4.10: Coefficient of consolidation c_v for both the SSC and LSC experiments

Column code	c_v [m²/s]	Column code	c_v [m²/s]
K-1	9.25E-09	MMIJ2-LSC1	3.39E-09
K-2	1.58E-09	MMIJ2-LSC2	1.14E-09
K-3	1.81E-09	MMIJ2-LSC3	1.28E-09
BN-1	8.74E-09	MMIJ2-LSC4	4.42E-09
BN-2	9.34E-09	MMIJ2-LSC5	1.68E-09
BN-3	2.08E-08	MMIJ2-LSC6	1.48E-09
MMIJ2-1	2.32E-09	MMIJ2-LSC7	1.21E-08
MMIJ2-2	1.19E-09	MMIJ2-LSC8	1.77E-09
MMIJ2-3	1.99E-09	MMIJ2-LSC9	1.54E-09

The three clay types are discussed separately.

Kaolinite

Because the consolidation process takes a rather short time for the kaolinite, the coefficient of consolidation is expected to be the largest of all clay types. However, this conclusion cannot be drawn based on the obtained data. The large differences in consolidation coefficient for the different pH values also suggest large differences in consolidation behaviour. These changes simply do not exist. The accuracy of the data collection could be an issue in determining the parameters of the fractal approach. The gelling concentration exceeded 200 g/l, and thus the volume is already small at the start of self-weight consolidation. Because of this, the interface readings with an accuracy of 1mm may have led to a flawed estimate of the first-phase consolidation parameters. Because these parameters are used in the calculation of the consolidation coefficient, possible errors may have also affected the calculated coefficients.

Bentonite

For the bentonite, the calculated coefficient of consolidation suggests the bed formed under alkaline consolidates fastest, i.e. a factor 2 faster than the beds formed under acidic and neutral conditions. Qualitatively interpreting the settling curves leads to a different conclusion. The settling curves show that the bed formed under alkaline consolidated slowest.

For the bentonite, the calculated fractal dimensions (calculated from Phase I consolidation) contradict with qualitative findings. This can also be seen in Table 4.8: the calculated fractal dimensions decrease with decreasing pH, but the corresponding final volumes also decrease with pH. This is contradictory because a smaller fractal dimension suggests more porous flocs and thus larger final volumes. These (large) changes in determined fractal dimension also affect the calculated coefficient of consolidation, leading to estimates for c_v that do not agree with qualitative findings.

Markermeer clay

The coefficients of consolidation calculated for the Markermeer clay agree with qualitative findings. It is remarkable that the fractal approach works best for the natural clay, because the natural clay contains not only clay but also sand, non-silicates and organic matter. However, the constitutive equations for the fractal approach derived by Merckelbach (2000) were actually derived for natural mud samples. In that respect, it makes sense they perform best for natural clay and mud samples.

The more porous beds formed under acidic conditions consolidate at a faster rate, which makes sense as these are the most porous, contain the largest flocs and thus the largest pores between the flocs. Even though they consolidate faster, they still have the largest final volume. The large spread

in calculated c_v for the 50 g/l initial concentrations also seems to be reflected by the settling curves, shown in Figure C.11.

The coefficient of consolidation also increased with increasing initial concentration for the acidic conditions, whereas it did not increase substantially for the neutral and alkaline conditions. A possible explanation, i.e. the dissolution of the calcium carbonate, is discussed in Section 5.1.2.

Taking into account these several aspects, also taking into account the parameters derived for the first and second phase of self-weight consolidation, it is concluded that the fractal approach can be utilized successfully to describe the self-weight consolidation of the Markermeer clay for the different initial concentrations and pH values.

4.4 Undrained shear strength

After consolidation, the undrained shear strength of the samples was determined using a shear vane test. A slightly different approach is followed than was done in the previous paragraphs, because the tested samples are discussed per experiment instead of per clay type.

4.4.1 Small settling column samples

After the last small settling column experiment, the settled beds were tested for undrained shear strength, as described in Section 3.7. Each sample was tested once, so three measurements were obtained for each clay type, each corresponding to either acid, neutral or alkaline conditions. The period the sediment had settled was either 42 days (Kaolinite) or 34 days (Bentonite and Markermeer clay). The difference in days was caused by the fact that the kaolinite settling test started earlier, but the settled beds were tested on the same date. This was done because of the limited availability of the used equipment.

Table 4.11: Settings for shear vane testing at BKD laboratory

Experimental variable	Setting
Rotation rate	0.1 rpm
Experiment duration	20 minutes
Total number of rotations	2

Before the tests commenced, the height of the settled bed was measured. These are listed in Table 4.12. It is noted that all three Kaolinite samples and the MM-2 sample did not meet the sample height requirement, which is $3*h_{vane}$. This may have influenced the results, but it was not possible to switch to a smaller vane because of the low undrained shear strength of the settled bed. The sample height of the three kaolinite samples ranged between 23-28 mm, which meant that the vane could be inserted into the bed completely, but that the sample height was only 1.4 to 1.7 times the vane height, which is 16 mm high. On the other hand, the requirement for sample width is satisfied because the sample diameter is $2.3*D_{vane}$, whereas $1.5\text{-}2.0*D_{vane}$ is required.

Table 4.12: Settled bed heights of SSC experiment

column code	h_{sample} [mm]	column code	h_{sample} [mm]	column code	h_{sample} [mm]
K-1	26	BN-1	90	MM-1	54
K-2	23	BN-2	137	MM-2	45
K-3	28	BN-3	157	MM-3	53

The settings listed in Table 4.11 were used in combination with the equipment specified in Table 3.16. Hereby, the peak strength τ_p and the undrained shear strength c_u were obtained, as shown in Table 4.13:

Table 4.13: Obtained peak and remoulded shear strengths for settled beds of SSC experiment

	τ_p [Pa]	c_u [Pa]		τ_p [Pa]	c_u [Pa]		τ_p [Pa]	c_u [Pa]
K-1	6.8	5.3	BN-1	27.1	7.0	MM-1	24.8	4.8
K-2	11.3	2.6	BN-2	28.8	8.5	MM-2	59.8	11.0
K-3	8.5	3.9	BN-3	26.0	5.2	MM-3	32.7	6.3

All measured undrained shear strengths are in the order of 1-10 Pascals, which is extremely low. In spite of having the lowest settled bed height (see Table 4.12), and hence the highest density, the average peak and undrained shear strengths are lowest for the Kaolinite.

4.4.2 Large settling column samples

After the large settling column experiment had ended, the samples were tested according to the procedure described in Section 3.7. As can be seen from Table 4.14, the rotational speed was set to a higher value than for the SSC experiments. This was caused by the used rheometer, for which the rotational rate could not be set lower than 0.5 rpm. The period the sediment had settled was 42 days (all samples).

Table 4.14: Settings for shear vane testing at Deltares FCL laboratory

Experimental variable	Setting
Rotation rate	0.5 rpm
Experiment duration	6 minutes
Total number of rotations	3

The obtained peak strength τ_p and the undrained shear strength c_u are presented in Table 4.15, together with the height of the settled bed. The undrained shear strength of the settled beds ranked in the same order as the height of the bed, when grouped according to initial concentration. Columns MMIJ2-LSC1 to LSC3 had an initial concentration c_0 of 30 g/l, MMIJ2-LSC4 to LSC6 had an initial concentration of 40 g/l and MMIJ2-LSC7 to LSC9 had an initial concentration of 50 g/l.

The sediment that settled in the acid water led to the highest settled volumes, and correspondingly to the lowest undrained shear strength. The sediment settling in the neutral water led to the smallest settled volumes, thus having the largest shear strength (except for columns MMIJ2-LSC8 and MMIJ2-LSC9).

Table 4.15: Settled bed heights, peak and remoulded shear strengths of settled beds for LSC experiments

column code	c_0 [gr]	chemical environment	τ_p [Pa]	c_u [Pa]	h_{sample} [mm]
MMIJ2-LSC1	30	acid	41.8	17.1	51
MMIJ2-LSC2	30	neutral	95.5	36.9	43
MMIJ2-LSC3	30	alkaline	52.8	17.5	46
MMIJ2-LSC4	40	acid	46.6	15.1	60
MMIJ2-LSC5	40	neutral	89.0	29.4	53
MMIJ2-LSC6	40	alkaline	76.6	17.9	56
MMIJ2-LSC7	50	acid	55.0	15.3	80
MMIJ2-LSC8	50	neutral	89.8	25.4	64
MMIJ2-LSC9	50	alkaline	88.6	26.0	69

4.4.3 Undrained shear strength versus consolidated volume

Figure 4.11, Figure 4.12 and Figure 4.13 show pictures of the settling columns at the BKD laboratory, prior to the shear vane testing. The consolidated volumes vary largely for the the different clay minerals. However, this is not reflected by the corresponding undrained shear strengths (Table 4.13). The absolute water content (cf. the bed density) is not the only factor determining undrained shear strength. This will be discussed in more detail in Section 5.3.

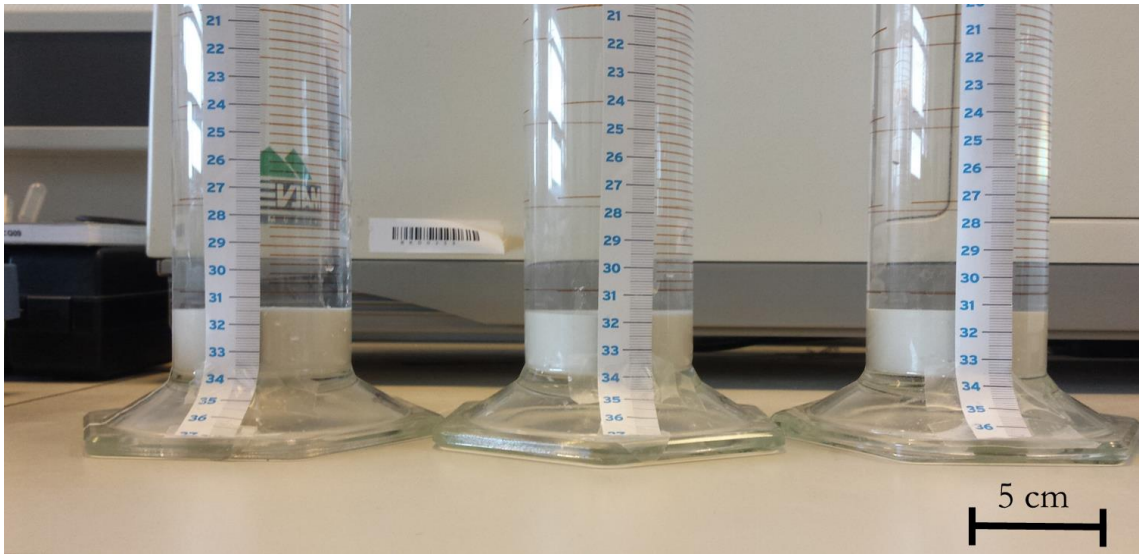

Figure 4.11: The consolidated volumes of the kaolinite, 42 days after starting the settling column test. The initial pH of the water increases from left to right for the three columns. The left column is acid, the middle column neutral and the right column is alkaline.

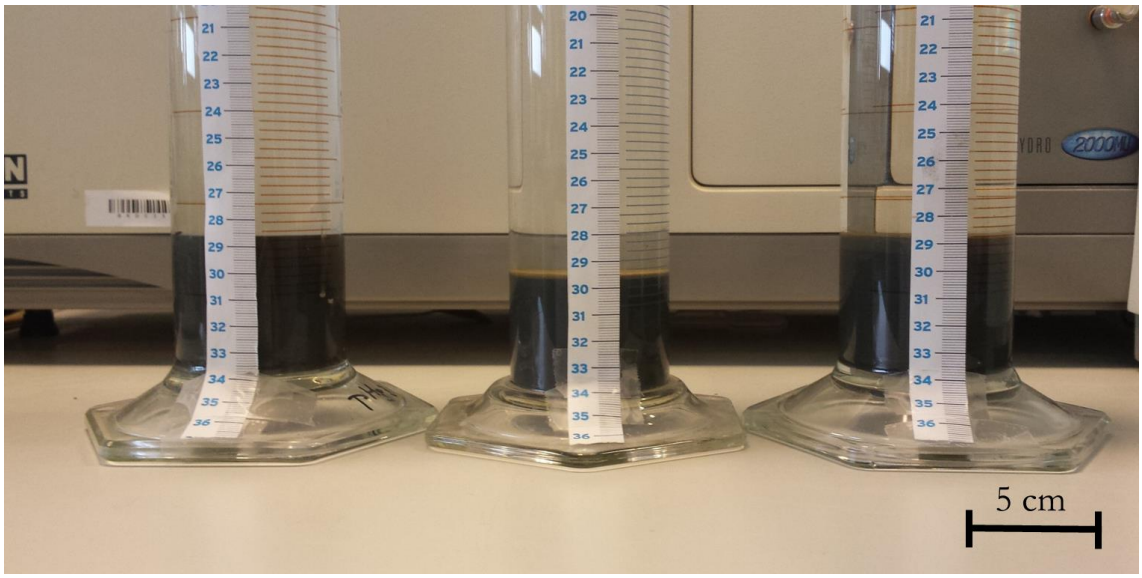

Figure 4.12: The consolidated volumes of the Markermeer clay, 35 days after starting the settling column test. The initial pH of the water increases from left to right for the three columns. The left column is acid, the middle column neutral and the right column is alkaline.

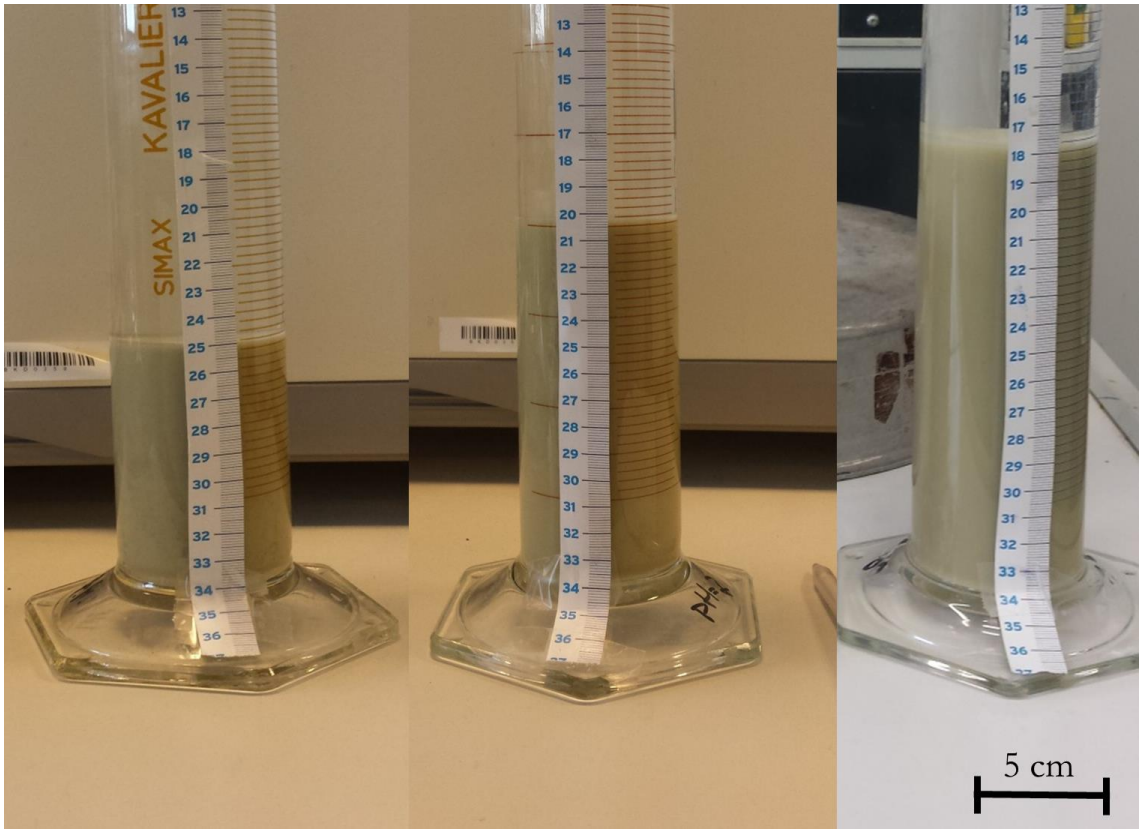

Figure 4.13: The consolidated volumes of the Bentonite, 35 days after starting the settling column test. The initial pH of the water increases from left to right for the three columns. The left column is acid, the middle column neutral and the right column is alkaline

5. Discussion

The experimental results are discussed in this chapter. The results are interpreted and related to existing literature. Next to that, the generated data are used for additional analyses.

5.1 The effect of varying acidity on the settling behaviour of mud

This section discusses the results of the settling column experiments and how these vary for different pore water chemistries. The three mud samples, of which two are artificial samples, showed large differences in settling behaviour among them. This resulted in large differences in the effective settling velocity and gelling concentrations.

Because there was no distinct settling phase for the bentonite mud (see Section 4.2.2), this will not be discussed separately.

5.1.1 Settling of kaolinite

The settling behaviour of the kaolinite mud sample, which has a low plasticity and is classified as a silty material (see Figure 4.1), shows a small dependency on suspension pH. The turbidity of the supernatant increased with increasing pH, but the effective settling velocity did not significant differ. This is in spite of the large range over which the pH was varied. The computed gelling concentrations were also not significantly affected by the changes in pH.

This finding is remarkable, because literature (i.e. Kaya et al. (2006), Palomino and Santamarina (2005)) suggests that variations in the suspension pH lead to changes in the flocculation behaviour of kaolinite. Under acidic conditions, larger flocs are formed which are also more porous than flocs formed under either neutral or alkaline conditions, with floc size decreasing with increasing pH (Mietta et al., 2009). The formation of more porous flocs should lead to a decrease in gelling concentration and thus, should also affect the effective settling velocity.

There are two possible reasons why the kaolinite used in this study did not show a significant pH-dependency. First, the flocculation of kaolinite only depends on the pH for low ionic strengths. Palomino and Santamarina (2005) mention a ionic strength threshold of $2*10^{-2}$ to $1*10^{-1}$ M NaCl. Below this threshold, a significant pH dependency is noted, while above the threshold, effective settling velocities show no clear pH dependency. The ionic strength applied in the current experiments was $1*10^{-2}$ M NaCl, which is slightly below the mentioned ionic strength threshold, but in the same order of magnitude.

Second, the kaolinite had a rather low plasticity. Other researchers used kaolinite clays which have a significantly larger clay-sized fraction. For instance, Kaya et al. (2006) used a kaolinite with a <2 μm fraction of 80% and Palomino and Santamarina (2005) used a kaolinite sample with a median diameter of 0.36 μm. According to Equation (2.18), the plasticity of those samples is probably much higher than that of the current kaolinite, thereby being more susceptible to changes in pH.

The threshold for which the flocculation process becomes pH-dependent, can be directly related to the thickness of the double diffuse layer (DDL) surrounding the clay particles. At a low ionic strength the DDL is thick but when the edges become positive because of the H^+, the clay particles do flocculate. With increasing ionic strength, the DDL becomes thinner and flocculation will readily occur (because of the van der Waals forces), regardless of the solution pH.

Whereas ionic concentrations of $1*10^{-2}$ M are regarded as high in laboratory environments, in surface waters such an ionic strength is quite common. For instance, tap water already has an electrical conductivity of approximately 500 μS/cm, which translates to an ionic strength of $5*10^{-3}$ M. Surface waters already encounter larger ionic concentrations, even more so for estuarine and coastal waters, because these waters are either brackish or saline. Hence, the pH-dependent effect on the flocculation of kaolinite will certainly not be relevant for saline water and may very well not be relevant for fresh water as well.

Dissolution of Kaolinite

Several researchers have shown that at low pH environments, aluminium dissociates preferentially from the kaolinite particles (i.e. Wieland and Stumm (1992)). As a result, Al^{3+} ions go into suspension. The influence of ion valence on flocculation scales with the power 6 (i.e. Sposito (1989)), hence aluminium ions have an enormous influence on flocculation. If aluminium dissolution is not accounted for, a too large pH-dependency may be attributed to the surface charge of kaolinite (Bolland, 1980). This is a possible explanation for the changes in floc size found by Mietta et al. (2009), because they changed the pH to more extreme values (pH 1.8 as the most extreme value) than was done in the current research. However, aluminium dissolution was not accounted for, which could have led to a large pH-dependency being observed, whereas the effect should be regarded as more indirect.

5.1.2 Settling of the Markermeer clay

The Markermeer clay sample, with a high plasticity, showed a pH dependency on the settling behaviour, with the effective settling velocity decreasing under acidic conditions. The gelling concentration also decreased for the acidic conditions, from which it can be concluded that more porous flocs were formed. The increase in porosity of the flocs leads to additional hindering of the flocs in suspension, thereby causing a decrease in the effective settling velocity.

Approximately 10% of the mass of this clay consists calcium carbonate ($CaCO_3$), as shown in Table 3.7. Upon addition of hydrochloric acid, the calcium carbonate dissolves according to the following reaction:

$$CaCO_3 + 2HCl \rightarrow Ca^{2+} + CO_2 + H_2O + 2Cl^- \tag{5.1}$$

Due to the dissolution of the present calcium carbonate in the natural clay, large amounts of hydrochloric acid needed to be added to arrive at stable low pH values. After enough hydrochloric acid was added to dissolve the calcium carbonate, the pH remained relatively stable. This is a strong indication that the observed buffering was actually caused by the present calcium carbonate.

The dissolution of calcium carbonate, and the subsequent release of calcium ions (Ca^{2+}) also influences the flocculation behaviour of clay. According to colloid chemistry theory ions with a valence of 2 have a 2^6= 64 times as large effect on the flocculation of pure clay particles when compared to valence 1 ions(Sposito, 1989). Hence, the influence of ion valence on flocculation is highly non-linear. This large effect of ion valence is shown by numerous authors, for instance by Ibanez et al. (2014). This is also confirmed for the Markermeer clay through zeta potential measurements, see Appendix C.1.3. This implies that the flocs formed under acidic conditions are not only influenced by the pH but also by the dissolution of the calcium carbonate. Of course, this is the case for this particular clay, but its validity for other clay and mud samples is not guaranteed.

5.1.3 Natural processes causing changes in pH

The Markermeer clay has a multitude of constituents, as shown in Table 3.7. The non-silicates in the clay, among which calcium carbonate, also interact in several geochemical processes. One of the non-silicates is pyrite, which makes up 0.6 % of the Markermeer clay. When pyrite comes in contact with oxygen, it oxidizes, thereby forming sulphuric acid. This was mentioned in Section 2.7.2, whilst the process of pyrite oxidation is discussed in greater detail in Appendix A.4. When significant amounts of pyrite are present, oxidation of the pyrite may lead to a decrease in soil pH.

Because the Markermeer lake bed also contains pyrite, it is calculated if the oxidation of pyrite could lead to acidification of the Markermeer clay. To conclude whether acidification is expected for the Markermeer, two values are calculated, both expressed in moles:

- The amount of H^+ that can be formed upon oxidation of all the pyrite present in the Markermeer clay
- The neutralizing capacity of the calcium carbonate present in the Markermeer clay

Considering a sample of 100 grams of Markermeer clay, the amount of pyrite and calcium carbonate are as follows (Table 5.1):

Table 5.1: Amounts of pyrite and calcium carbonate in the Markermeer clay

Constituent	Amount [gr]	molar mass [gr/mol]	Amount [moles]
Pyrite (FeS_2)	0.6	120	0.005
Calcium carbonate ($CaCO_3$)	9.1	100	0.091

If all the available pyrite oxidizes according to Equation A.2 (See Appendix A), 0.02 moles of H^+ are formed. For every mole of $CaCO_3$, 2 moles of H^+ can be neutralized, thereby leading to a neutralizing capacity of 0.182 moles. Hence, the neutralizing capacity of the present calcium carbonate in the Markermeer is a factor 9 larger than the possible release of H^+, and no significant decrease in pH is expected in the Markermeer mud because of the possible oxidation of pyrite. This confirms findings by Saaltink et al. (2016). Apart from the neutralizing capacity of calcium carbonate, clay minerals and the fresh water also have a neutralizing capacity, thereby leading to an even greater total neutralizing capacity.

5.1.4 Comparing the effect of pH and mineralogy

Apart from the solution pH, other factors influence the settling behaviour of the mud samples as well. For instance, the mineralogy of the solid clay particles is found to largely influence settling behaviour. Although initial concentrations were kept constant at c_0=40 g/l, large differences in settling behaviour existed for the small settling column experiments.

The effects of mineralogy and pH on the settling behaviour of the three mud samples are deduced from Figure 5.1. In this figure, the height of the mud-water interface is plotted as a function of time for the first three hours of the final small settling column experiment. This particular experiment involved all three mud samples, for which the initial ionic strength was kept constant. The measured interface heights for the mud samples are grouped per mud type, thereby enabling to distinguish the pH influence from the mineralogy influence on settling. The following conclusions can be drawn based on this data:

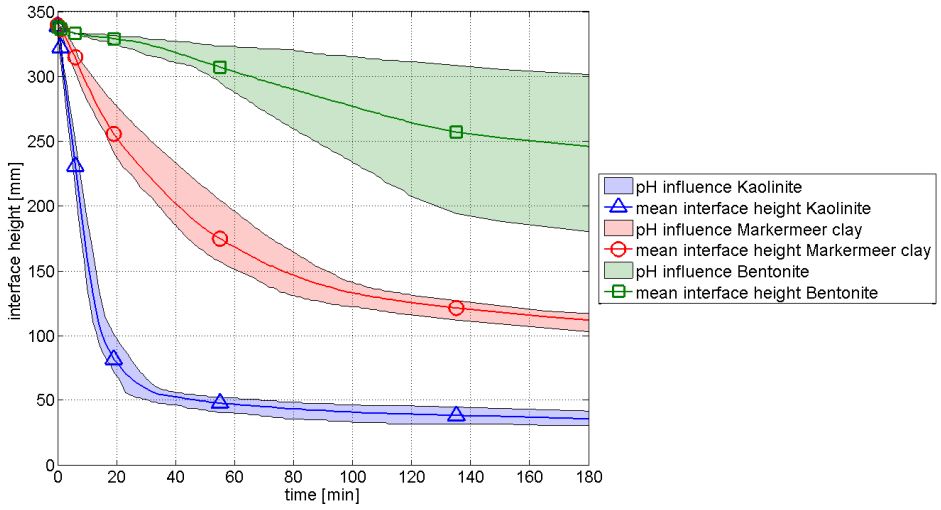

Figure 5.1: Measured interface heights for the three different mud samples, with the differences for pore water chemistry grouped in an envelope around the mean interface height. The time plotted spans from 0 to 180 minutes, thereby encompassing the settling phase, but also a part of self-weight consolidation phase I. The initial concentration c_0 is constant: c_0= 40 g/l.

- The influence of pH is largest for the extremely high plasticity clay. Strictly speaking, this is not an influence on the settling phase but on the first phase of consolidation. However, the settling curves differ significantly.
- The influence of the pH on the settling behaviour decreases with decreasing plasticity. For the Markermeer clay sample it is still noticeable, but for the Kaolinite the influence of pH is rather limited.
- The settling behaviour of the three mud samples is influenced to a much larger extent by clay mineralogy than by the suspension pH.

5.2 The effect of varying acidity on the consolidation behaviour of mud

Similar to the previous section, this section also discusses the results of the settling column experiments, but will now discuss the consolidation phase for the three different mud samples. For the Markermeer clay samples, this section will both discuss the results of the small (1L) and large (2L) settling column experiments. When reference is made to final volumes, this indicates the volumes after a certain period of self-weight consolidation.

5.2.1 Consolidation of kaolinite

The consolidation parameters for the kaolinite based on the curve fitting procedure, as they were presented in Section 4.3, predict large differences in consolidation behaviour. They are repeated in Table 5.2 for convenience:

Table 5.2: Consolidation parameters for the kaolinite mud samples

Mud sample	c_0 [g/l]	n_f [-]	K_k [m/s]	K_p [Pa]
Kaolinite - acidic	40	2.59	2.46E-10	7.51E+04
Kaolinite - neutral	40	2.64	2.68E-11	1.05E+05
Kaolinite - alkaline	40	2.71	9.89E-13	2.65E+06

Based on the permeability parameter K_k, that differs several orders of magnitude for different suspension acidity, and the changes in fractal dimension n_f, large differences in the consolidation behaviour would be expected. Large differences in the settling curves should reflect this. However, as Figure 5.2 shows, the settling curves do not show large differences at all for different pH. During the consolidation process the interface height lowered from 50-55 mm to approximately 30 mm, and the differences in consolidation behaviour between the three different samples are in the order of millimetres, which is a negligible difference compared to the large difference in acidity.

The final sample heights also indicated small differences in consolidated volumes. The large difference in effective stress parameter is probably an error that propagated from the fractal dimension n_f that was determined for the first phase of consolidation.

Conclusion: there are only small differences in consolidation behaviour, in spite of large variations in pH.

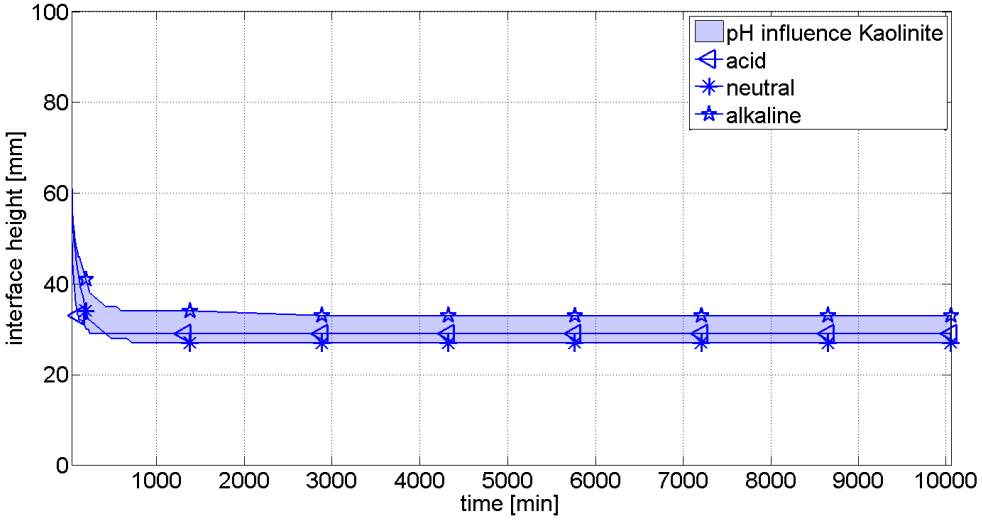

Figure 5.2: Settling curves for the kaolinite mud, displaying the first and second phase of self-weight consolidation. In spite of zooming in on the settling curve (the x-axis ranges from 0 to 100 mm only), differences in the settling curve are still small.

It is noted that the heights that were observed after one week, are not identical to the h_∞ height measured after 6 weeks (42 days). These heights rank differently, with the final volume in acidic conditions being largest, followed by the alkaline and neutral conditions.

5.2.2 Consolidation of Markermeer clay

The self-weight consolidation of the Markermeer clay will be discussed in two separate parts. First, the results for the small settling columns are discussed and secondly, the results for the large settling columns are discussed. In the latter, not only the pH but also the initial concentration was varied.

Small settling column results

The consolidation parameters for the Markermeer clay based on the curve fitting procedure, as they were presented in Section 4.3, predict a self-weight consolidation process that is largely the same for the three different pH values considered. The found parameters are repeated in Table 5.3 for convenience:

Table 5.3: Consolidation parameters for the Markermeer clay samples

Mud sample	c_0 [g/l]	n_f [-]	K_k [m/s]	K_p [Pa]
Markermeer clay - acidic	40	2.65	1.26E-13	3.14E+07
Markermeer clay - neutral	40	2.66	1.65E-13	1.21E+07
Markermeer clay - alkaline	40	2.65	1.26E-13	2.70E+07

If the settling curves are also studied for these consolidation phases (Figure 5.3), it appears that these curves are largely similar. The samples do consolidate to different heights, but this can also be attributed to the different concentrations (i.e. the changes in gelling concentration) for which the self-weight consolidation phases began.

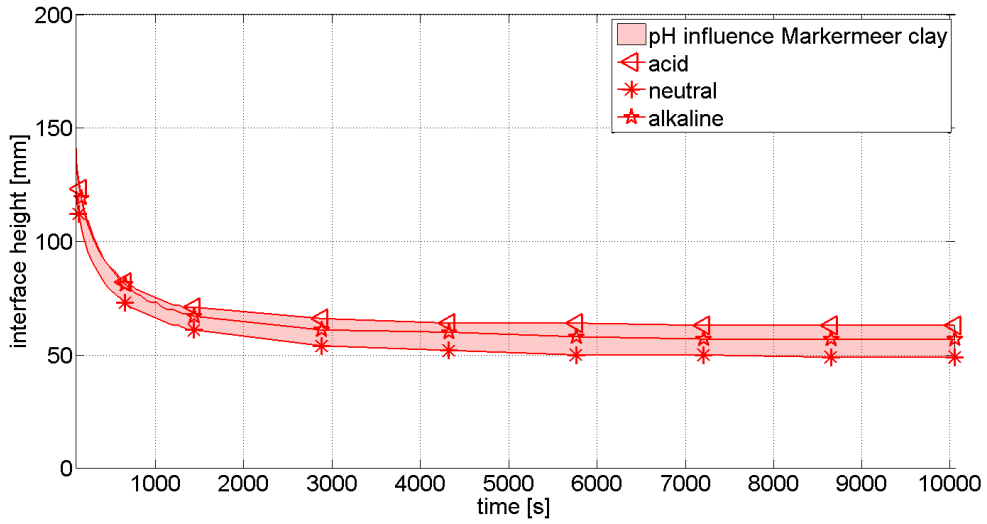

Figure 5.3: Settling curves for the Markermeer clay, displaying the first and second phase of self-weight consolidation.

Large settling columns

The large settling columns show a somewhat different behaviour compared to the small settling column results. Two trends for the fractal dimension and the permeability parameter, shown in Figure 5.4 as a function of both pH and initial concentration, are discussed:

1. The fractal dimension decreases with decreasing pH. For the mud that settled in the acidic water, this also led to the highest consolidated volume. For the neutral and alkaline conditions, the trend reversed: in spite of having a slightly larger fractal dimension, the beds for the alkaline conditions were more voluminous than those for the neutral conditions. Although changes in fractal dimension from 2.6 to 2.7 may seem small, these changes have a profound impact on consolidation. This is due to the highly nonlinear influence the fractal dimension has on the permeability and development of effective stresses.

2. The fractal dimension decreases, and the permeability parameter increases with increasing concentration for the acidic conditions. The trend for the neutral and alkaline conditions is different: the fractal dimension is largest for the highest initial concentration and thus the permeability parameter is lowest. These different trends can be understood by realizing that for the acidic suspensions to remain at a stable, low pH, all the calcium carbonate had to be dissolved.

Logically, larger initial concentrations lead to larger amounts of calcium carbonate that are dissolved before a steady pH is reached. With an absolute increase in dissolved calcium carbonate, the amount of Ca^{2+} in the water also increases. Because the effect of ion valence on the tendency of clay particles to flocculate is highly nonlinear, it scales to the power 6 (i.e. Sposito (1989)), the release of the additional Ca^{2+} causes the suspension to become more unstable (in a colloidal sense). This causes faster flocculation, hence leading to larger flocs that are more porous. This is also reflected in the consolidation parameters. This effect, combined with the pH-dependent effect, leads to the changes in self-weight consolidation behaviour.

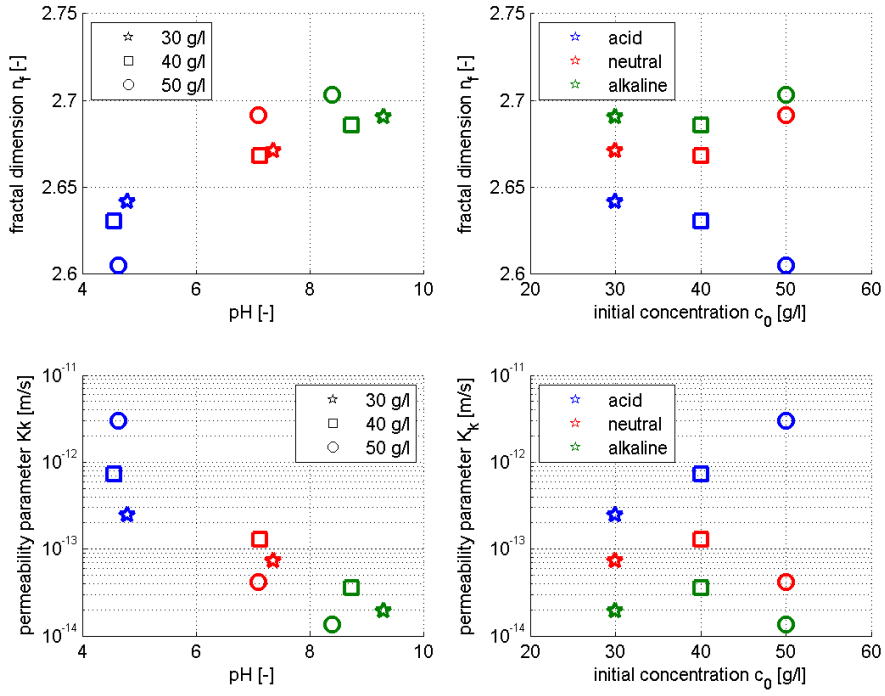

Figure 5.4: The determined parameters K_k and n_f for the first phase of self-weight consolidation, plotted as a function of both suspension pH and initial concentration c_0. These parameters were determined from interface readings for the large (2L) settling column experiments.

Comparing the data to literature shows that the K_k parameter values for the acidic columns are on the high end of the spectrum for K_k, and the fractal dimension n_f is rather low. Barciela Rial (2015) determined the consolidation parameters for the Markermeer clay, that was sampled from the same batch as the clay tested in the current research. These results can be compared with the neutral conditions, in spite of different ionic strengths, and show a similar trend: n_f increases with initial concentration.

The large differences in fractal dimension found between the current results and the results reported by Merckelbach (2000) are attributed to the large differences in initial concentration, as Merckelbach (2000) used initial concentrations c_0 in the order of 120-130 g/l for the experiments from which the self-weight consolidation parameters were deduced.

Table 5.4: Determined n_f and K_k for the Markermeer clay, compared with other research

reference	used material	n_f [-]	K_k [m/s]
current - acid	Markermeer clay IJ2	2.61-2.64	2.48E-13 – 2.98E-12
current - neutral	Markermeer clay IJ2	2.67-2.69	4.14E-14 – 1.28E-13
current - alkaline	Markermeer clay IJ2	2.69-2.70	1.34E-15 – 3.58E-14
Barciela Rial (2015)	Markermeer clay IJ2	2.64-2.75	1.63E-16 – 6.66E-14
De Lucas Pardo (2014)	Markermeer mud	2.69	7.85E-14 – 9.03E-14
Merckelbach (2000)	Caland-Beer mud	2.72-2.75	9.9E-16 – 2.2E-14
Merckelbach (2000)	Dollard mud	2.76	1.8E-14

The final volumes ranked as follows for the three different chemical environments: the volume of the consolidated beds in the acidic conditions are larger than those for the alkaline and neutral conditions, in that particular order. The difference in final volumes is in the order of 10-20%. Furthermore, it is found that the determined effective stress parameter K_p depends more on the obtained fractal dimension n_f than on the final volume. The determined K_p parameter values agree largely with literature. The effective stress parameters obtained for the acidic beds are somewhat lower, which is attributed to their lower fractal dimension and thus more porous structure.

Table 5.5: Determined n_f and K_p for the Markermeer clay, compared with other research

reference	used material	n_f [-]	K_p [m/s]
current - acid	Markermeer clay IJ2	2.61-2.64	7.84E+06 – 2.40E+07
current - neutral	Markermeer clay IJ2	2.67-2.69	2.13E+07 – 6.46E+07
current - alkaline	Markermeer clay IJ2	2.69-2.70	6.35E+07 – 1.67E+08
Barciela Rial (2015)	Markermeer clay IJ2	2.64-2.75	1.41E+07 – 6.66E+09
De Lucas Pardo (2014)	Markermeer mud	2.69	1.1E+07 – 2.5E+07
Merckelbach (2000)	Caland-Beer & Dollard mud	2.72-2.75	7.0E+07 – 4.0E+09

5.2.3 Consolidation of bentonite

The consolidation parameters for the bentonite based on the curve fitting procedure, as they were presented in Section 4.3, predict large differences in consolidation behaviour. They are repeated in Table 5.6 for convenience:

Table 5.6: Consolidation parameters for the bentonite mud samples

Mud sample	c_0 [g/l]	n_f [-]	K_k [m/s]	K_p [Pa]
Bentonite - acidic	40	2.64	7.60E-14	2.06E+08
Bentonite - neutral	40	2.66	2.27E-15	6.92E+09
Bentonite - alkaline	40	2.75	1.57E-18	1.66E+13

Large differences in the permeability parameters are determined. This qualitatively agrees with interface readings. The parameter K_k obtained for the bentonite is several orders of magnitude

smaller than the K_k obtained for the kaolinite and Markermeer clay samples. This relates well to knowledge from geotechnical engineering, from which it is known that bentonite has a low permeability (Mitchell and Soga, 2005).

The obtained fractal dimensions for the three samples are proportional to the final volumes, which is a contradictory finding. The fractal dimension is a measure for the packing density of flocs, and for equal initial concentrations, lower fractal dimensions should theoretically lead to the largest consolidated volume. However, it is exactly the opposite for the bentonite mud.

Of course, this finding only holds for the assumption that the fractal dimension does not change during the consolidation process, an assumption that is also made by Merckelbach and Kranenburg (2004). The effective stress parameter was found to be highest for the largest consolidated volume, while you would expect exactly the opposite. Again, this points at the influence of the fractal dimension n_f and the associated error propagation in the determination of K_p when using the fractal approach.

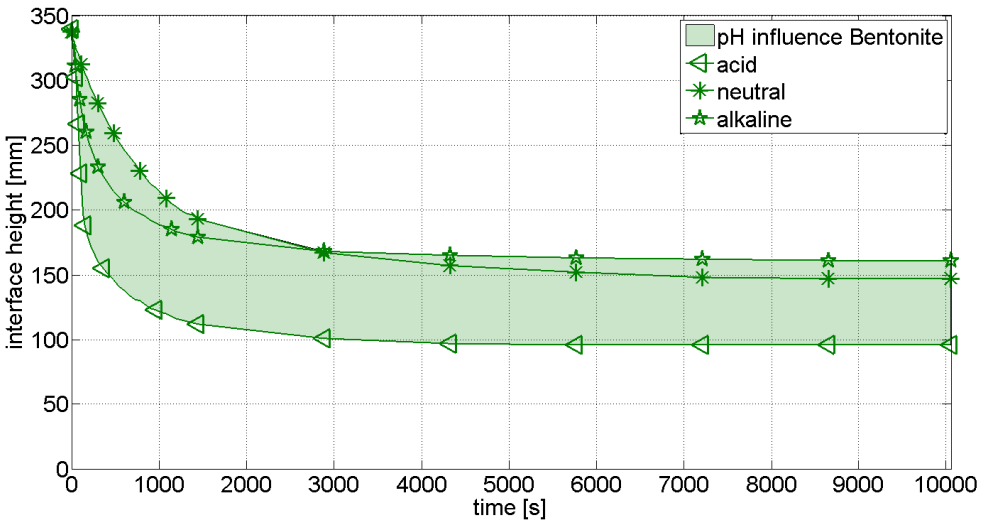

Figure 5.5: Settling curves for the bentonite mud, displaying the first and second phase of self-weight consolidation. Large differences in consolidation can be observed.

Regardless of the fractal approach, large changes in the consolidation behaviour of the bentonite mud exist (see Figure 5.5). These changes cannot be explained by flocculation theory alone: the largest flocs are expected with decreasing pH, thereby leading to the largest settled volumes. Trend in settled volumes is exactly opposite: alkaline > neutral > acid. This directly corresponds with the amount of acid added to the bentonite, as also hydrochloric acid needed to be added to obtain even a neutral solution. (mixing the clay powder with water led to a rise from pH 7 to pH 10). To restore

the pH to neutral values, the addition of 8 ml of hydrochloric acid (pH=0) was required. To make the water acidic, 20 mL of hydrochloric acid was required, bringing the pH to 4.8.

5.2.4 Comparing the effect of pH and mineralogy

The results for the self-weight consolidation of the three different muds are compared in this section. As shown in Figure 5.6, the mineralogy of the solid clay particles is found to largely influence the self-weight consolidation behaviour. The final consolidated volumes and the influence range of pH increase with increasing plasticity. The low plasticity mud, i.e. the kaolinite, consolidated quickly compared to the high plasticity mud samples.

The length of the self-weight consolidation was mainly governed by the plasticity of the mud samples, with increasing plasticity leading to longer consolidation periods.

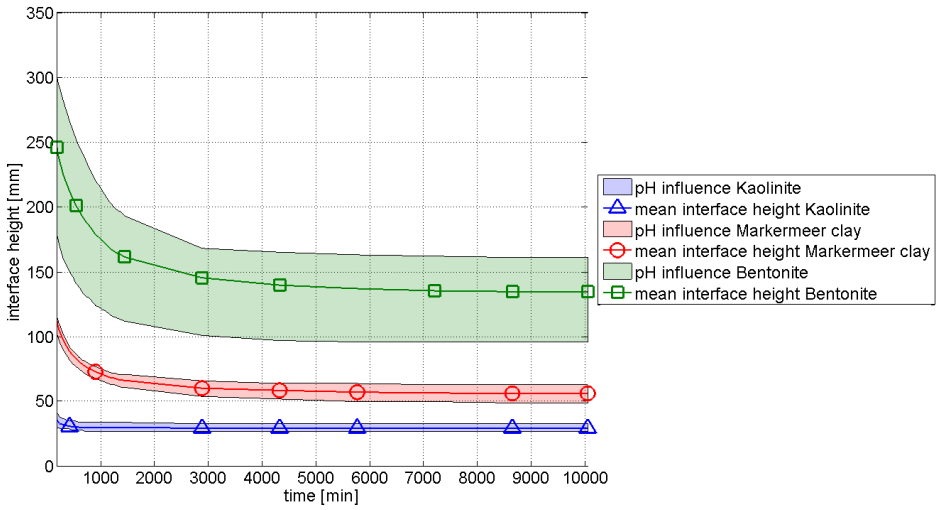

Figure 5.6: Measured interface heights for the three different mud samples, with the differences for pore water chemistry grouped in an envelope around the mean interface height. The time plotted spans from 180 to 10.050 minutes, thereby encompassing the largest part of the first and second phases of self-weight consolidation.

The effect of pH is significant for high and extremely high plasticity mud samples, but this effect decreases with decreasing plasticity. This can be understood from a soil mechanical point of view: the factors determining the plasticity, namely the specific surface area and surface charge, also determine the amount of electrostatic interactions between the clay particles. If the electrostatic interactions between clay particles are small, the effect of pH is also expected to be small.

5.2.5 Concluding remarks regarding the self-weight consolidation of the different mud samples

The self-weight consolidation of the different mud samples showed large differences. The low plasticity mud consolidated relatively quick and consolidated to a small volume. Because of the small differences in interface heights during the self-weight consolidation process, the curve fitting

procedure is prone to errors for the kaolinite. Fitting the power-law relation on curves that differ only marginally leads to large differences in fractal dimension n_f.

The estimates for n_f of the bentonite mud contradict with qualitative findings, as discussed in Section 5.2.3. The fractal approach worked best for the natural clay.

Furthermore, it is noted that self-weight consolidation continued after one week. Hence, the h_∞-interface heights (Table 4.8 and Table 4.9), measured after 6 to 7 weeks, differed from the final interface heights plotted in this section, albeit only marginally. Recalling, the h_∞ interface heights were used to calculate the K_p parameter.

When using the fractal approach to determine parameters describing the self-weight consolidation process, one should be aware of error propagation from K_k & n_f to K_p and c_v. Furthermore, it is important to note that the consolidation coefficient c_v describes the rate at which consolidation occurs, but does not give us information about the equilibrium situation.

5.3 Undrained shear strength as a function of Liquidity Index

As presented in Section 4.4, the obtained shear strengths of the tested samples were found to be in the order of several Pascals. The obtained shear strengths did not show a clear correlation with the corresponding void ratios of the consolidated samples. The void ratio expresses the absolute water content of the consolidated samples.

As was discussed in Section 2.6.3, it is preferable to express the undrained shear strength of settled beds or soils as a function of their relative water content. This relative water content indicates how much water a soil holds, compared to its Atterberg Limits, and is known to have a large influence on the mechanical behaviour of a soil or slurry. This relative water content is expressed as the Liquidity Index (for the formal definition see Equation (2.19)).

5.3.1 Undrained shear strength as a function of Liquidity Index

The average Liquidity Indices of the settled beds, after the small settling column experiment, are listed in Table 5.7. These are calculated from the settled bed height, by using the procedure described in Appendix B.1. For the three different clay types these were calculated as follows:

- Kaolinite: the average void ratios of the acid, neutral and alkaline suspension settled beds were normalized with the Atterberg Limits determined for the corresponding pore water chemistries.
- Bentonite: the average void ratios were normalized through the Atterberg Limits determined for the clay powder with 0.02M NaCl pore water.
- Markermeer clay: the average void ratios of all settled beds were normalized through the Atterberg Limits for the clay with its natural pore water.

Table 5.7: The average Liquidity Indices of the consolidated samples, for the three different clay types with different pore water chemistries.

Clay type	suspension pH	Average Liquidity Index [-]
Kaolinite	acid	7.9
Kaolinite	neutral	6.4
Kaolinite	alkaline	8.9
Bentonite	acid	4.3
Bentonite	neutral	6.9
Bentonite	alkaline	8.0
Markermeer clay	acid	3.7
Markermeer clay	neutral	2.9
Markermeer clay	alkaline	3.6

The height of the settled kaolinite beds was much lower than the heights of the bentonite and Markermeer clay, but when expressed as a Liquidity Index it becomes apparent why the undrained shear strength of the kaolinite was the lowest on average. This is because the kaolinite has a low plasticity, reflected in its Plasticity Index of approximately 15%. Therefore, it cannot hold large amounts of water and despite its settled volume which is relatively low, the consolidated samples have a high average Liquidity Index.

The Markermeer clay and bentonite both have a much higher plasticity, and in spite of the consolidated volumes being larger, they both have lower average Liquidity Indices. The bentonite shows a large spread in Liquidity Index, which cannot be explained properly. A possible indication could be the fact that hydrochloric acid needed to be added for both the acid and neutral environments. This was done because the bentonite had a strong tendency to buffer the suspension pH towards a value of pH=10.

Plotting the measured shear strengths as a function of LI yields the following result (Figure 5.7). Empirical relations between the undrained shear strength and the Liquidity Index, as proposed by Locat and Demers (1988), Houston and Mitchell (1969) and Leroueil et al. (1983) are also plotted as a reference. Comparing these relations with the data show that the undrained shear strengths are orders of magnitude lower than the empirical relations, which were devised from a soil mechanical point of view. The two artificial mud samples do not show a clear trend between Liquidity Index and undrained shear strength, whereas the natural clay samples does show a more pronounced trend: with increasing Liquidity Index, the undrained shear strength decreases. This decrease happens in a similar fashion to the trend lines found by Houston and Mitchell (1969), although the Markermeer clay samples have a rather low undrained shear strength compared to their Liquidity Index. Possible reasons include inaccuracies in the determination of the Liquidity Index (discussed in 5.3.2), or the experimental procedure.

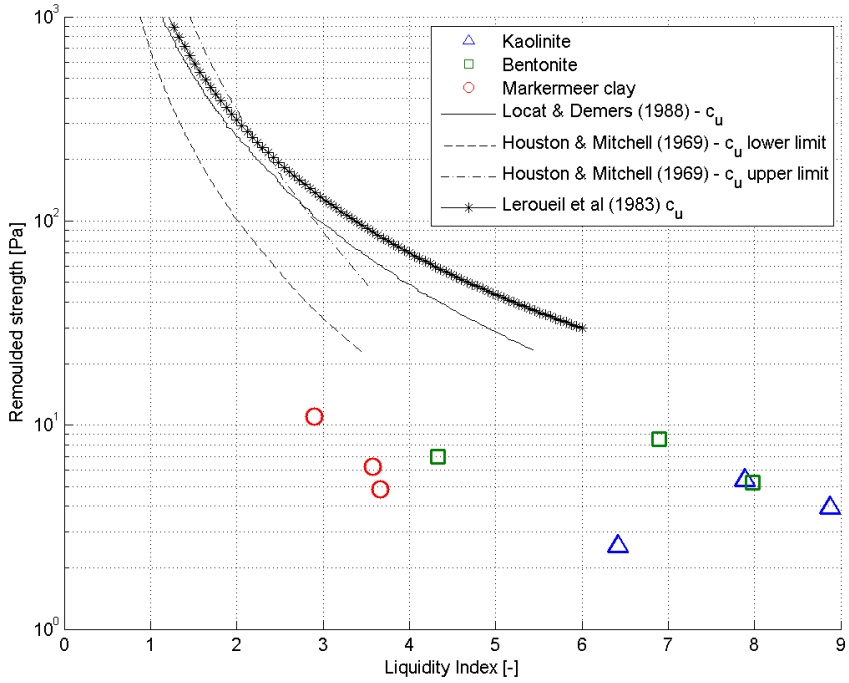

Figure 5.7: The undrained shear strengths of the consolidated kaolinite, bentonite and Markermeer clay samples, plotted as function of their respective average Liquidity Indices.

For the large settling columns, the Liquidity Index of all the tested samples was calculated as described for the Markermeer clay. This resulted in the values as they are listed in Table 5.8.

Table 5.8: The average Liquidity Indices of the consolidated samples for the large (2L) settling column experiments. Markermeer clay with varying initial concentrations and different suspension pH.

Clay type	suspension pH	initial concentration [g/l]	Average Liquidity Index [-]
Markermeer clay	acid	30	3.9
Markermeer clay	neutral	30	3.0
Markermeer clay	alkaline	30	3.4
Markermeer clay	acid	40	3.4
Markermeer clay	neutral	40	2.8
Markermeer clay	alkaline	40	3.0
Markermeer clay	acid	50	3.6
Markermeer clay	neutral	50	2.8
Markermeer clay	alkaline	50	3.0

For the Markermeer clay, the suspension pH caused the largest differences in Liquidity Index, whereas the initial concentration had a more limited impact on the Liquidity Index of the consolidated sample. Of course, the consolidated volumes were different for the different initial concentrations, but the average water content of the consolidated samples did not differ substantially.

If the undrained shear strength of the samples is again plotted as a function of the Liquidity Index, the following result is obtained (Figure 5.8):

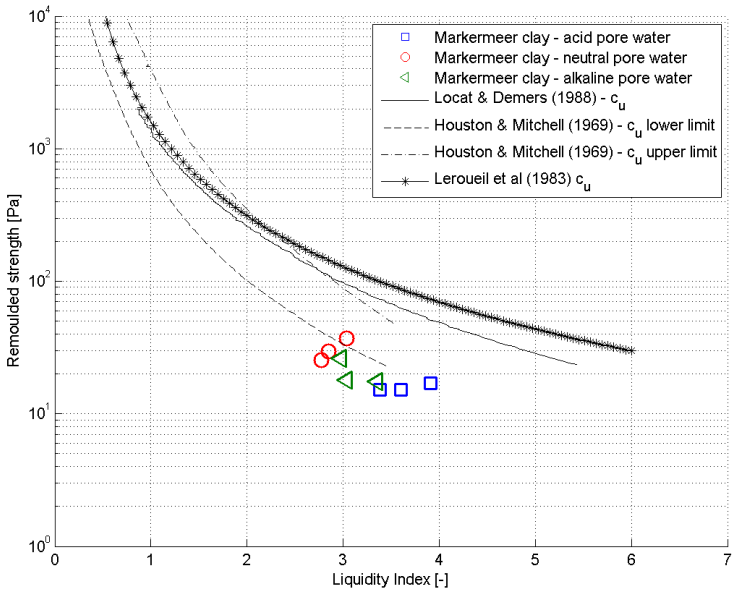

Figure 5.8: The undrained shear strengths of the consolidated Markermeer clay samples, plotted as function of their respective average Liquidity Indices. These results are for the large settling column tests.

The mud that settled and consolidated in the neutral suspensions, resulting in the lowest Liquidity Indices, also exhibits the highest undrained shear strengths. The mud that consolidated in the alkaline and acid suspensions shows lower undrained shear strengths. This agrees with the larger volumes they consolidated to, and thus a higher Liquidity Index. When compared to the empirical correlations in literature, the found undrained shear strengths are still on the lower side of the spectrum.

The undrained shear strengths vary between 15-30 Pascals. Although this is all quite low, the clay that consolidated in the neutral conditions developed twice as much strength as the samples that consolidated in the acid conditions. Those differences are significant, despite the consolidated volumes that differed by 10-15% only.

5.3.2 Sources of inaccuracy in the determination of the Liquidity Index

The Liquidity Index is used to express the undrained shear strength of the tested samples. This appears to be a promising method for estimating the undrained shear strength of these samples, as it enables to compare different types of mud with different plasticities. However, normalizing the water content by means of the Atterberg Limits should be done carefully, especially for varying pore water chemistry. In the current study there are two possible sources of inaccuracy for the results that were presented in the previous section. These are:

1. The Atterberg Limits differ for varying pore water chemistry, if the clay has a high plasticity (van Paassen, 2004). This is also shown in Figure 4.2: the Liquid Limit of bentonite decreases with increasing ionic strength. The experimental procedure involved the addition of hydrochloric acid, with a resulting ionic strength corresponding to 0.02 M NaCl for the different samples. Therefore, the water contents for the consolidated bentonite samples were normalized by using the Atterberg Limits of the bentonite clay with 0.02M NaCl pore water. In spite of having the correct ionic strength, the addition of the hydrochloric acid could have affected the Atterberg Limits as well, thus caution should be exercised when interpreting the data.

For the Markermeer clay the normalization procedure has probably led to an underestimation of the Liquidity Index for the consolidated samples. The Atterberg Limits were only determined for the natural pore water, as the water content of the natural clay was already close to the Liquid Limit. However, the Markermeer clay also is a highly plasticity clay and thus, its Liquid Limit is likely to decrease with increasing ionic strength. Recalling that the Liquidity Index, written in terms of void ratio, is defined as:

$$LI = \frac{\bar{e} - e_{PL}}{e_{LL} - e_{PL}} \tag{5.2}$$

Assuming the Plastic Limit remains constant with increasing ionic strength (this is based on the small differences in Plastic Limit for the Bentonite, despite changes in pore water chemistry), a decrease in Liquid Limit leads to a subsequent decrease in Liquidity Index. This can be interpreted from Equation (5.2). The possible impact this approach has on the determined Liquidity Index is quantified by assuming a maximum decrease of 10% in the Liquid Limit because of the increase in ionic strength to approximately 0.1M NaCl. This assumption is based on the empirical formulation proposed by Schmitz and van Paassen (2003). The differences in Liquidity Index are plotted in Figure 5.9. In this case, a decrease of 10% of the Liquid Limit would lead to an increase in LI of approximately 0.5 for the consolidated Markermeer clay samples.

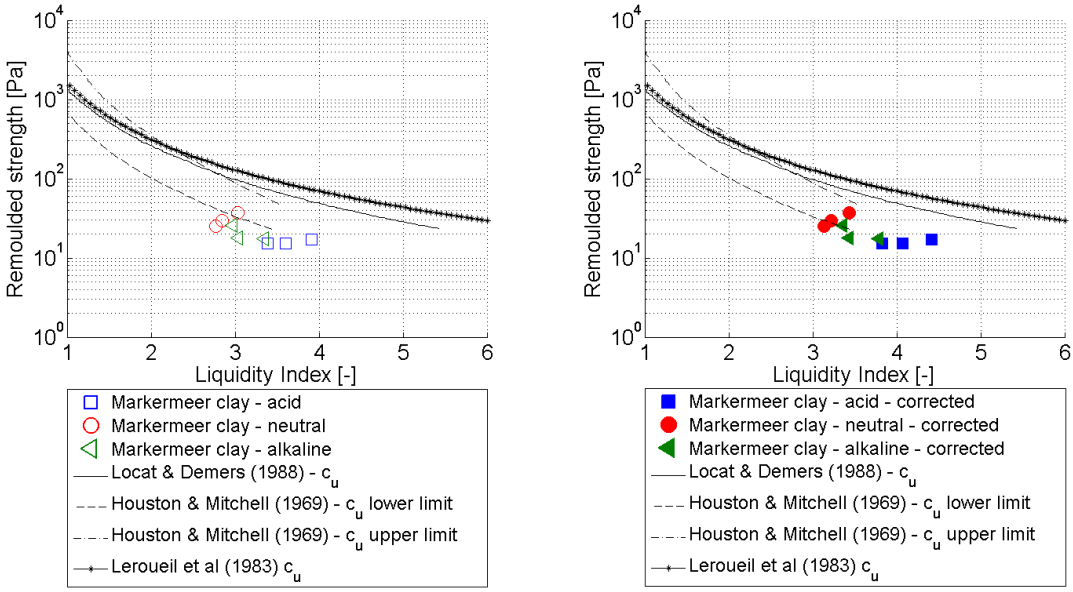

Figure 5.9: The influence of changes in the Atterberg Limits on the calculation of the Liquidity Indices for the settled beds. The left panel shows the LI corresponding to the natural pore water of the Markermeer clay. The right panel shows the LI, if the Liquid Limit decreases with 10%, leading to an increase in LI of approximately 0.5 for the tested samples.

2. The Liquidity Index of the settled beds is approximated by its average Liquidity Index. These shear strengths are measured in the middle of the beds (see Figure 3.8 for a sketch) but the assumption that the average Liquidity Index corresponds with the actual Liquidity Index on this height is only correct if the Liquidity Index varies linearly over the bed. Been (1980) measured density profiles in mud layers that consolidated due to their own weight and found an almost linear increase in density with increasing depth in the bed. However, a much more dense base layer formed, due to segregation. Merckelbach (2000) measured similar density profiles, that decreased linearly from the top of the consolidated bed, until there is a steep increase in measured density for the lower layer. Again, this is attributed to segregation in the settling columns.

Although segregation is not considered in this research, the assumption of a density profile that increases linearly with depth over the full height of the consolidated sample appears to be a rather crude approximation which may lead to inaccuracies in the determination of the Liquidity Index of the sample. To get a more precise estimate of the Liquidity Index, density measurements are necessary.

5.3.3 Concluding remarks about the undrained shear strength versus the Liquidity Index

In Section 5.3.1 it is shown that the Liquidity Index can be utilized to obtain a first indication of the undrained shear strength of a consolidated mud bed. However, there are some remarks that require further attention.

The indication for the undrained shear strength given by the Liquidity Index is best for the natural mud samples, when compared to empirical relationships between c_u and LI. These empirical relations were determined for a variety of natural clay samples, hence it makes sense they show a better fit with the obtained undrained shear strengths for the natural clay sample than the artificial mud samples.

However, the obtained shear strengths are rather low when compared to literature. This could be due to the testing procedures, in which the current research differs from literature. In this research, the undrained shear strength was determined using a shear vane in combination with a rheometer, an approach similar to Merckelbach (2000) and Jacobs (2011). On the other hand, most researchers from the field of soil mechanics used a Swedish fall cone to determine the undrained shear strength of their samples (i.e. Locat and Demers (1988) and Leroueil et al. (1983)). Hence, due consideration should be given to the experimental procedure when assessing undrained shear strength data, which was also acknowledged by Houston and Mitchell (1969). They mention experimental procedures as the main reason for the large variability in determined undrained shear strengths for similar Liquidity Indices.

The kaolinite and bentonite showed different behaviour, that cannot be explained by the changes in Liquidity Index alone. Liquidity Indices for these samples were very low, making them susceptible to measurement errors (because of the very low undrained shear strengths). They deserve further attention, but this is beyond the scope of this research.

5.4 Linking fluid and soil mechanics

As stated already in Section 1.1, this research is on the boundary of both fluid and soil mechanics. This section elaborates on making the crossover between these two fields.

5.4.1 Using the same variables

Fluid and soil mechanics do not always use the same variables. In fluid mechanics, the settling and self-weight consolidation of mud is mostly expressed in terms of either: sediment concentration c [g/l], volumetric concentration φ [-] or void ratio e [-]. On the other hand, soil mechanics characterizes the mechanical behaviour of soils in terms of water content, or its normalized equivalent: the Liquidity Index. The self-weight consolidation equation proposed by Gibson, and the parameters linked to it, are expressed in terms of the void ratio e.

It is shown in Appendix B.1 that, under the assumption that the mud-water mixture is fully saturated (S=1):

- The average concentration c of a mud-water suspension can be rewritten into an averaged void ratio
- The Atterberg Limits, and the corresponding Liquidity Index can also be expressed in terms of void ratio, instead of the water content

Combining these findings enables us to convert the settling curves into liquidity index curves, a curve that shows the liquidity index of a suspension or settled bed as a function of time. The main advantage of this conversion is the ability to incorporate the material properties of different clayey materials into the settling curves. The need to incorporate these material properties became apparent during the small settling column experiments: large differences existed between the settling and consolidation behaviour of the various used clays. However, the initial concentration of these clays was equal (c_0=40 g/l) for all the small settling column experiments. These differences were shortly touched upon in Chapter 4 but will be elaborated more extensively here.

5.4.2 Normalizing the settling curves through the Atterberg Limits

Settling curves have a major drawback. The interface height, that can be translated to an average density, can only be used to compare the results of mud samples with identical properties. When mud with different plasticities are tested, it is not appropriate to compare their results by the specific density alone. Therefore, it is proposed to normalize the settling curves of different mud, albeit artificial or natural, by means of the Atterberg Limits. Through this normalization, the average Liquidity Index of the mixture or bed is obtained. Expressing either one of these in terms of an average Liquidity Index has two advantages:

- The properties of the clayey material are also reflected in the Liquidity Index curve. For instance, the settling and self-weight consolidation of the two artificial muds shows that 40 g/l of kaolinite is thoroughly different mixture than 40 g/l of bentonite. Liquidity index curves reflect these differences, see Figure 5.10
- Empirical relationships between the undrained shear strength (or yield stress) of a slurry/soil and its Liquidity Index exist. By using these relationships, the undrained shear strength can be expressed as well.

Comparing the Liquidity Index curves of different mud samples

By converting the interface height to an average Liquidity Index, the settling curves as they are shown in Sections 5.1 and 5.2, can be converted to Liquidity Index curves. This curve gives the average Liquidity Index of the bed (or suspension) as a function of time. An example of such a

curve is plotted in Figure 5.10, displaying the mean Liquidity Index of the small settling column experiments for the kaolinite and bentonite mud samples.

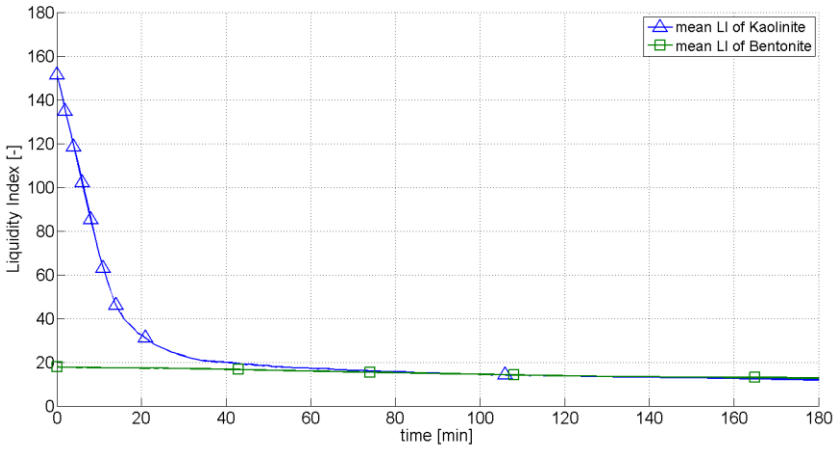

Figure 5.10: Liquidity Index plotted as a function of time, for the mean LI of the kaolinite and bentonite mud samples. Although the initial concentration c_0 was constant, the Liquidity Index differs by a factor 8. The plot shows the first 180 minutes of the small settling column experiment.

This curve can be interpreted qualitatively, and shows that the experiments with the kaolinite and bentonite started at vastly different Liquidity Indices. From a soil mechanical point of view, this explains why such large differences in settling behaviour were observed. The settling column experiment for the kaolinite started at a Liquidity Index of 150-160. This means that the water content of the suspension at the start of the experiment is around 150 times the water content at the Liquid Limit of the tested kaolinite. The bentonite, for which the initial LI was approximately 20, barely shows a settling phase, which can be understood as its LI was much lower than that of the kaolinite. It is already much more a slurry than the kaolinite, in spite of the equal initial concentrations. 70 minutes into the settling column experiment, the Liquidity Indices for the two mixtures converge (they diverge later on), which is a possible indication for a similar consolidated state at that moment.

When the Liquidity Index curves are plotted for the self-weight consolidation phase (Figure 5.11) it can be seen why the Markermeer clay samples developed more strength than the bentonite samples, which in turn developed more strength than the kaolinite samples. The Liquidity Indices rank in the opposite order, indicating that the relative water content is smallest for the Markermeer clay, followed by the bentonite and kaolinite. This shows that the Liquidity Index curves are indeed a more qualitative tool for assessing the mechanical behaviour of consolidating mud layers, than the settling curves alone. Unfortunately, assessing the Liquidity Index curves quantitatively is not possible: information about the actual Atterberg Limits of the Markermeer clay and the bentonite is lacking. The Atterberg Limits used to convert the interface height were the same as those used in Section 5.3.1, meaning that in determining the LI of the Markermeer clay samples, the influence of pH or ionic strength was not accounted for. For the bentonite mud, the ionic strength was

accounted for in determining the Atterberg Limits, but not the changes in acidity. Despite these drawbacks, this method is still regarded as a useful tool for comparing the self-weight consolidation behaviour of different mud samples.

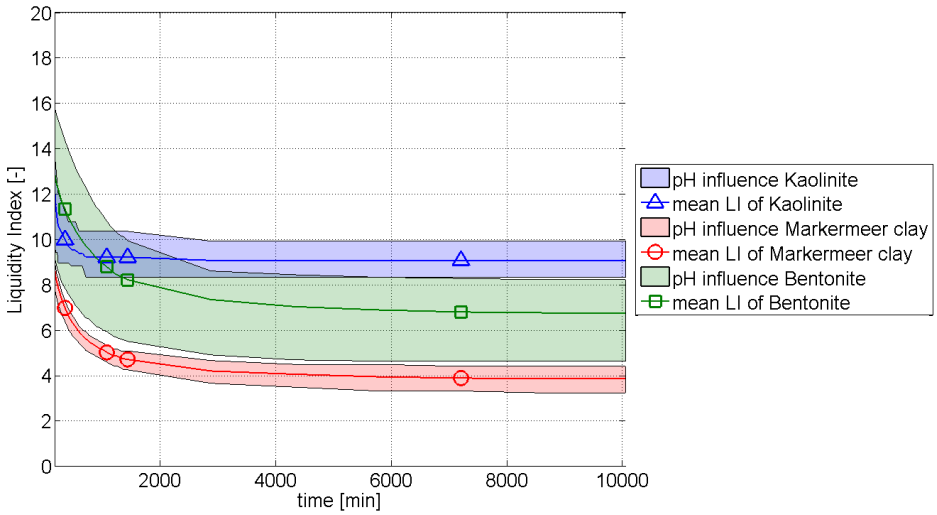

Figure 5.11: Liquidity Index plotted as a function of time, for the self-weight consolidation phase of the small settling column experiment. The influence of pH is also indicated for the different curves.

Comparing the Liquidity Index curves for different initial concentrations

In the large settling column experiments, the initial concentration was also varied. Therefore, the interface height differs for the mud settling under the same chemical conditions, i.e. acidic, neutral or alkaline. However, this does not necessarily tell us something about the mechanical behaviour of the consolidated layer.

Again, the Liquidity Index of the beds is plotted as a function of time, but now only for the consolidation phase, because it shows the bandwidth of the different clay samples.

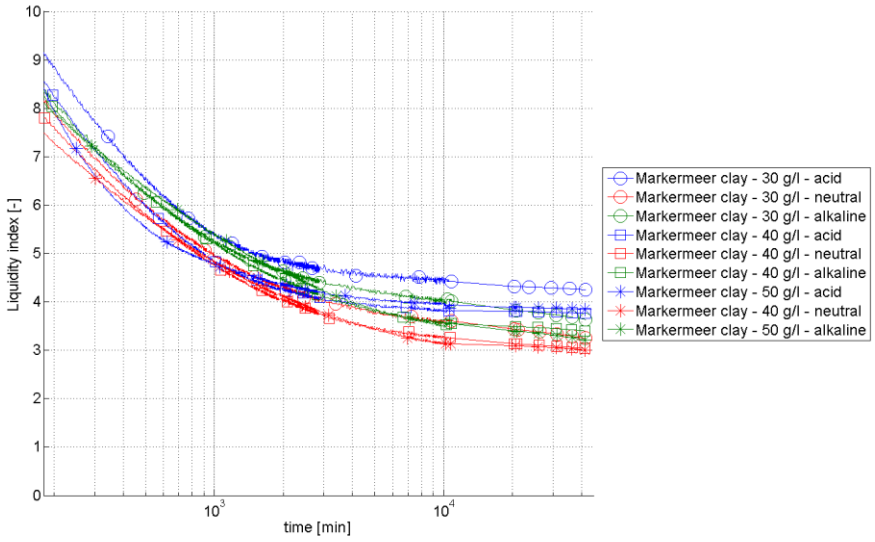

Figure 5.12: Liquidity Index as a function of time for the large settling column experiments. The Liquidity Indices at the end of the experiment appear to be grouped per chemical condition (i.e. acid, neutral or alkaline).

5.4.3 Relating the gelling concentration to the Plasticity Index

The gelling concentration, discussed in Section 2.5.3, indicates the concentration at which the transition from hindered settling to self-weight consolidation takes place.

Gelling concentration expressed as a concentration

For the three clayey materials used in this research, large differences in gelling concentration were found. These gelling concentrations are listed in Table 5.9. One possible explanation lies in the different method through which they were determined: the gelling concentration for the Kaolinite was determined by measuring the height of the deflection of the settling curve, translating this to a specific concentration, a method proposed by Dankers (2006). For the bentonite and the Markermeer clay, the gelling concentration was determined by setting up settling columns with at least 2 different initial concentrations, thereby obtaining a solution for Equation (2.4). Following this approach, the gelling concentration can also be deduced.

Table 5.9: Gelling concentrations found for clayey materials in current research

Clay type	Gelling concentration range [g/l]
Kaolinite	170-260
Bentonite	55
Markermeer clay	80-90

Dankers (2006) noted that the first mentioned method is likely to overestimate the gelling concentration, as the concentration of the suspension is affected by consolidation of the lower

layers. Regardless of these differences, a large spread in gelling concentration will continue to exist, as is also reflected by the large differences in settling behaviour, see Section 4.2.

Also in literature, large differences in gelling concentration exist. Dankers (2006) summarized found values from literature, which are listed in the rows 4-10 of Table 5.10. These results are supplemented with the results from the current research and the work by Been (1980) and Barciela Rial (2015).

Table 5.10: Estimates of gelling concentrations from literature and current research. Estimates are rounded per 5 g/l

c_{gel} [g/l]	Material	Source
170-260	Kaolinite	current research
55	Bentonite	current research
80-90	Markermeer clay (NL)	current research
50-130	Polystyrene, silica and attapulgite	Buscall et al. (1988)
80	estuarine mud (Severn, UK)	Odd and Cooper (1989)
130	N/A	Toorman (1992)
30-180	N/A	Williams and Williams (1989)
280	Bauxite mining waste	Sills (1998)
65-90	Kaolinite	Dankers (2006)
80-105	estuarine mud (Caland-Beer canal, NL)	Dankers (2006)
80	Markermeer clay	Barciela Rial (2015)
170-265	Kaolinite	Been (1980)

Table 5.10 shows that the found gelling concentrations in the current research are comparable to literature. As can be seen from this table, the gelling concentrations reported in literature vary between values as small as 30 g/l, to values as large as 280 g/l, which is a ninefold difference. A possible explanation for these large differences is the lack of physics in the description of the gelling concentration.

Gelling concentration expressed as a Liquidity Index

As discussed at the start of this section, normalizing the settling curves by means of the Atterberg Limits yields the Liquidity Index. Likewise, the gelling concentrations can also be converted into a Liquidity Index, given that the Atterberg Limits for the material have also been determined. Of the research listed in Table 5.10, this was done by Sills (1998), Barciela Rial (2015) and Been (1980). The found gelling concentrations, combined with the values found in this research, are converted into a Liquidity Index. The results is plotted in Figure 5.13, with the Liquidity index plotted as a function of gelling concentration.

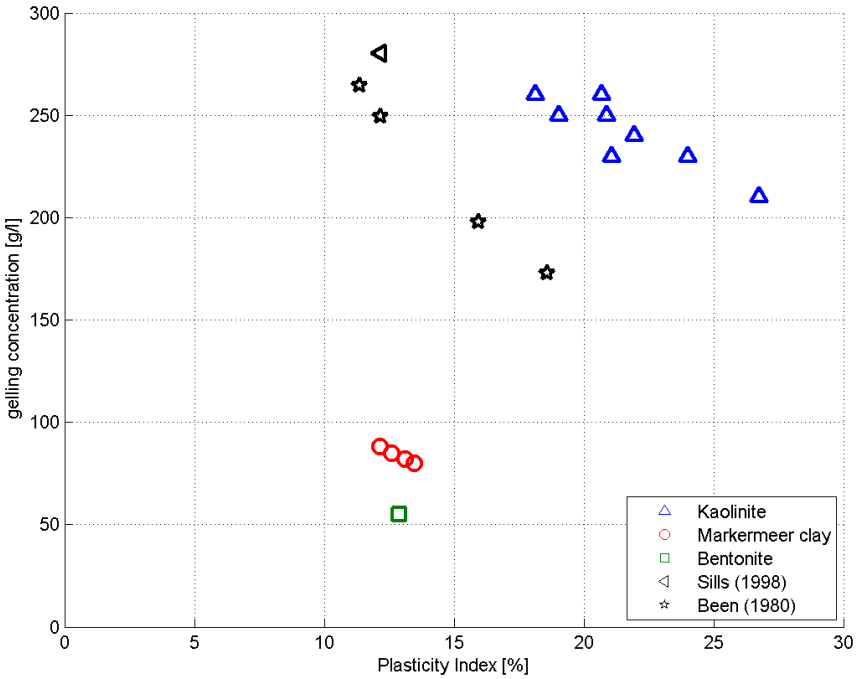

Figure 5.13: Liquidity index plotted as a function of gelling concentration.

The large spread noticed for the gelling concentration has decreased, from a gelling concentration ranging from 30-280 g/l, to a Liquidity Index ranging from 10-25 (roughly). Hence, the material properties as they are reflected by the Atterberg Limits also have some validity for the gelling concentration. However, the Liquidity Index is converted from the gelling concentration by normalizing it through the Atterberg limits: these two parameters are coupled. Therefore, it is not entirely justified to plot one value as a function of the other.

Linking the gelling concentration to the Plasticity Index yields more promising results, as can be seen in Figure 5.14. If the gelling concentrations are plotted as a function of their respective Plasticity Indices, it can be seen that there is a steep increase in the gelling concentration for the mud mixtures with a low plasticity. If the data is plotted on double log axes, it becomes apparent that a power-law fit describes the relation between the PI and the gelling concentration.

The existence of such a relation has two important implications: it supports the view of mud flocs as fractal structures and hence its influence on the gelling concentration, and provides a direct relation between material properties and the gelling concentration. Hence, a first estimate of the gelling concentration for different mud samples can be computed based on the Atterberg Limits of a mud sample.

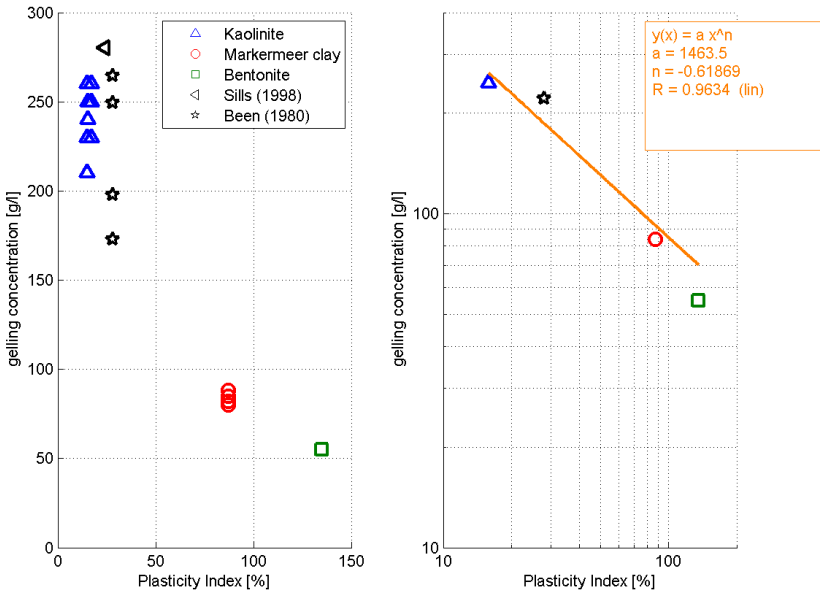

Figure 5.14: Found gelling concentrations plotted as a function of Plasticity Index. On the left panel, the gelling concentrations found in this research are compared with reference literature. In the right panel, a power law fit is fitted to a selection of the gelling concentrations

The power-law relation between the PI and the gelling concentration is found to be:

$$c_{gel} = 1464 * PI^{-0.619} \tag{5.3}$$

The following remarks are made about the selected data points for the curve fitting:

- In order to not place emphasis on the low plasticity mud mixtures, only one value is chosen for both the kaolinite dataset (this research) and the research by Been (1980). These values are the mean gelling concentrations.
- The gelling concentrations for the kaolinite and Been (1980) were based on interface readings, a method which is known to overestimate the gelling concentration (Dankers, 2006). However, to not overly influence the power law fit, the mean of the obtained gelling concentrations is chosen. Taking the estimates on the lower end of the spectra for the obtained gelling concentrations obviously influences the obtained power law fit.
- The found gelling concentration by Sills (1998) is not included because in that research, it was actually bauxite mining waste that was tested, with a much larger particle density (ϱ_s=3470 kg/m^3).

Considerations on relating the gelling concentration and the Atterberg Limits

Both the gelling concentration and the Plasticity Index, which were introduced in Sections 2.5.2 and 2.6.2 respectively, can be used to express the properties of a slurry or soil, given a certain water content. In the case of the gelling concentration, it is used to express the volumetric concentration of mud flocs, termed φ ($\varphi = c/c_{gel}$). In the case of the Plasticity Index, it is used to convert the water content W of a soil or slurry to the Liquidity Index (not exactly though). Obtaining a relationship between these parameters may prove to be useful tool for estimating the gelling concentration, by obtaining the Atterberg Limits of a mud sample through which a first estimate of the gelling concentration can be obtained.

PI decreases with increasing salt concentration, while void ratio e increases.(larger flocs, higher porosity!) will then be larger with increasing salt concentration. (hence it will not be constant for the same clay mineral in different aqueous environments)

However:

- For high plasticity clays, the Liquid Limit decreases with increasing salt concentration (see Section 4.1)
- Hence, the PI also decreases, assuming the Plastic Limit stays approximately the same.
- With increasing salt concentration, flocculation is promoted and more porous flocs are formed (up to 10 ppt, (Mehta, 2014)). This leads to a decrease in gelling concentration.

As can be seen from Figure 5.14, the trend with decreasing Plasticity Index is an increase in gelling concentration. This is exactly the opposite of the influence of increasing ionic concentration. Hence, caution should be exercised when relating the gelling concentration and the Plasticity Index to one another.

6. Conclusions and recommendations

6.1 Conclusions

The goal of this thesis is to gain more understanding of factors influencing the settling and self-weight consolidation of mud. Factors studied are the pH and the composition of the solid particles.

To examine the effect of pH, an experimental study was performed. In these experiments, the initial pH of the suspension was systematically varied. It was found that, because the pH and the ionic strength of the suspension are coupled, the ionic strength needs to be kept constant in order to study the effect of pH. To investigate the effect of the solids composition, two artificial mud samples, i.e. a kaolinite and bentonite clay powder, and one natural mud sample were tested. From the experimental results it can be concluded that:

- The mineralogy of the present clay minerals exerts a large influence on the settling and self-weight consolidation process

The mineralogy of the present clay minerals, reflected through the plasticity of the mud sample, exerts a large influence on settling and self-weight consolidation. This is reflected by large differences in gelling concentration and consolidated volumes between the three different mud samples. The gelling concentration of mud samples decreases with increasing plasticity and also, the self-weight consolidation process takes longer for higher plasticity mud samples.

- There is an influence of pH on the settling and self-weight consolidation of mud, but mainly for samples with high to extremely high plasticities. The different clay types show different trends for variations in the pH

For the kaolinite, a low plasticity mud, the effect of pH is limited. The settling and the self-weight consolidation behaviour of kaolinite, an artificial mud sample with a low plasticity, showed only a

small dependency on pH. The effective settling velocities showed no clear trend on suspension pH, and the final volumes of samples that consolidated in either acidic, neutral or alkaline suspensions showed a 10% variation in final consolidated volume. Because of the small settled volumes, these variations do not exceed the uncertainties in measurement procedures. Therefore they are regarded as insignificant.

The natural mud sample from the Markermeer, with a high plasticity, showed a significant pH dependency on the settling behaviour. The mud settled with a lower effective settling velocity in acidic suspensions. This is caused by the formation of flocs that are more porous, which is indicated by a decrease in gelling concentration. These more porous flocs lead to a larger hindrance for settling mud flocs, thereby decreasing the effective settling velocity. Due to the dissolution of calcium carbonate in the natural clay, large amounts of hydrochloric acid needed to be added to arrive at stable low pH values. This dissolution process led to the release of calcium (Ca^{2+}) ions. Because of the divalent ions, the suspension became more unstable thereby leading to faster flocculation. Hence, the observed changes in settling and self-weight consolidation behaviour cannot only be regarded as a pH-dependant effect.

Based on an analysis following the fractal approach, it was found that during self-weight consolidation the natural mud layers were most porous and permeable under acidic conditions. The mud samples in the acidic conditions consolidated to the largest final volumes, followed by samples that consolidated under alkaline and neutral conditions, respectively.

The extremely high plasticity mud sample did not show a clear settling phase, but the self-weight consolidation was largely influenced by the pH. The final volumes decrease with decreasing pH, which is opposite to the natural mud sample. The consolidated volumes for acidic and alkaline suspensions differ by a factor 1.7. This behaviour cannot be explained by changes in flocculation and should be studied further.

Concluding: the effect of pH is significant for high and extremely high plasticity mud samples, but this effect decreases with decreasing plasticity. This can be understood from a soil mechanical point of view: the factors determining the plasticity, namely the specific surface area and surface charge (or CEC), also determine the amount of electrostatic interactions between the clay particles. If the electrostatic interactions between clay particles are small, the effect of pH is also expected to be small.

The undrained shear strength of the consolidated mud layers is also measured. The kaolinite consolidated to the lowest final volumes and showed the lowest undrained shear strengths, of approximately 5 Pascal. The natural clay developed larger undrained shear strengths, in the order of 5-10 Pascal. The measured undrained shear strengths of the bentonite mud layers are in the order of 5-10 Pascals, and hence somewhat stronger than the low plasticity clay beds. This is in spite of

the consolidated volumes that were at least 5 times as large as the consolidated volumes for the kaolinite.

In large settling columns, the undrained shear strength of the natural mud varied between 15-30 Pascal. The undrained shear strength of the natural mud in the acidic suspensions is, on average, twice as small as those for the neutral suspensions. These undrained shear strengths correspond with the respective Liquidity Indices for the consolidated beds.

- Consolidation parameters obtained using the fractal approach correctly predict the self-weight consolidation of the natural mud. For the artificial mud samples, this method is prone to errors.

For the kaolinite these errors are a result of the small differences in interface heights during the self-weight consolidation process. For the bentonite the obtained fractal dimensions contradict with qualitative findings. The fractal approach works best for the natural clay, yielding values that agree with qualitative observations.

However, error propagation from the parameters determined for the first phase of self-weight consolidation can lead to erroneous values for the parameters describing the second phase of self-weight consolidation.

Besides the main objectives, the following additional conclusions can be drawn from this research:

- No large changes in acidity are expected in the Markermeer environment, in spite of the presence of pyrite in the Markermeer bed.

Because of the large neutralizing capacity of both the fresh water and the natural mud, no large changes in acidity are expected for the Markermeer environment. For natural mud samples, this neutralizing capacity can either stem from the presence of calcium carbonate or the clay minerals themselves. In the Markermeer clay, 10 % of the mass consisted of calcium carbonate (Barciela Rial, 2015), therefore it has a very high neutralizing capacity.

The oxidation of pyrite (discussed in Appendix A) could, in case of low buffering capacities, lead to a drop in soil pH. This oxidation process takes place when clay that contains pyrite is brought from an anoxic to oxic state, which is exactly what happens when dredging clay from a lake bed. Because of the presence of large amounts of calcium carbonate, this is not expected to be relevant for the Markermeer.

- The relative water content of a suspension or mud layer, that can be expressed as a Liquidity Index enables us to compare the settling and self-weight consolidation of different types of mud. Next to that, this relative water content also determines the undrained shear strength of mud, rather than the absolute water content.

The mineralogy of the clay particles, in combination with the chemical environment, determine the plasticity of clay. This plasticity, reflected by the Atterberg Limits, can be used to normalize the settling curves of different mud samples. This yields the average Liquidity Index of the various mud samples as a function of time. The average Liquidity Index of a settling bed can be used to get a first indication of the settling and self-weight consolidation behaviour.

To compare the mechanical behaviour of different mud samples, it is advised to normalize the average water content of the consolidated beds through the Atterberg Limits. The measured undrained shear strength of the settled beds are shown to depend on the Liquidity Index rather than their bulk density. For the natural clay used in this research the undrained shear strength as a function of LI showed a fair agreement with empirical relations between LI and c_u, given by Locat and Demers (1988) and Houston and Mitchell (1969). The undrained shear strengths of the artificial mud samples show no trend with their respective Liquidity Indices.

- A power law relation can be established between the gelling concentration and the Plasticity Index (Figure 5.14)

The gelling concentration, a state parameter which is often used in cohesive transport modelling, is related to a material property of mud, namely the Plasticity Index. A power-law relation is established, based on the determined gelling concentrations and corresponding Atterberg limits of the three different mud samples. Experimental data obtained by Been (1980) were also utilized to obtain this fit. Although the power law relation is fitted to relatively few data points, the existence of such a relation has two important implications: it supports the view of mud flocs as fractal structures and hence its influence on the gelling concentration, and provides a direct relation between material properties and the gelling concentration. Hence, a first estimate of the gelling concentration for different mud samples can be computed based on the Atterberg Limits of a mud sample. This means a large improvement: the Atterberg Limits can be determined by means of a standardized test, whereas the current methods to determine the gelling concentration are laborious and rather subjective

6.1.1 Reflection on the research

This research is initiated because of the emerging demand to use mud as fill material for reclamations, in line with the mindset of Building with Nature. This research is not geared towards solving the practical issues related to building with muddy materials. However, it can prove to be very useful in the design of such reclamations.

As a part of understanding the material behaviour of mud, factors influencing the electrostatic interactions between clay particles were studied. The electrostatic interactions between the clay particles are influenced by the pH and solids composition, providing an answer to the engineering question posed in this research. But it is also important to interpret how this research slots into the domains of fluid and soil mechanics. Keeping in mind the bigger picture, an adapted version of Figure 1.2 is presented below (Figure 6.1):

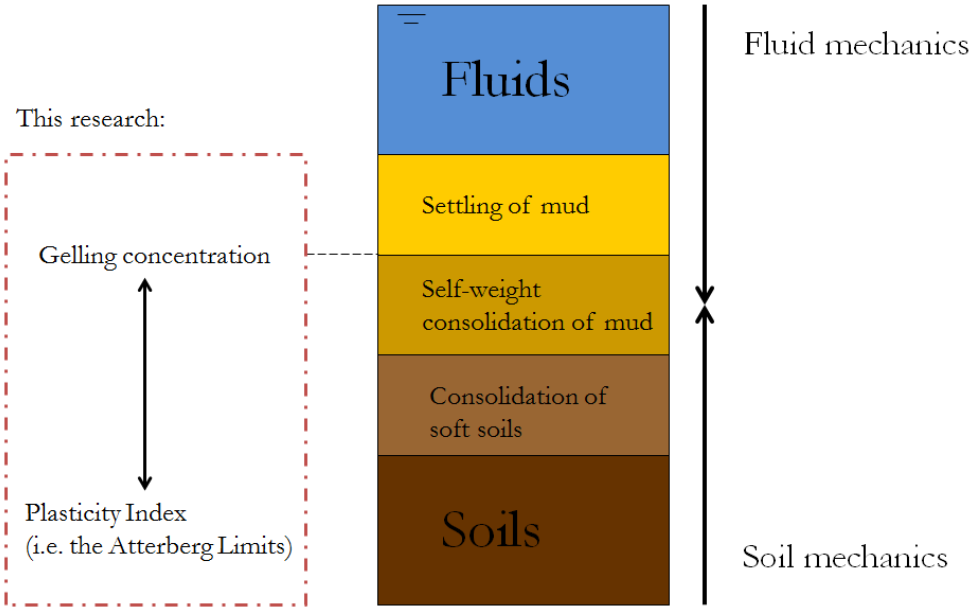

Figure 6.1: Interface of fluid and soil mechanics, with indication of the contribution of this research to both fields.

The strength of the material tested in this research is several orders of magnitude too low to serve any geotechnical purpose. The mud layers are still (very) soft, having a strength and consistency comparable to a watery slurry, such as yoghurt. However, characterising this material by means of its Liquidity Index, already for these liquid states (from a soil mechanical point of view) allows us to better understand, track and possibly predict the material behaviour in subsequent consolidation and strength development. The goal of building with mud is to let the mud become a soft soil, from which point onward, further development is possible. This work provides a means with which the strength development can be predicted, already from the gelling concentration onwards.

It also appears that it works the other way round: the influence of clay plasticity extends into the domain of fluid mechanics as well. It is related to the gelling concentration, which is one of the most important state parameters in cohesive sediment transport. In that respect, the established relation between the gelling concentration and Plasticity Index enables us to actually link fluid and soil mechanics. Therefore, this is a substantial step forward in linking these two research fields.

6.2 Recommendations

For daily practice:

- If you want to study the settling and self-weight consolidation for different clay types, it is advisable to start with comparable initial Liquidity Indices. This ensures that the settling tests start from comparable initial states (from a soil mechanical perspective).
- More generally speaking: to properly compare the settling and self-weight consolidation behaviour of different mud types, normalize the results through the Atterberg Limits. This can be done for both settling curves and consolidated volumes.
- Although it was concluded that pyrite oxidation will probably not impact the pH of the Markermeer substantially, other soils and mud layers containing pyrite should be treated with caution. Dredging the mud, thereby bringing the mud from an anoxic to oxic state can cause the pyrite to oxidize. If no calcium carbonate is present to buffer it, the soil pH can fall to values of 3-4. This may have grave influences on the flora and fauna in and on the reclamations that are created.

For future research:

- Compare the results from this study with numerical models solving the Gibson equation. This way, it can be verified whether the outcomes of this research can be reproduced with numerical models.
- The settling and self-weight consolidation behaviour of the Bentonite cannot be properly explained from a fluid mechanical point of view. The used initial concentration is close to the found gelling concentration, thereby limiting the possibility for floc formation. However, the settled volumes differed greatly and the consolidated volumes ranked oppositely as was to be expected based on flocculation theory. Further study seems appropriate.
- If the gelling concentrations of other mud samples are determined, also determine the Plasticity Index of these samples. By doing so, the power law relation that was found in this research can be verified. Additional data can also be used to improve the statistical reliability of the found power law relation.

Appendix A: Acid Sulphate Soils

This appendix contains information on Acid Sulphate Soils. Originally, this was one of the main subjects of the thesis. During the course of the research, incorporating this into the research was no longer feasible. A desk study was already performed, the results of which are presented in this Appendix.

It was thought that one of the possible factors that may be of interest is acidification of the soil, when it is brought into contact with oxygen. The soils which exhibit this behaviour are called acid sulphate soils (ASS). This soil type is discussed in this paragraph.

A.1 Introduction to Acid Sulphate Soils

Acid sulphate soils are coastal and near-coastal soils, sediments or other materials which are rich in iron sulphides. They are environmentally benign when left undisturbed in an aqueous, anoxic environment, but when exposed to oxygen the iron sulphides break down, releasing sulphuric acid and soluble iron. Both substances have considerable ability to degrade the natural and built environment, and the acid may additionally mobilise other pollutants (e.g. aluminium, lead, zinc) if present in the soil. The primary source of inorganic acidity in ASS is iron disulphide, also known as pyrite (FeS_2) (Dear, 2014).

It is stressed that soils containing pyrite are only potential acid sulphate soils if the potential acidity represented by the pyrite is greater than the acid-neutralising capacity of the soil. This neutralising capacity could be provided by carbonates, exchangeable bases or easily-weathered silicates (Dent, 1986). Of these three, calcium carbonate stands out in both rate of reaction and neutralising capacity, and therefore a guideline whether a soil is classified as an acid sulphate soil is based on the pyrite ánd the calcium carbonate content. This is expressed in the Soil Taxonomy manual, where potential acid sulphate soils are specified as: 'waterlogged mineral or organic soil materials that contain 0.75 per cent or more sulphur (dry weight) mostly in the form of sulphides and that have less than three times as much carbonate ($CaCO_3$ equivalent) as sulphur' (Soil Survey Staff, 1975).

Acid sulphate soils occur in environments which share five common factors, which are crucial to the formation of pyrite. The list presented here is based on the research by Ritsema et al. (2000), and Sammut et al. (1996): ASS occur in environments with the following characteristics (1) a supply of organic matter, (2) severely reducing conditions brought about by continuous waterlogging, (3) a supply of SO_4^{2-} (sulphate), usually from seawater, that is reduced to sulphides by bacteria decomposing the organic matter, (4) a supply of iron from the sediment for the accumulation of iron sulphides and (5) anoxic circumstances.

To see why the above conditions play a role in the formation of pyrite, this formation process is further elaborated upon in the following section.

A.2 Pyrite formation

The description of pyrite formation is largely based on the work by Berner (1984): Sedimentary pyrite forms during shallow burial, via the reaction of detrital iron minerals with H_2S. The H_2S, in turn, is produced by the reduction of interstitial dissolved sulphate by bacteria using sedimentary organic matter as a reducing agent and energy source. The initial product of this reaction is not, in fact, pyrite but rather a series of metastable iron monosulfides which transform to pyrite under most conditions, but by a process that is rather poorly understood, according to Berner (1984). The process is illustrated in Figure A.1.

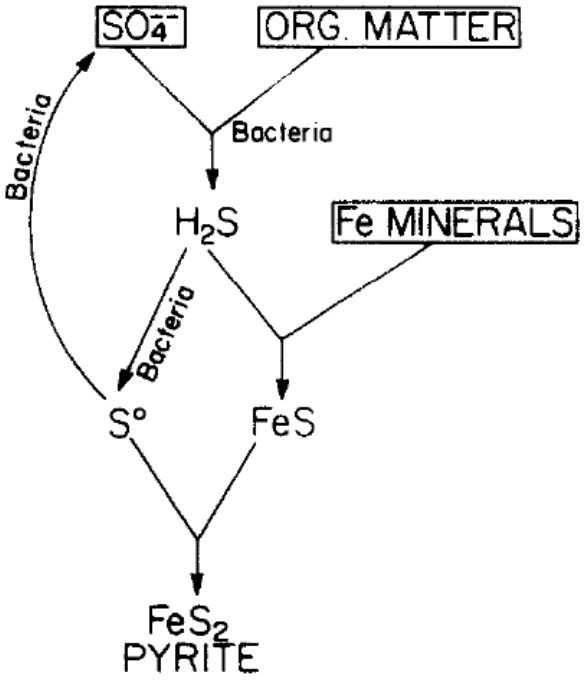

Figure A.1: Diagrammatic representation of the overall process of sedimentary pyrite formation (Berner, 1984)

In freshwater sediments this process is limited by low concentrations of dissolved sulphate and as a result, little pyrite is formed. In normal marine sediments (those deposited in oxygen-containing bottom waters), pyrite formation is limited mainly by the amount and reactivity of organic matter buried in the sediment. In euxenic marine sediments (those deposited in anoxic, H_2S-containing bottom waters), a plentiful supply of both organic matter and hydrogen sulphide brings about the formation of high concentrations of pyrite which are limited only by the reactivity of the iron minerals brought to the site of deposition (Berner, 1984). The latter category is found in tidal swamps and salt marshes, which abundantly fulfill (Ritsema et al., 2000) the five characteristics as described in Appendix A.1.

Now that the mechanisms of pyrite formation, and hence, the genesis of acid sulphate soils are known, it is useful to elaborate on where these soils occur. The next paragraph will address the occurrence of this soil type worldwide.

A.3 Occurrence of acid sulphate soils

Andriesse and van Mensvoort (2006) provided an estimate of the occurrence of ASS; they stated that potential and actual acid sulphate soils occupy an area of some 17 million ha worldwide, where the topsoil is severely acid or will become so if drained. In addition, there may be as much acid sulphate soils which are covered by layers of peat and/or nonsulfidic alluvium (Dent, 1986). Therefore, but also because of scanty field surveys, even fewer reliable laboratory data and also, variable definition, estimates of the extent and distribution of ASS prove not to be highly reliable. The current estimates, given per continent, are shown in Figure A.2.

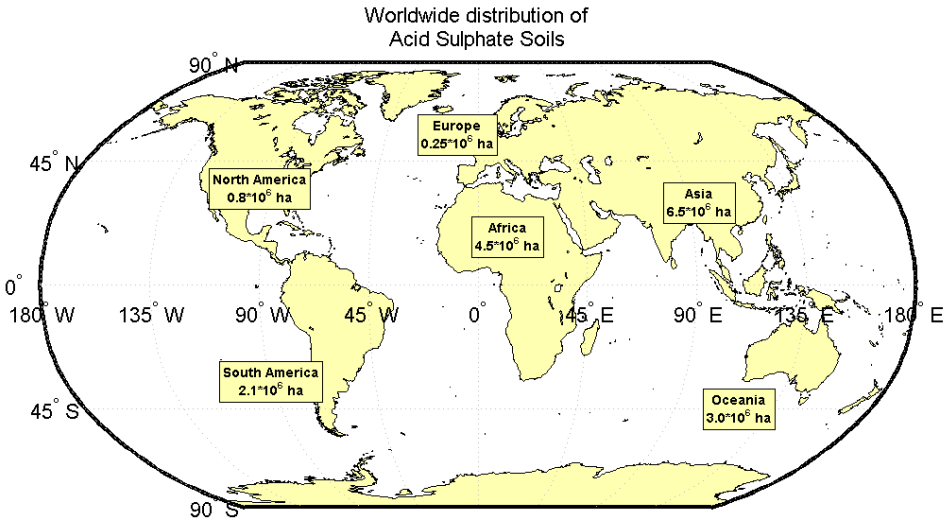

Figure A.2: Worldwide distribution of Acid Sulphate Soils, grouped per continent. Estimates based on Andriesse and van Mensvoort (2006)

More significant than their actual area is their location: ASS are concentrated in otherwise densely populated coastal and floodplains, mostly in the tropics, where development pressures are intense and little suitable alternative land for expansion of farming or urban and industrial development exists (Ritsema et al., 2000). Large extensions of ASS occur in South and Southeast Asia, Australia, West Africa and along the north-eastern coast of South America. Smaller areas are found in coastal regions of Eastern and Southern Africa, and in the Caribbean. In Southeast Asia, the bulk of the ASS is found in Indonesia, Thailand and Vietnam (Andriesse and van Mensvoort, 2006). An overview of the acreages per continent, as presented by Andriesse and van Mensvoort (2006), is given in Appendix A.5.

Other researchers showed that these soils also exist in countries with a cold or moderate climate, such as Finland (Palko, 1994) and areas in the Netherlands, which were reported as being ASS already in the 19th century (van Bemmelen, 1886).

It must be noted that ASS exhibit large spatial variations, tied to the highly dynamic estuarine, deltaic and flood plain environments of which they are a part. For instance, if sedimentation or

erosion occurs slowly, tidal marshes stay in place, and extensive plains of acid sulphate soil develop. Where there has been heavy sedimentation, older sulphidic clays have been buried by non-sulphidic alluvium. Apart from spatial variations, ASS also exhibit very significant temporal variability, not least in their defining characteristics of acidity and related toxicities.

Now that the occurrence of these soils has been identified, it is useful to elaborate on the possible consequences of exposing these soils to oxygen, which is likely to happen when they are dredged.

A.4 Pyrite oxidation

As was stated before, the presence of pyrite does not have a detrimental effect on the environment, when it is left under anoxic conditions. However, when it is brought into contact with oxygen, the pyrite oxidizes. When pyrite oxidizes, it forms: ferrous sulphate, ferric oxide, jarosite and sulphuric acid. During oxidation of pyrite, the supply of O_2 is rate limiting. Upon slow oxidation of pyritic soil in situ, buffering by clay minerals, jarosite, and ferric oxide, keeps pace with acid formation, and the pH remains between 3 and 4. Lower pH values may develop with rapid oxidation as in excavated soil and aerated pyritic soil samples (van Breemen, 1982).

When pyrite is exposed to air and water, the following overall stoichiometric reactions may characterize the oxidation of pyrite (Stumm and Morgan, 1996):

$$2\ FeS_2 + 7\ O_{2\,(aq)} + 2\ H_2O \dashrightarrow 2\ Fe^{2+} + 4\ SO_4^{2-} + 4\ H^+$$

$$4\ Fe^{2+} + 4\ O_{2\,(aq)} + 4\ H^+ \dashrightarrow 4\ Fe^{3+} + 2\ H_2O \qquad \text{(A.1)}$$

$$FeS_2 + 14\ Fe^{3+} + 8\ H_2O \dashrightarrow 15\ Fe^{2+} + 2\ SO_4^{2-} + 16\ H^+$$

The overall pyrite oxidation reaction has also been expressed as (van Breemen, 1976):

$$4\ FeS_2 + 15\ O_2 + 14\ H_2O \dashrightarrow 4\ Fe(OH)_3 + 8\ SO_4^{2-} + 16\ H^+ \qquad \text{(A.2)}$$

The main conclusion from these chemical reactions is the fact that upon oxidation of pyrite, sulphuric acid is formed, which causes a significant drop in pH, when no buffering capacity is present. However, a couple of remarks should be made regarding the oxidation of pyrite:

- Buffering capacity can be provided by seawater and calcareous soils (rich in $CaCO_3$). It can also be done by available shells, or when processing acid sulphate soil industrially, with agricultural lime (Dear, 2014). The reaction of calcium carbonate with sulphuric acid is as follows: $CaCO_3 + H_2SO_4 \dashrightarrow CaSO_4 + H_2O + CO_2$
- Pyrite is not the only material available in mud which is able to oxidize. Organic matter is also oxidizing, thereby consuming part of the available oxygen. As was stated before, the

supply of oxygen is rate-limiting in the pyrite oxidation process. It could be possible that the available oxygen is used up by oxidizing organic matter.

Another question is what the relevant timescales are for pyrite oxidation: van Breemen (1976) artificially aerated acid sulphate soil samples, and found that the pH decreased, but that its timescale was of the order weeks to months. Ritsema et al. (2000) noted that bacteria-catalysed oxidation of FeS_2 is most important as chemical reactions are very slow and the presence of bacteria enhances the oxidation process by orders of magnitude. Therefore, he advised to perform analyses of ASS before gross chemical changes take place, or the samples must be dried quickly. Otherwise, the pH may fall from 7 to less than 3 within days or weeks. The question remains how dredging and depositing the soil relates to artificially aerating soil samples.

A.5 Overview of Acid Sulphate Soils acreages per continent

Andriesse and van Mensvoort (2006) published estimates of Acid Sulphate Soil acreages per country and continent. Table A.1 lists the estimates per continent.

Table A.1: Acid Sulphate Soil occurrence estimates. After Andriesse and van Mensvoort (2006).

Occurrence of ASS on different continents, area (1000 ha)			
Region/Country	**FAO 1974 estimate**	**Revised estimate: Langenhoff (1986)**	**Revised estimate: Andriesse (2002)**
Africa	3655	4415	4490
Asia	5610	5770	6515
Australia	-	-	3000
Latin America and the Caribbean	2720	275	2800
North America	100	100	100
Europe	5	10	235
Total	12090	13080	17100

Appendix B: Relations between fluid and soil mechanics

B.1 Sediment concentration expressed as a void ratio

In Section 2.5, the settling and self-weight consolidation behaviour of mud was expressed in terms of either: sediment concentration c [g/l], volumetric concentration φ [-] or void ratio e [-].

However, the Atterberg limits, as they were introduced in Section 2.6.2, are a function of the water content of a soil or slurry. It may be convenient to express the Atterberg Limits and the indices related to it in terms of one of the above parameters.

As the self-weight consolidation equation, as proposed by Gibson, and the parameters linked to it, are expressed in terms of the void ratio e, the choice is made to express Liquidity Index (LI) in terms of void ratio.

To do so, first the average concentration of the suspension (/settled bed) is given by:

$$\bar{c} = c_0 * \frac{h_0}{h(t)} \tag{B.1}$$

Figure B.1 shows a sketch of these terms.

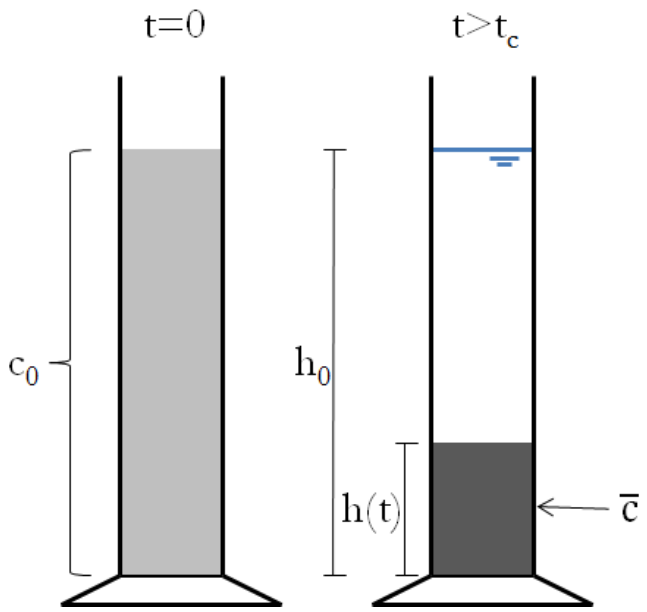

Figure B.1: Schematized settling column with indication of terms in Equation B.1.

If the average concentration is known, the average void ratio can be computed according to:

$$\bar{e} = \frac{\rho_s - \bar{c}}{\bar{c}} \tag{B.2}$$

And, if all the pores in the sediment bed are filled with water, the void ratio is linked to the water content as follows (by definition):

$$e \overset{\text{def}}{\equiv} W \frac{\rho_s}{\rho_w} \tag{B.3}$$

Assuming that these densities do not change during the consolidation process, combining Equations (2.19) and Equation B.3, leads to the Liquidity Index which can be written as:

$$LI = \frac{\bar{e} * \left(\frac{\rho_w}{\rho_s}\right) - e_{PL} * \left(\frac{\rho_w}{\rho_s}\right)}{e_{LL} * \left(\frac{\rho_w}{\rho_s}\right) - e_{PL} * \left(\frac{\rho_w}{\rho_s}\right)} \xrightarrow{yields} LI = \frac{\left(\frac{\rho_w}{\rho_s}\right) * (\bar{e} - e_{PL})}{\left(\frac{\rho_w}{\rho_s}\right) * (e_{LL} - e_{PL})} \tag{B.4}$$

And hence:

$$LI = \frac{\bar{e} - e_{PL}}{e_{LL} - e_{PL}} \tag{B.5}$$

Appendix C: Experimental results

In this appendix experimental results are included. The measured results include:

- Material properties (C.1)
- Settling curves (C.2)
- Undrained shear strength (C.5)

Calculated and fitted data include:

- Gelling concentrations (C.3)
- Consolidation parameters (C.4)

C.1 Material properties

The material properties that were determined for the Kaolinite, Bentonite and Markermeer clay. Also the tap water specifications for the tap water used in the settling column experiments at the BKD laboratory.

C.1.1 Kaolinite

Following properties are presented in this section:

- Particle size distribution
- Cation Exchange Capacity
- Water content

Particle size distribution (psd)

The particle size distribution of the kaolinite clay powder is determined using a Malvern Mastersizer with a Hydro 2000MU measuring cell. Results are plotted in Figure C.1.

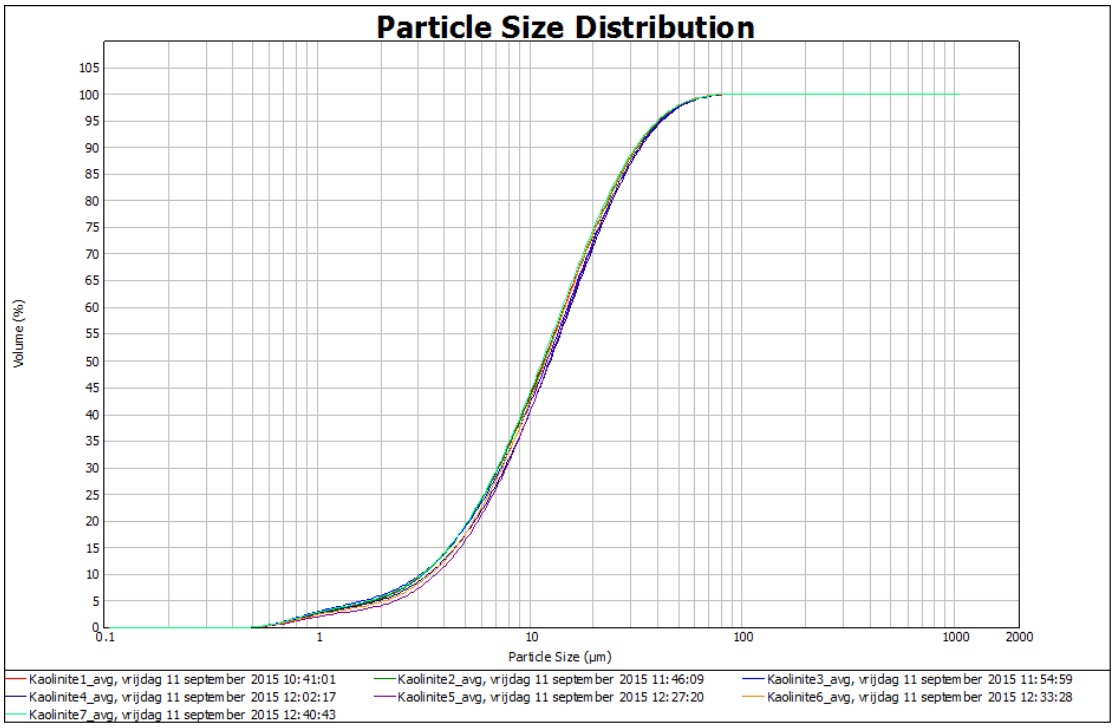

Figure C.1: Particle size distribution of kaolinite clay powder

The seven different coloured lines correspond to the seven experimental runs performed with the Malvern Mastersizer. The experimental runs and their settings are listed in Table C.1. The peptisator used for run 2-7 is sodium pyrophosphate.

Table C.1: Settings for psd determination of kaolinite with Malvern Mastersizer

Run	Suspension	RPM	Ultrasonic bath
1	Demineralized water	1500	No
2	Peptisator	1500	No
3	Peptisator	1500	Yes
4	Peptisator	1000	Yes
5	Peptisator	600	No
6	Peptisator	1000	No
7	Peptisator	1500	No

Cation exchange capacity

Table C.2: Cation exchange capacity of kaolinite clay powder. Determined with Methylene blue absorption test

Sample number	Dry weight	Volume MB added	Concentration MB	Methylene Blue Absorption	Cation Exchange Capacity
	(g)	(ml)	(g/l)	(g/100g)	meq/100g
K-1	2.01	6.00	3.20	1.0	2.99
K-2	2.40	7.00	3.20	0.9	2.92

Water content

Table C.3: Water content of kaolinite clay powder

Sample name	Mass container(gr)	Combined mass container and wet sample (gr)	Combined mass container and dry sample (gr)	Water content (%)
K-1	9.34	50.22	50.10	0.3

C.1.2 Bentonite

The particle size distribution of the bentonite clay powder is determined using a Malvern Mastersizer with a Hydro 2000MU measuring cell.

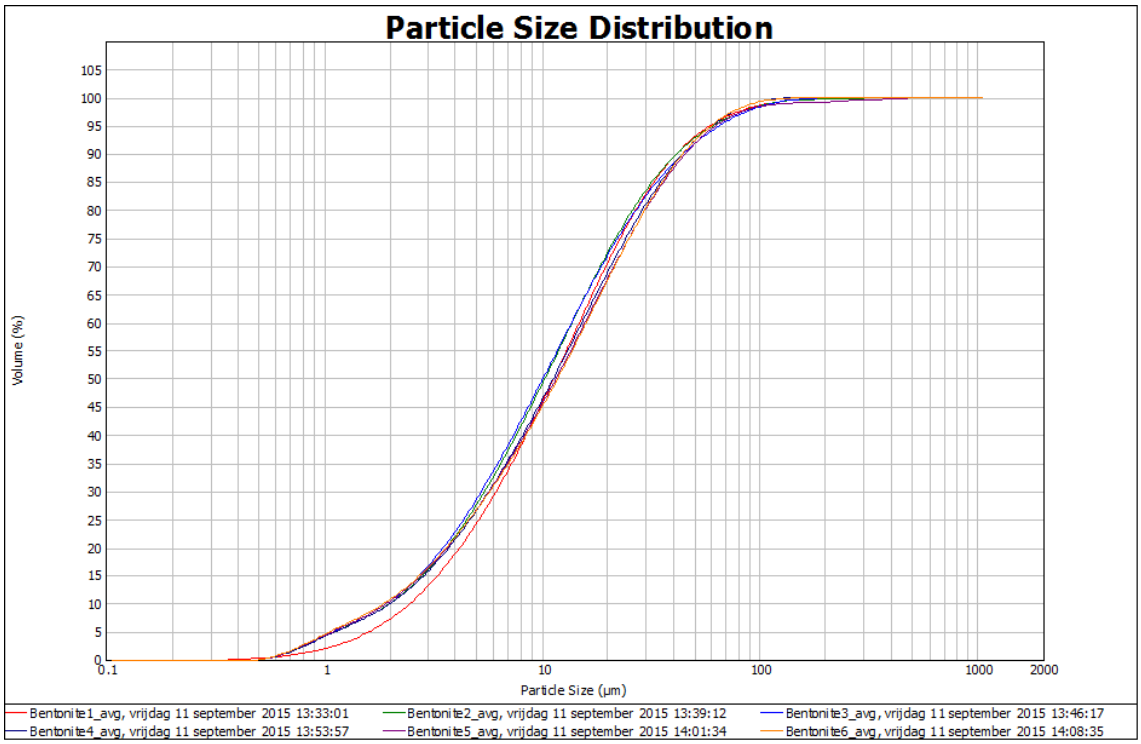

Figure C.2: Particle size distribution of bentonite clay powder

The six different coloured lines correspond to the seven experimental runs performed with the Malvern Mastersizer. The experimental runs and their settings are listed in Table C.4. The peptisator used for all runs is sodium pyrophosphate.

Table C.4: Settings for psd determination of bentonite with Malvern Mastersizer

Run	Suspension	RPM	Ultrasonic bath
1	Peptisator	600	No
2	Peptisator	1000	No
3	Peptisator	1500	No
4	Peptisator	600	Yes
5	Peptisator	1000	Yes
6	Peptisator	1500	Yes

Cation exchange capacity

Table C.5: Cation exchange capacity of bentonite clay powder. Determined with Methylene blue absorption test

Sample number	Dry weight	Volume MB added	Concentration MB	Methylene Blue Absorption	Cation Exchange Capacity
	(g)	(ml)	(g/l)	(g/100g)	meq/100g
BN-1	0.21	16.00	3.20	24.4	76.39
BN-2	0.25	20.00	3.20	25.6	80.21

Water content

Sample name	Mass container(gr)	Combined mass container and wet sample (gr)	Combined mass container and dry sample (gr)	Water content (%)
BN-1	9.44	52.90	48.56	11.1

C.1.3 Markermeer clay

The Markermeer clay was sampled from the location as indicated in Figure C.3. The coordinates of this location are WGS84: 52.3795, 5.0209.

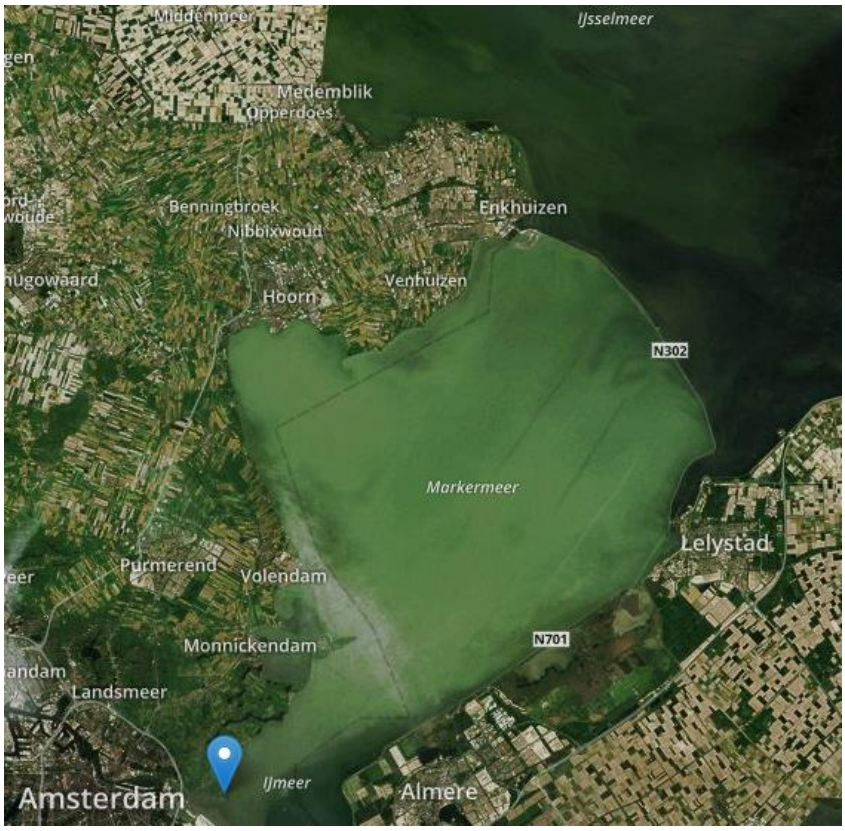

Figure C.3: Satellite image of Markermeer, with the blue marker (in the bottom left corner) indicating the sampling site of the MM-IJ2 sample. Image retrieved from Boskalis.world web portal on 20-01-2016

Particle size distribution

To verify the experimentally determined particle size distribution of Barciela Rial (2015), the mud fraction (<63 μm) is determined according to the Dutch RAW standard (CROW, 2000). Results listed in Table C.6.

Table C.6: Determined mud fraction of MM-IJ2 clay sample

Sample name	Mass beaker glass (gr)	Mass sample (gr)	Combined mass beaker and sample >63 μm (gr)	Fraction <63 μm (%)
MM-IJ2	199.01	107.08	209.50	90.2

Loss on ignition

Check with BKD lab the relevant procedure for the loss on ignition.

Table C.7: Loss on ignition of MM-IJ2 clay sample

Sample name	Mass crucible (gr)	Mass crucible and sample, dried (gr)	Mass crucible and sample, after ignition (gr)	loss on ignition (%)
MM-IJ2-A	32.26	46.03	44.75	9.3
MM-IJ2-B	32.48	47.65	46.29	8.9

Water content

Sample name	Mass container(gr)	Combined mass container and wet sample (gr)	Combined mass container and dry sample (gr)	Water content (%)
MM-IJ2-1	9.45	237.07	102.37	145.0
MM-IJ2-2	9.38	271.85	115.51	147.3
MM-IJ2-MBR	N/A	28.2	11.8	139.0

Zeta potential of samples

The zeta-potential was determined for three samples from the LSC experiment. Samples LSC-1, LSC-2 and LSC-3 were sampled from their respective columns after shear vane testing. These samples were diluted with demineralized water, and then brought to constant ionic strengths with either calcium chloride ($CaCl_2$) or potassium chloride (KCl). This way the effect of mono- and divalent ions on the mud sample could be determined. The results are plotted in Figure C.4.

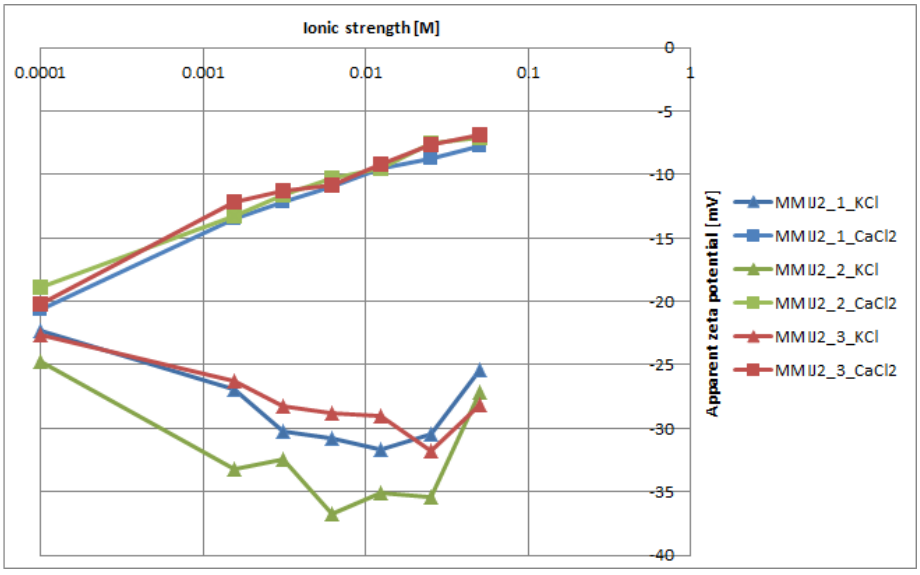

Figure C.4: Measured zeta potential for Markermeer clay samples, borught to constant ionic strengths either with monovalent (KCl) or divalent salt (CaCl2).

C.1.4 Tap water characteristics

For the majority of the small settling column experiments (1 L), tap water was used. Tap water contains a variety of dissolved ions, that depend on catchment area and treatment. The characteristics of the tap water in Papendrecht (at the BKD laboratory) were retrieved from the OASEN drinking water company on 17-09-2015. Table C.8 is an excerpt of this data, displaying the relevant information. The 3rd quarter of 2015 is chosen as the relevant period because the majority of the experiments were conducted during this period.

Table C.8: Tap water characteristics for 3rd quarter of 2015 at WPS Alblasserdam, the Netherlands

Factsheet: water composition measured at water pumping station Alblasserdam				
Parameter	unit	Minimum 2015	Mean of 3rd quarter 2015	Maximum 2015
Descriptive parameters				
Acidity level at 20° C	pH	7.78	7.98	8.23
Electrical conductivity	mS/cm	0.42	0.53	0.64
Total organic carbon (TOC)	mg/l	1.35	1.58	1.81
Water hardness	mmol/l	1.28	1.83	2.34
Dissolved ions (major)				
Chloride	mg/l	59.8	81.4	103.0
Hydrogen carbonate	mg/l	123.0	163.6	185.5
Sodium	mg/l	47.5	51.0	57.0
Sulphate	mg/l	33.5	44.7	62.4
Dissolved ions (minor)				
Aluminum	µg/l	2.06	7.04	14.96
Ammonium	mg/l	<0.03	<0.03	<0.03
Iron	mg/l	<0.01	<0.01	<0.01
Manganese	mg/l	<0.005	<0.005	<0.005
Oxygen	mg/l	9.02	10.12	11.03

C.2 Settling curves

The settling curves for both the small settling column (1L) and large settling column (2L) experiments are presented here. A distinction is made between the settling phase and the consolidation phase. For the latter, the x-axis is set to logarithmic scale.

C.2.1 Hindered settling phase – Small and Large settling column experiments

Because the Bentonite showed no clear settling phase, only the results for the kaolinite and Markermeer clay are included.

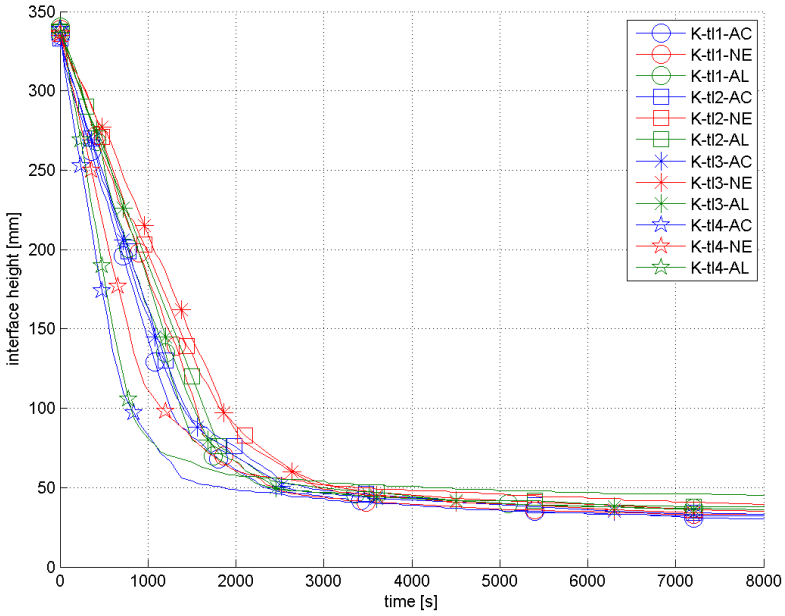

Figure C.5: Settling curves for hindered settling phase of SSC experiment. Material: Kaolinite

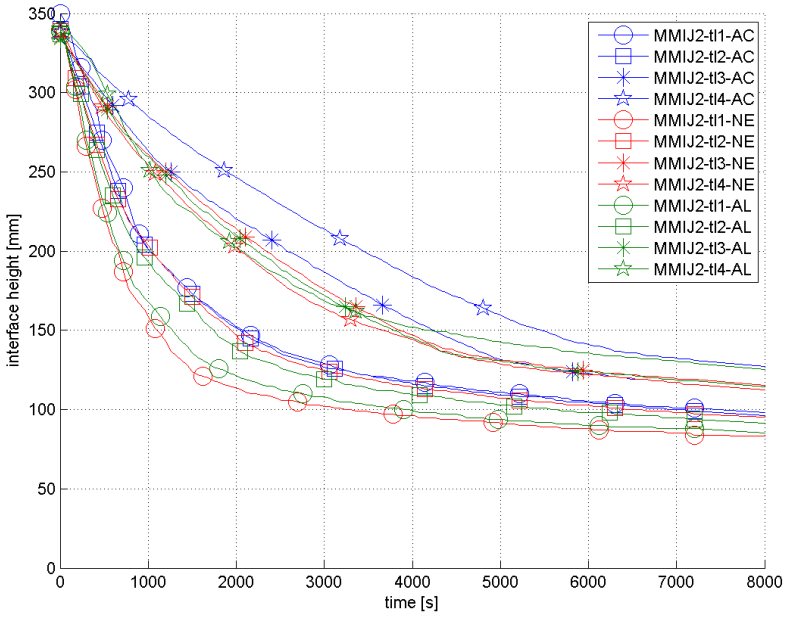

Figure C.6: Settling curves for hindered settling phase of SSC experiment. Material: Markermeer clay

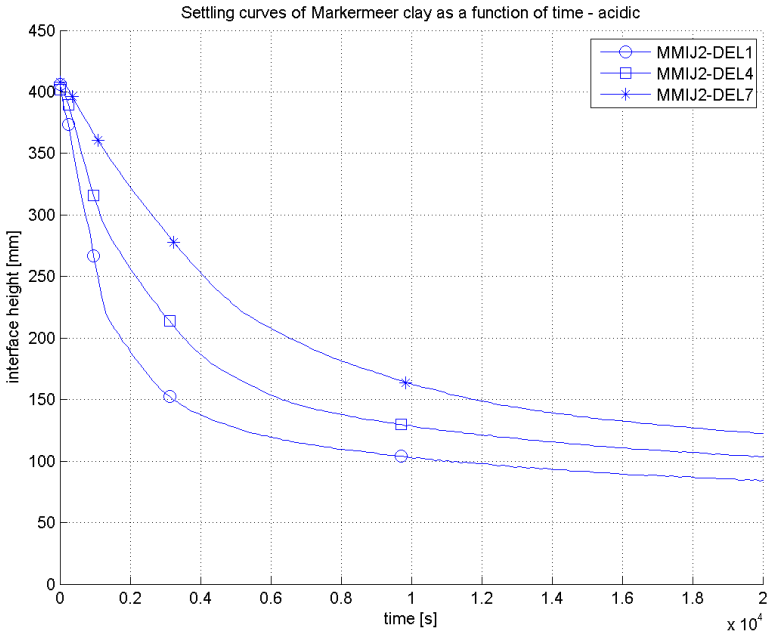

Figure C.7: Settling curves for hindered settling phase of LSC experiment. Material: Markermeer clay. Initial concentrations vary between 30, 40 and 50 g/l. pH conditions: acid

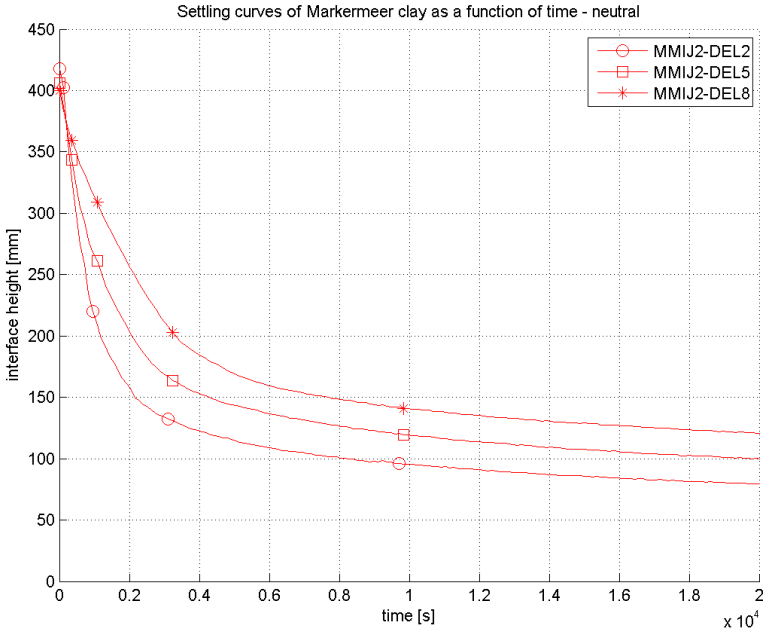

Figure C.8: Settling curves for hindered settling phase of LSC experiment. Material: Markermeer clay. Initial concentrations vary between 30, 40 and 50 g/l. pH conditions: neutral

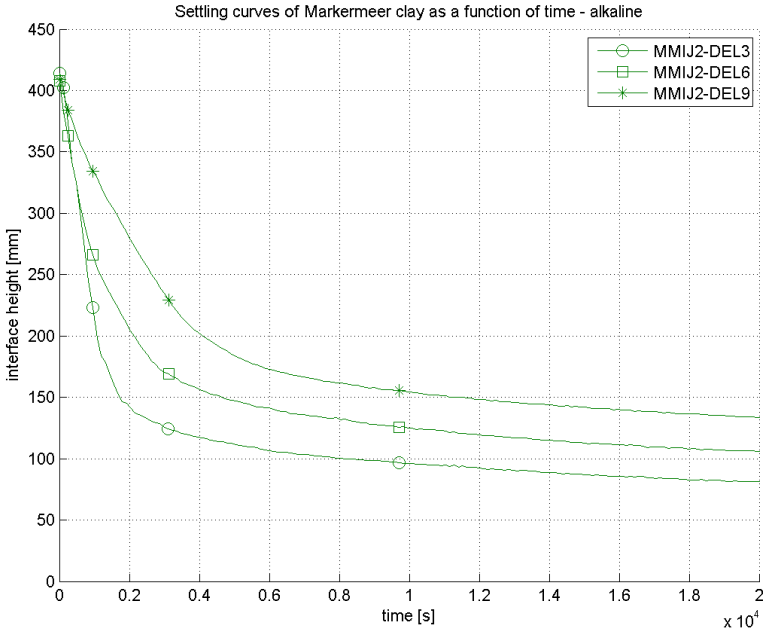

Figure C.9: Settling curves for hindered settling phase of LSC experiment. Material: Markermeer clay. Initial concentrations vary between 30, 40 and 50 g/l. pH conditions: alkali

C.2.2 Self-weight consolidation phase – Small and Large settling column experiments

Only the last of the small settling column experiments was geared towards studying the consolidation phase. Therefore, this is the only experiment that is included. For the large settling column experiment, all settling curves are included.

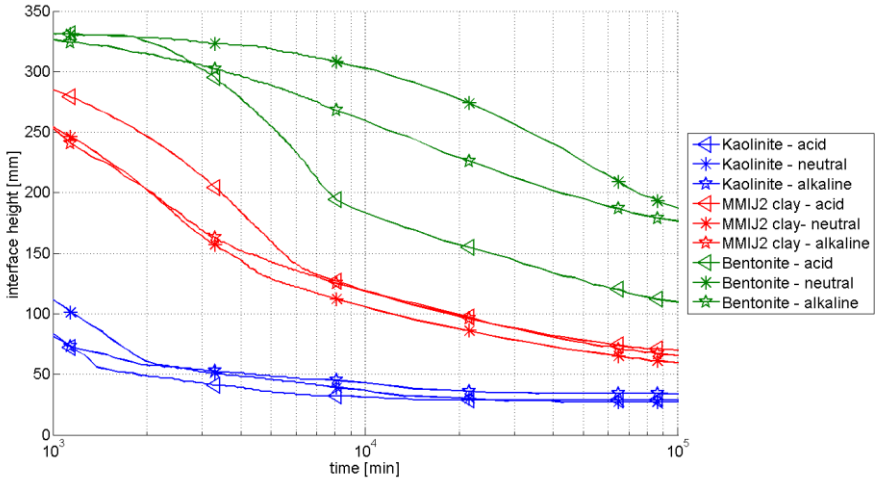

Figure C.10: Settling curves for self-weight consolidation phase of SSC experiment. Materials: Kaolinite, Markermeer clay and Bentonite. Initial concentration: 40 g/l. pH conditions vary between acid, neutral and alkaline

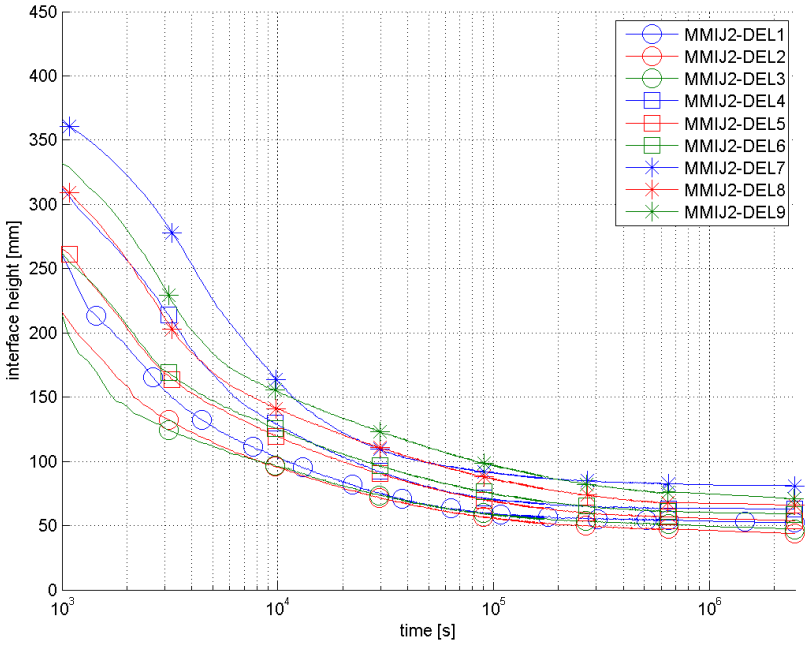

Figure C.11: Settling curves for self-weight consolidation phase of LSC experiment. Material: Markermeer clay. Initial concentrations vary between 30, 40 and 50 g/l. pH conditions vary between acid, neutral and alkaline

C.3 Gelling concentration

C.3.1 Bentonite

The gelling concentration could not be determined from the SSC experiments. This was because the initial concentration was approximately the gelling concentration.

A separate experiment was set up, with initial concentrations of 5 and 10 g/l. By fitting the effective settling velocity formula to the measured interface data, the gelling concentration c_{gel}, and the reference settling velocity, $w_{s,0}$ are determined. The curve fit is shown in Figure C.12.

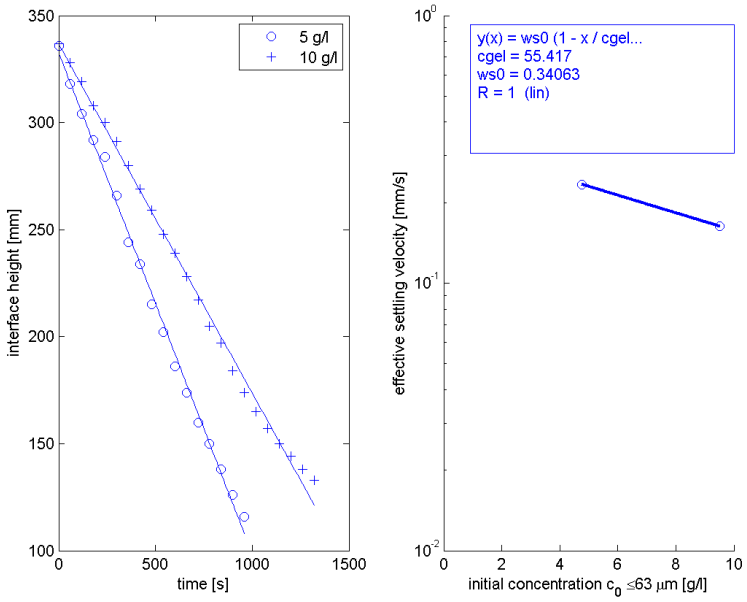

Figure C.12: Gelling concentration fit for bentonite clay. Suspension of demineralized water with ionic strength of 0.02M

C.3.2 Markermeer clay

The gelling concentrations for the large settling column experiments were determined by tracking the suspension-water interface during the hindered settling phase. This was done for all nine columns set up during this experiment. Effective settling velocities were determined by fitting curves through the data, hereby obtaining an estimate for the gelling concentration, c_{gel}, and the reference settling velocity, $w_{s,0}$. The curve fits are shown in Figure C.13, Figure C.14 and Figure C.15.

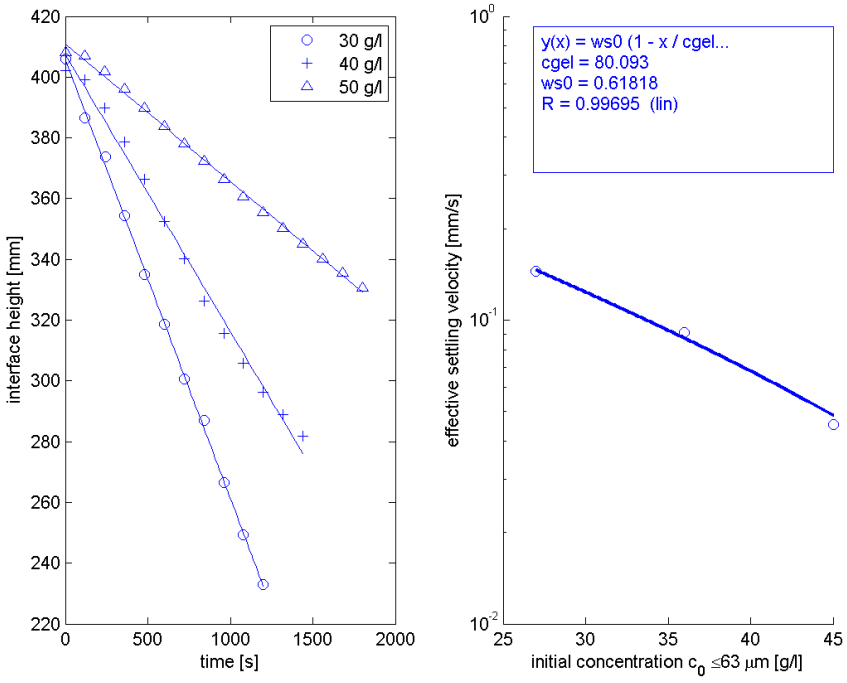

Figure C.13: Gelling concentration fit for acidic conditions. Clay sample: MM-IJ2

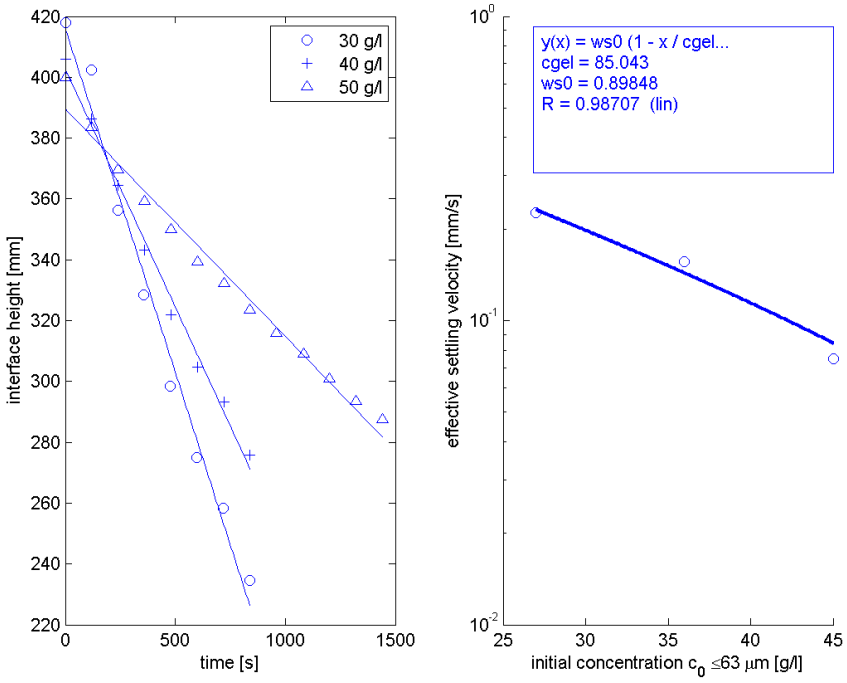

Figure C.14: Gelling concentration fit for neutral conditions. Clay sample: MM-IJ2

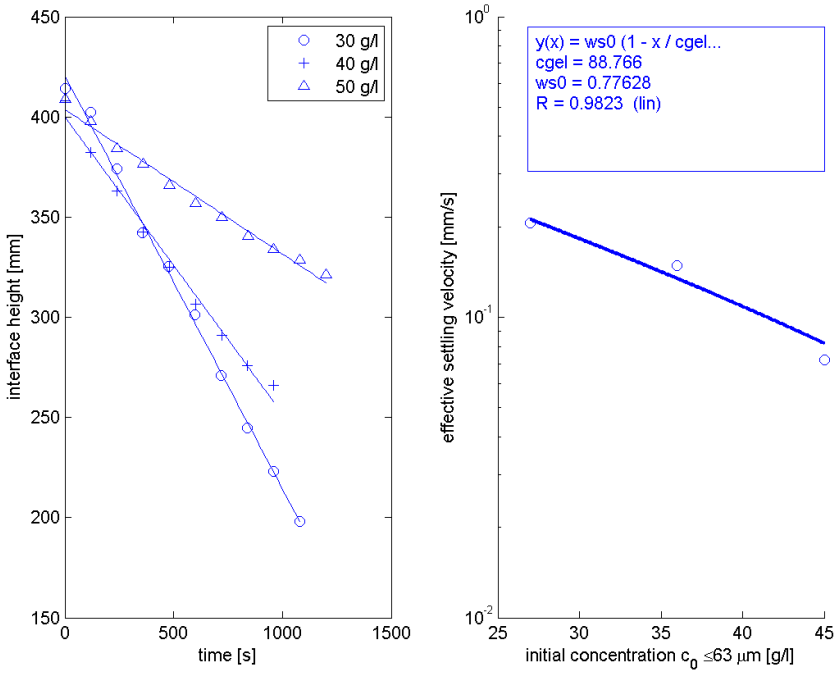

Figure C.15: Gelling concentration fit for alkaline conditions. Clay sample: MM-IJ2

C.4 Consolidation

In this section, the results for the curve fits of consolidation phase I are presented. Equation (2.14) is fitted to the interface measurement data to obtain the parameters K_k and n_f. These parameters are presented in Section 4.3.

For all nine small settling columns, curves were fitted to the measured data. The starting and ending time for these curve fits are listed in Table C.9.

Table C.9: Lower and upper limits for data selection for curve fits of first phase consolidation for SSC experiment

Column code	Lower time limit [s]	Upper time limit [s]
K-1	1.5E+03	7.0E+03
K-2	2.0E+03	7.0E+03
K-3	1.5E+03	7.0E+03
BN-1	1.0E+03	1.0E+05
BN-2	2.0E+04	1.0E+05
BN-3	1.0E+01	1.0E+05
MMIJ2-1	6.0E+03	7.0E+04
MMIJ2-2	4.0E+03	7.0E+04
MMIJ2-3	4.0E+03	7.0E+04

Table C.10: Lower and upper limits for data selection for curve fits of first phase consolidation for LSC experiment

Column code	Lower time limit [s]	Upper time limit [s]
MMIJ2-LSC1	4.0E+03	7.0E+04
MMIJ2-LSC2	4.0E+03	1.0E+05
MMIJ2-LSC3	4.0E+03	1.0E+05
MMIJ2-LSC4	6.0E+03	7.0E+04
MMIJ2-LSC5	4.0E+03	1.0E+05
MMIJ2-LSC6	4.0E+03	1.0E+05
MMIJ2-LSC7	5.0E+03	7.0E+04
MMIJ2-LSC8	4.0E+03	1.0E+05
MMIJ2-LSC9	4.0E+03	1.0E+05

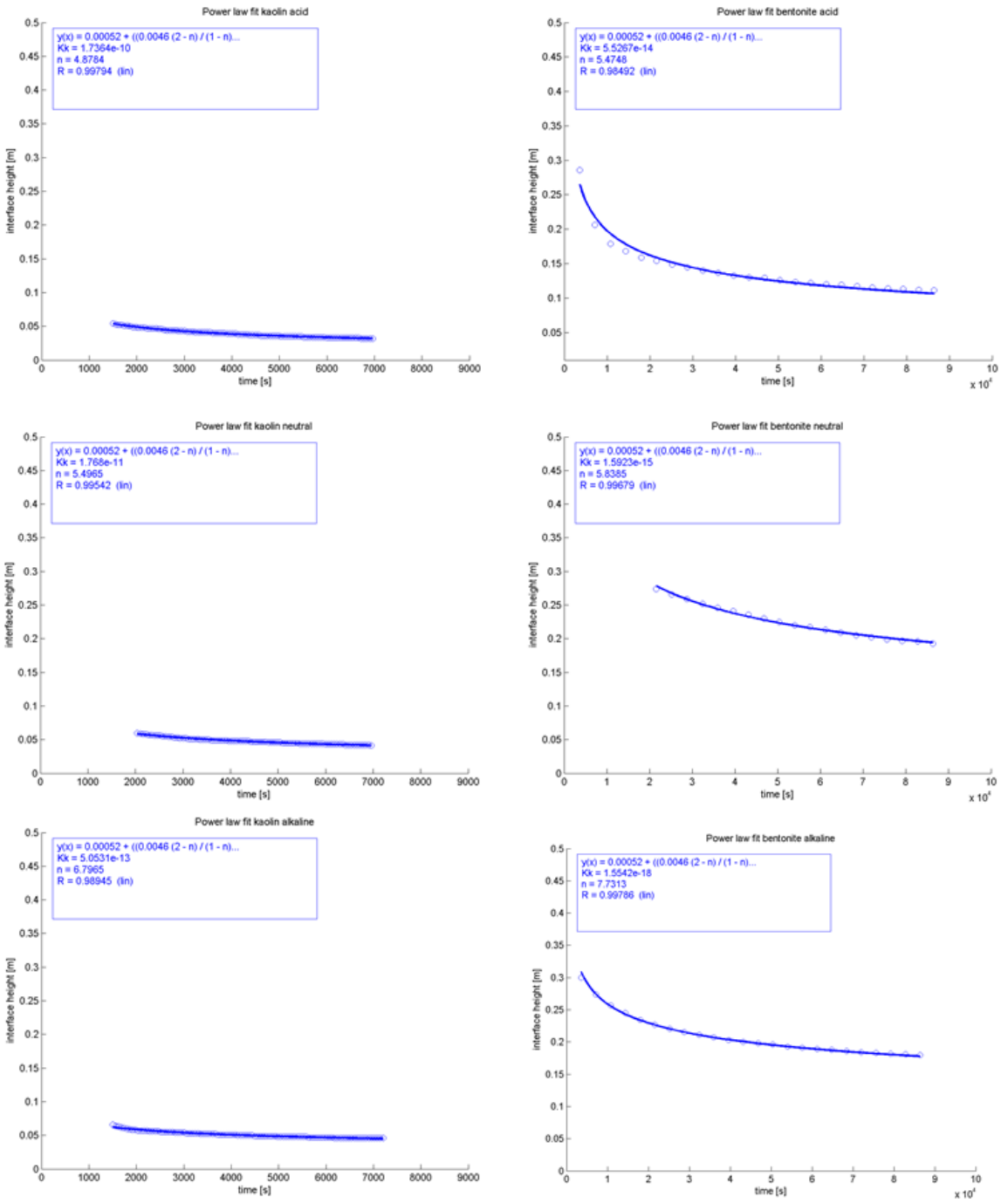

Figure C.16: Curve fits for kaolinite and bentonite for SSC experiment

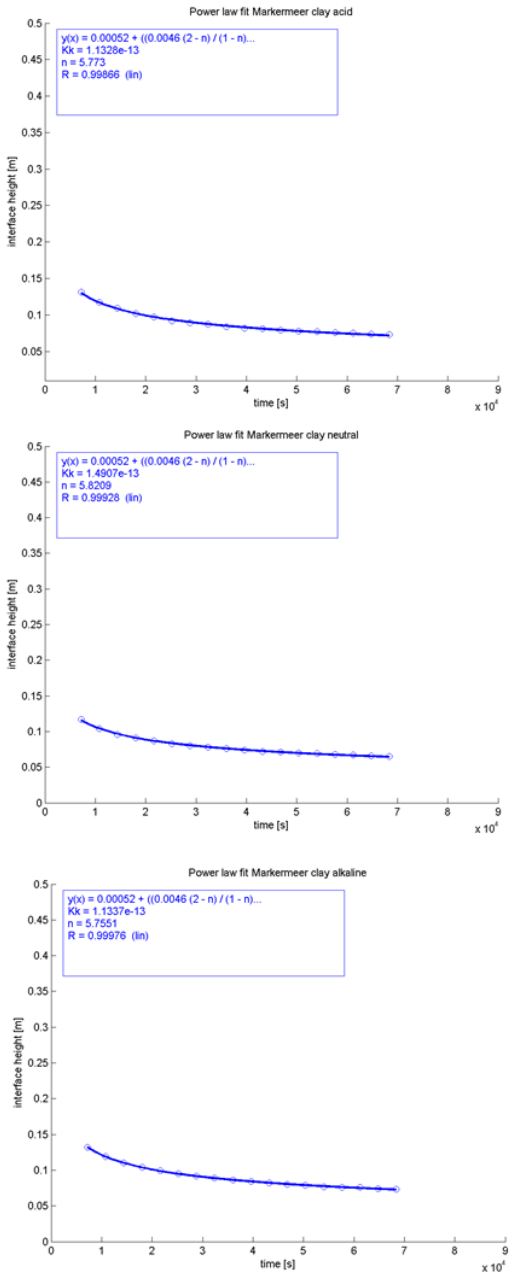

Figure C.17: Curve fits for Markermeer clay for SSC experiments

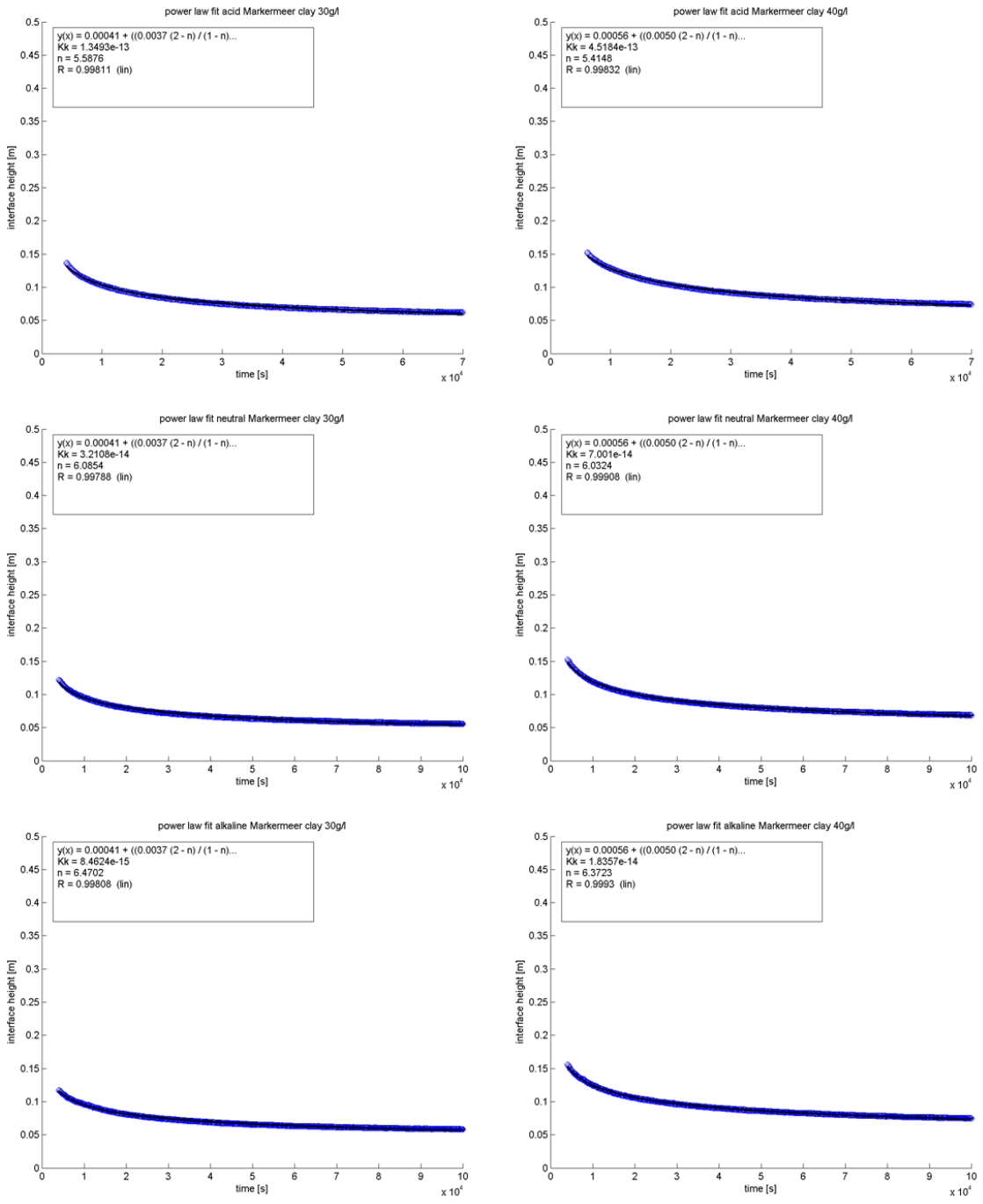

Figure C.18: Curve fits for 30 and 40 g/l Markermeer clay suspensions. LSC experiment

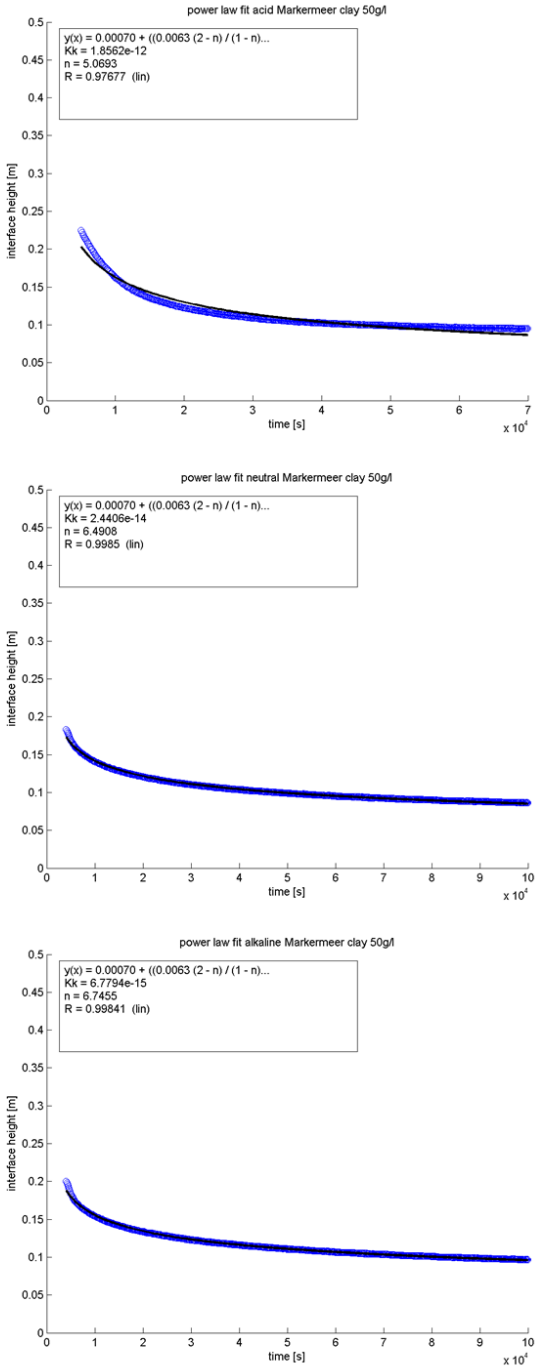

Figure C.19: Curve fits for 50 g/l Markermeer clay suspensions. LSC experiment

C.5 Undrained shear strength

The shear stress curves for the tested samples are presented here. The two features characterising these shear stress curves, the peak strength τ_p and the undrained shear strength c_u are listed in Table 4.13 and Table 4.15.

C.5.1 Small settling column shear stress curves

Output of Haake Viscotester VT550, with FL100 vane. For experimental settings, see Table 4.11.

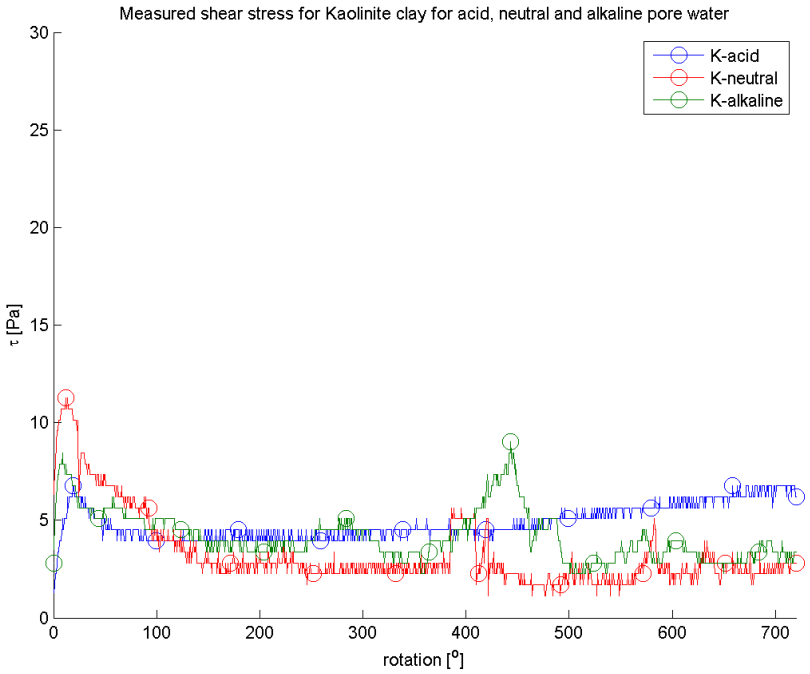

Figure C.20: Measured shear stress curves for kaolinite samples at BKD laboratory.

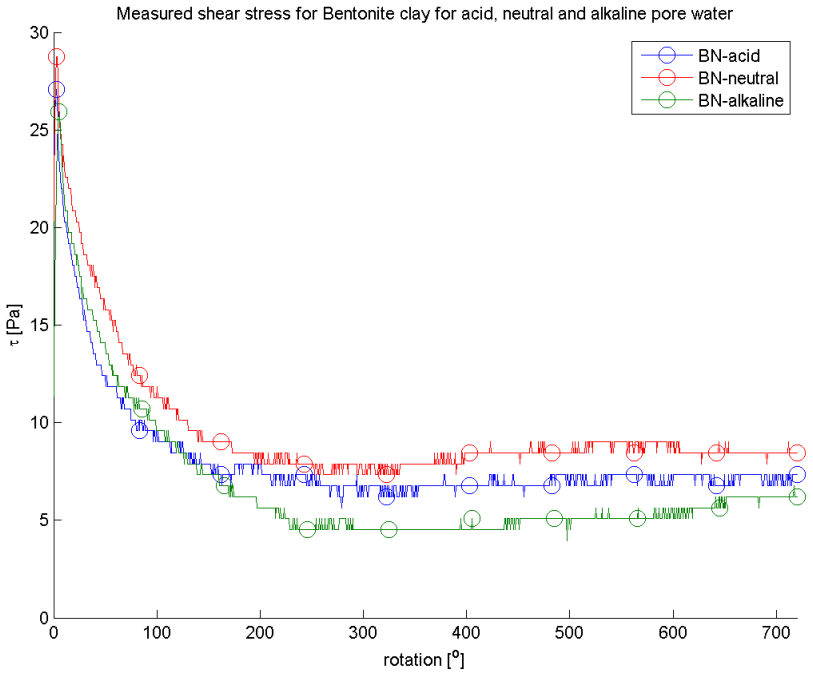

Figure C.21: Measured shear stress curves for bentonite samples at BKD laboratory.

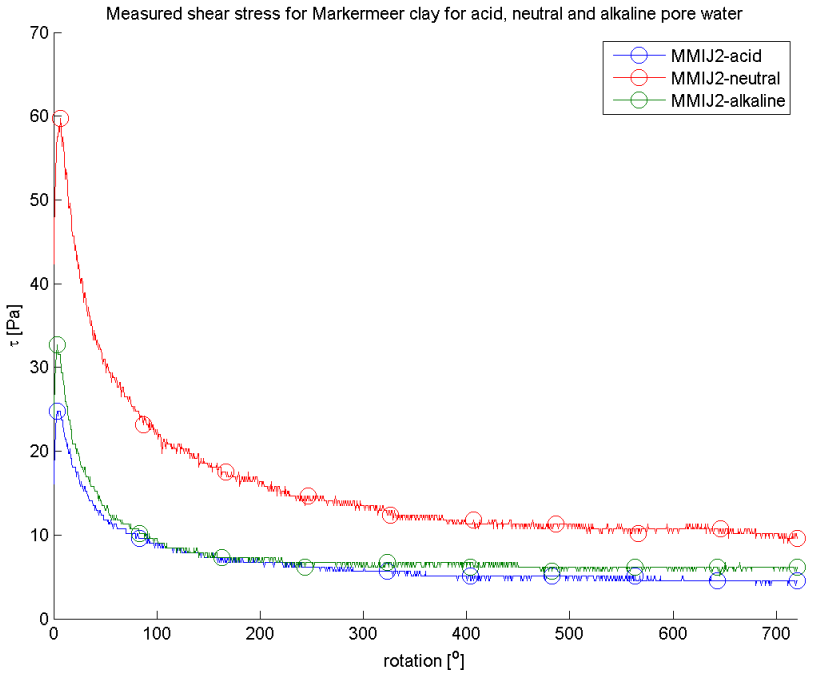

Figure C.22: Measured shear stress curves for Markermeer clay samples at BKD laboratory.

C.5.2 Large settling column shear stress curves

Output of Haake Viscotester VT550, with FL100 vane. For experimental settings, see Table 4.14. Curves plotted in blue correspond with acidic conditions, the red lines are neutral conditions and the green lines are for alkaline conditions.

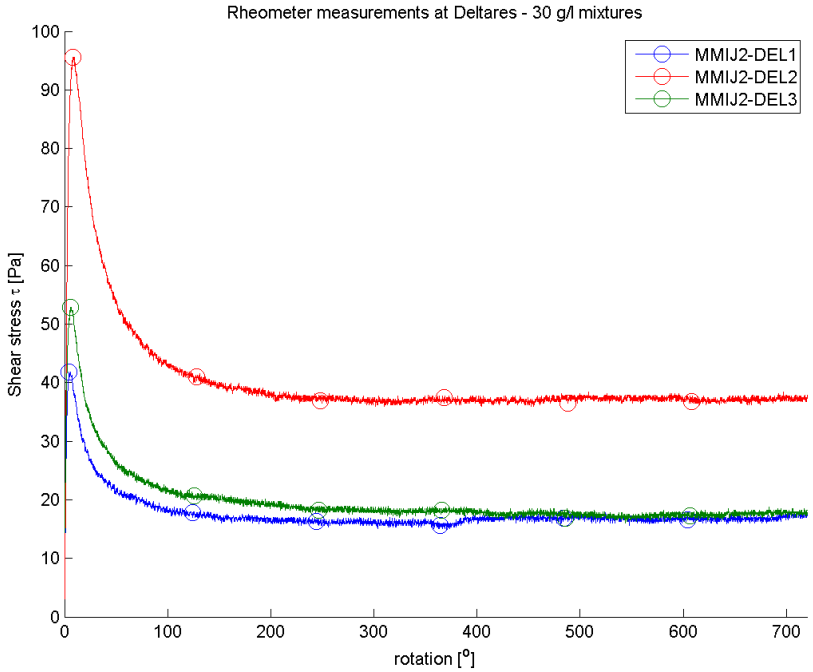

Figure C.23: Measured shear stress curves of 30g/l Markermeer clay mixtures at Deltares FCL laboratory

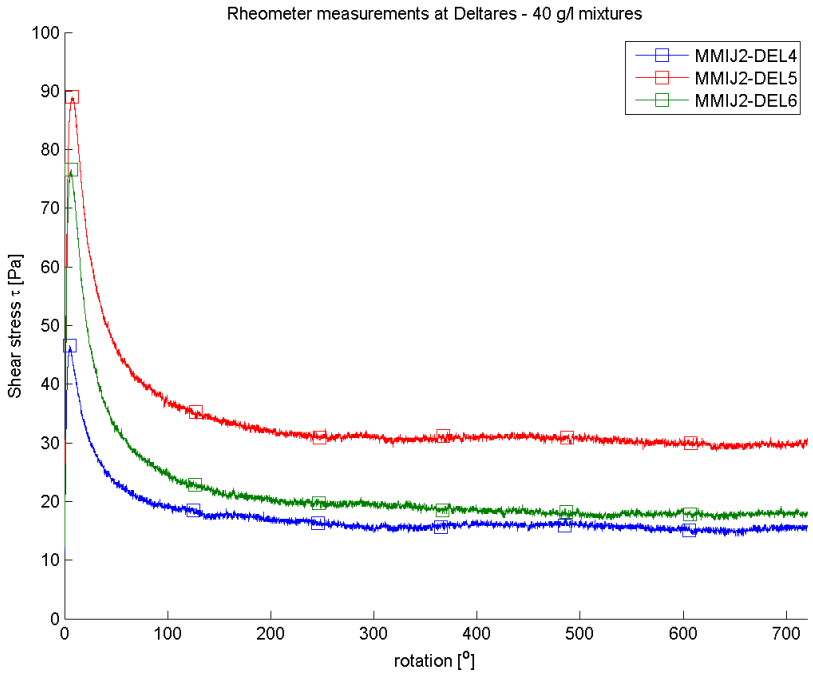

Figure C.24: Measured shear stress curves of 40g/l Markermeer clay mixtures at Deltares FCL laboratory

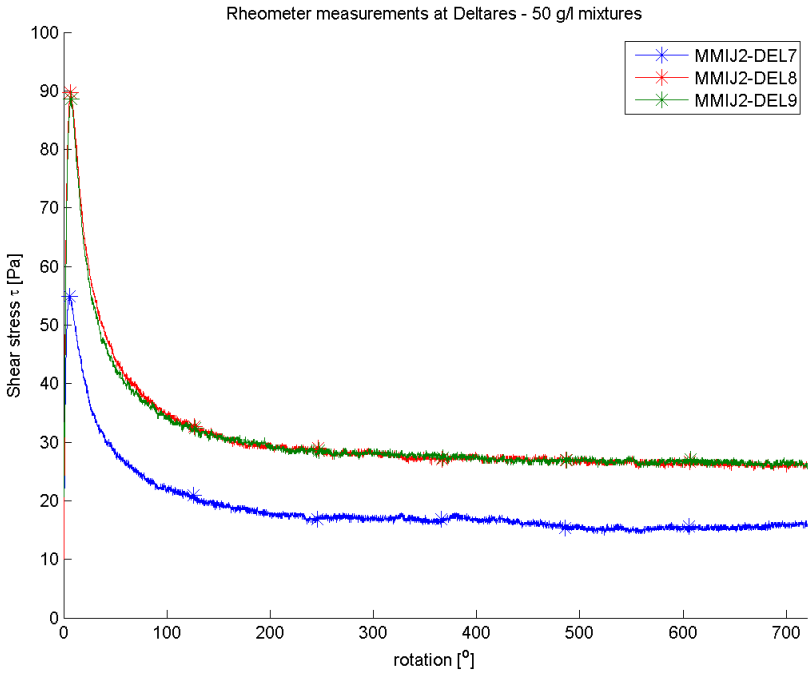

Figure C.25: Measured shear stress curves of 50g/l Markermeer clay mixtures at Deltares FCL laboratory

Appendix D: Nomenclature

D.1.1 List of symbols

Symbol	Description	Unit
Latin		
A	activity of clay	-
c	sediment concentration	kg/m^3
c_0	initial sediment concentration	kg/m^3
$\bar{c}$	averaged sediment concentration	kg/m^3
c_{gel}	gelling concentration	kg/m^3
c_u	undrained shear strength	Pa
c_v	coefficient of consolidation	m^2/s
CEC	Cation Exchange Capacity	meq/100 gr
D	particle diameter	m
D_p	primary particle diameter	m
D_f	mud floc diameter	m
D_{vane}	shear vane diameter	m
e	void ratio	-
$\bar{e}$	averaged void ratio	-
e_{LL}	void ratio corresponding to the Liquid Limit	-
e_{PI}	void ratio corresponding to the Plasticity Index	-
e_{PL}	void ratio corresponding to the Plastic Limit	-
EC	electrical conductivity	S/m
g	gravitational acceleration	m/s^2
G	shear rate	1/s
h	height of mud-water interface	m
h_0	settling column height	m
h_∞	height of mud-water interface after self-weight consolidation	m
h_{sample}	height of sample at moment of shear vane testing	m
h_{vane}	shear vane height	m
k	permeability	m/s
K_k	permeability parameter – fractal approach	m/s
K_p	effective stress parameter – fractal approach	Pa
LI	Liquidity Index	-
LL	Liquid Limit	%
n	number of particles in mud floc	-
n_f	fractal dimension	-
pH	-log of H^+ concentration	-
PI	Plasticity Index	%
PL	Plastic Limit	%
r	diameter of mixing rod plate	m
R	diameter of settling column	m

Symbol	Description	Unit
S_p	mixing jar impeller speed	rpm
t	time	s
t_c	time of contraction	s
w_s	effective settling velocity	m/s
$w_{s,0}$	reference settling velocity of single mud floc	m/s
W	absolute water content as a fraction of solids	-
W_{rel}	relative water content	-
Greek		
α	floc shape factor	-
β	floc shape factor	-
ζ	zeta-potential of double diffuse layer	V
ζ_s	Gibson height – sand fraction	m
ζ_m	Gibson height – mud fraction	m
μ	dynamic viscosity	Pa·s
ξ_{cl}	solids fraction of clay	%
$\xi_{cl,0}$	critical clay content for cohesive behaviour	%
ρ_s	specific density of solids	kg/m^3
ρ_w	density of water	kg/m^3
ϕ	volumetric concentration of flocs	-
ϕ_p	volumetric concentration of primary particles	-

D.1.2 Abbreviations

Abbreviation	Description
Experiments	
BKD	Boskalis Dolman laboratory
FCL	Deltares Fysisch Chemisch Laboratorium
LSC	Large (2L) settling columns
SSC	Small (1L) settling columns
Clay types	
BN	Bentonite
K	Kaolinite
MMIJ2	Markermeer clay – sampled at the IJmeer

References

Andriesse, W. & van Mensvoort, M. E. F. 2006. Acid Sulfate Soils: Distribution and Extent. *In:* Lal, R. (ed.) *Encyclopedia of soil science.* New York, N.Y.: Taylor & Francis.

Barciela Rial, M. 2015. *RE: Sediment heterogeneity in Lake Markermeer.*

Been, K. 1980. *Stress strain behaviour of a cohesive soil deposited under water*, University of Oxford.

Been, K. & Sills, G. C. 1981. Self-weight consolidation of soft soils - an experimental and theoretical study. *Geotechnique,* 31**,** 519-535.

Berner, R. A. 1984. Sedimentary pyrite formation - an update. *Geochimica Et Cosmochimica Acta,* 48**,** 605-615.

Bolland, M. D. A. 1980. pH-Independent and pH-Dependent Surface Charges on Kaolinite. *Clays and Clay Minerals,* 28**,** 412-418.

Bora, P. K. & Sharma, B. 2003. Plastic Limit, Liquid Limit and Undrained Shear Strength of Soil - Reappraisal. *Journal of Geotechnical and Geoenvironmental Engineering,* 129**,** 774-777.

Bouyer, D., Coufort, C., Liné, A. & Do-Quang, Z. 2005. Experimental analysis of floc size distributions in a 1-L jar under different hydrodynamics and physicochemical conditions. *Journal of Colloid and Interface Science,* 292**,** 413-428.

Boyle, P., Berthier, D., Holding, G., Ameratunga, J. & De Bok, C. 2010. Successful application of vacuum consolidation at port of Brisbane. *Ground Improvement Technologies and Case Histories***,** 747-753.

Buscall, R., Mills, P. D. A., Goodwin, J. W. & Lawson, D. W. 1988. Scaling behaviour of the rheology of aggregate networks formed from colloidal particles. *J. Chem. Soc., Faraday Trans. 1 Journal of the Chemical Society, Faraday Transactions 1: Physical Chemistry in Condensed Phases,* 84**,** 42-49.

CIRIA 1996. *Beach management manual,* London, Construction Industry Research and Information Association.

CROW 2000. *Standaard RAW bepalingen 2000,* Ede, CROW.

Dankers, P. J. T. 2006. *On the hindered settling of suspensions and mud-sand mixtures.* PhD Thesis, TU Delft.

Dankers, P. J. T. & Winterwerp, J. C. 2007. Hindered settling of mud flocs: Theory and validation. *Continental Shelf Research,* 27**,** 1893-1907.

De Lucas Pardo, M. A. 2014. *Effect of biota on fine sediment transport processes: A study of Lake Markermeer.* PhD Thesis, TU Delft.

de Wit, P. J. 1992. Liquefaction and erosion of mud due to waves and current. TU Delft.

Dear, S.-E., Ahern, C. R., O'Brien, L. E., Dobos, S. K., McElnea, A. E., Moore, N. G. & Watling, K. M. 2014. Queensland Acid Sulfate Soil Technical Manual: Soil Management Guidelines. *In:* Brisbane: Department of Science, I. T., Innovation and the Arts, Queensland Government. (ed.).

Dent, D. L. 1986. *Acid sulphate soils : a baseline for research and development,* Wageningen, Netherlands, International Institute for Land Reclamation and Improvement/ILRI.

Dyer, K. R. 1989. Sediment processes in estuaries: Future research requirements. *Journal of Geophysical Research: Oceans,* 94**,** 14327-14339.

Gibson, R. E., England, G. L. & Hussey, M. J. L. 1967. Theory of 1-dimensional consolidation of saturated clays. *Geotechnique,* 17**,** 261-273.

Houston, W. N. & Mitchell, J. K. 1969. Property interrelationships in sensitive clays. *Journal of the Soil Mechanics & Foundations Division (ASCE),* 95(SM4)**,** 1037-1062.

Hunt, J. R. 1980. Prediction of Oceanic Particle Size Distributions from Coagulation and Sedimentation Mechanisms. *Particulates in Water.* American Chemical Society.

Ibanez, M., Wijdeveld, A. & Chassagne, C. 2014. The role of mono- and divalent ions in the stability of kaolinite suspensions and fine tailings. *Clays and clay minerals,* 62**,** 374-385.

Jacobs, W. 2011. *Sand-mud erosion from a soil mechanical perspective.* PhD Thesis, TU Delft.

Kandiah, A. 1974. *Fundamental aspects of surface erosion of cohesive soils.* PhD Thesis, University of California, USA.

Kaya, A., Oren, A. H. & Yukselen-Aksoy, Y. 2006. Settling of kaolinite in different aqueous environment. *Marine Georesources & Geotechnology,* 24**,** 203-218.

Kranenburg, C. 1994. The Fractal Structure of Cohesive Sediment Aggregates. *Estuarine, Coastal and Shelf Science,* 39**,** 451-460.

Krone, R. B. 1963. *A study of rheologic properties of estuarial sediments,* Berkeley, USA, Hydraulic Engineering Laboratory and Sanitary Engineering Research Laboratory, University of California.

Kynch, G. J. 1952. A theory of sedimentation. *Transactions of the Faraday Society,* 48.

Lee, S. L., Karunaratne, G. P., Yong, K. Y. & Ganeshan, V. 1987. Layered clay-sand scheme of land reclamation. *Journal of Geotechnical Engineering-Asce,* 113**,** 984-995.

Leroueil, S., Tavenas, F. & Bihan, J.-P. L. 1983. Propriétés caractéristiques des argiles de l'est du Canada. *Canadian Geotechnical Journal,* 20**,** 681-705.

Locat, J. & Demers, D. 1988. Viscosity, yield stress, remolded strength, and liquidity index relationships for sensitive clays. *Canadian Geotechnical Journal,* 25**,** 799-806.

Maggi, F. 2005. *Flocculation dynamics of cohesive sediment.* PhD Thesis, TU Delft.

Mehta, A. J. 2014. *An introduction to hydraulics of fine sediment transport,* Hackensack, World Scientific.

Merckelbach, L. M. 2000. *Consolidation and strength evolution of soft mud layers.* PhD Thesis, TU Delft.

Merckelbach, L. M. & Kranenburg, C. 2004. Determining effective stress and permeability equations for soft mud from simple laboratory experiments. *Géotechnique,* 54**,** 581-591.

Merckelbach, L. M. & Kranenburg, C. 2004. Equations for effective stress and permeability of soft mud–sand mixtures. *Géotechnique,* 54**,** 235-243.

Mietta, F. 2010. *Evolution of the floc size distribution of cohesive sediments.* PhD Thesis, TU Delft.

Mietta, F., Chassagne, C., Manning, A. J. & Winterwerp, J. C. 2009. Influence of shear rate, organic matter content, pH and salinity on mud flocculation. *Ocean Dynamics,* 59**,** 751-763.

Mietta, F., Chassagne, C. & Winterwerp, J. C. 2009. Shear-induced flocculation of a suspension of kaolinite as function of pH and salt concentration. *Journal of Colloid and Interface Science,* 336**,** 134-141.

Mitchell, J. K. & Soga, K. 2005. *Fundamentals of soil behavior,* Hoboken, N.J., John Wiley & Sons.

Nasser, M. S. & James, A. E. 2008. Degree of flocculation and viscoelastic behaviour of kaolinite-sodium chloride dispersions. *Colloids and Surfaces a-Physicochemical and Engineering Aspects,* 315**,** 165-175.

NEN 2013. NEN-EN-ISO 14688-1+A1:2013 nl. *In:* NEN (ed.).

Nooy van der Kolff, A. H., Lesemann, D. & Petereit, K. The use of dredged sludge as a fill in the Osthafen, Bremerhaven, Germany. PIANC MMX Congress, 10-14 May 2010 2010 Liverpool.

O'Melia, C. R. 1980. Aquasols: the behavior of small particles in aquatic systems. *Environmental Science & Technology,* 14**,** 1052-1060.

Odd, N. V. M. & Cooper, A. J. 1989. A Two-Dimensional Model of the Movement of Fluid Mud in a High Energy Turbid Estuary. *Journal of Coastal Research***,** 185-193.

Palko, J. 1994. *Acid sulphate soils and their agricultural and environmental problems in Finland.* PhD Thesis, University of Oulu.

Palomino, A. M. & Santamarina, J. C. 2005. Fabric map for kaolinite: effects of pH and ionic concentration on behavior. *Clays and clay minerals,* 53**,** 211-223.

Rand, B. & Melton, I. E. 1977. Particle interactions in aqueous kaolinite suspension .1. Effect of pH and electrolyte upon mode of particle interaction in homoionic sodium kaolinite suspensions. *Journal of Colloid and Interface Science,* 60**,** 308-320.

Ritsema, C. J., van Mensvoort, M. E. F., Dent, D. L., Tan, Y., van den Bosch, H. & van Wijk, A. L. M. 2000. Acid sulfate soils. *In:* Sumner, M. E. (ed.) *Handbook of soil science.* CRC Press.

Saaltink, R. M., Dekker, S. C., Griffioen, J. & Wassen, M. J. 2016. Wetland eco-engineering: measuring and modeling feedbacks of oxidation processes between plants and clay-rich material. *in press.*

Safar, Z., Ibanez, M., van Paassen, L. A. & Chassagne, C. 2015. A systematic laboratory study of flocculated clay settling rates as function of polyelectrolyte charge, concentration and shear history. *unpublished.*

Sammut, J., White, I. & Melville, M. D. 1996. Acidification of an estuarine tributary in eastern Australia due to drainage of acid sulfate soils. *Marine and Freshwater Research,* 47**,** 669-684.

Sampath, A. 2009. *Sedimentation of Lake Apopka mud and comparison with other sediments.* MSc Thesis, University of Florida.

Schmitz, R. M. & van Paassen, L. A. 2003. The Decay of Liquid Limit of Clays with increasing Salt Concentration. *Ingeokring newsletter,* 9**,** 10-14.

Serra, T. & Casamitjana, X. 1997. Modelling the Aggregation and Break-up of Fractal Aggregates in a Shear Flow. *Applied Scientific Research,* 59**,** 255-268.

Serra, T., Colomer, J. & Logan, B. E. 2008. Efficiency of different shear devices on flocculation. *Water research,* 42**,** 1113-21.

Sills, G. C. 1998. Development of structure in sedimenting soils. *Philosophical Transactions: Mathematical, Physical and Engineering Sciences,* 356**,** 2515.

Skempton, A. W. & Northey, R. D. 1952. The Sensitivity of Clays. *Géotechnique,* 3**,** 30-53.

Soil Survey Staff, U. S. 1975. *Soil taxonomy : a basic system of soil classification for making and interpreting soil surveys,* Washington, D.C., Soil Conservation Service, U.S. Dept. of Agriculture.

Sposito, G. 1989. *The chemistry of soils,* New York, Oxford University Press.

Stolzenbach, K. D. & Elimelech, M. 1994. The effect of particle density on collisions between sinking particles: implications for particle aggregation in the ocean. *Deep Sea Research Part I: Oceanographic Research Papers,* 41**,** 469-483.

Stumm, W. & Morgan, J. J. 1996. *Aquatic chemistry : chemical equilibria and rates in natural waters,* New York, Wiley.

Terashi, M. & Katagiri, M. 2005. Key issues in the application of vertical drains to a sea reclamation by extremely soft clay slurry. *Ground Improvement - Case Histories,* 3**,** 119-143.

Terzaghi, K., Peck, R. B. & Mesri, G. 1996. *Soil mechanics in engineering practice,* New York, Wiley.

Tombacz, E. & Szekeres, M. 2004. Colloidal behavior of aqueous montmorillonite suspensions: the specific role of pH in the presence of indifferent electrolytes. *Applied Clay Science,* 27**,** 75-94.

Toorman, E. A. 1992. *Modelling of fluid mud flow and consolidation.* PhD Thesis, Katholieke Universiteit Leuven.

Toorman, E. A. & Berlamont, J. 2015. *Dynamics of mud transport* [Online]. Available: http://www.coastalwiki.org/wiki/Dynamics_of_mud_transport [Accessed 02 November 2015].

van 't Hoff, J. & Nooy van der Kolff, A. H. 2012. *Hydraulic fill manual; for dredging and reclamation works,* Leiden, CRC Press/Balkema.

van Bemmelen, J. M. 1886. De samenstelling en vorming van de zure gronden in het Nederlandse alluvium. *Bijdragen tot de kennis van den alluvialen bodem in Nederland.* Amsterdam: Johannes Müller.

van Breemen, N. 1976. *Genesis and solution chemistry of acid sulfate soils in Thailand,* Wageningen, Pudoc, Centre for Agricultural Publishing and Documentation.

van Breemen, N. 1982. Genesis, Morphology, and Classification of Acid Sulfate Soils in Coastal Plains. *In:* Kittrick, J. A., Fanning, D. S. & Hossner, L. R. (eds.) *Acid Sulfate Weathering.* Madison, WI: Soil Science Society of America.

van Leussen, W. 1994. *Estuarine macroflocs and their role in fine-grained sediment transport.* PhD Thesis, Universiteit Utrecht.

Van Olphen, H. 1977. *An introduction to clay colloid chemistry : for clay technologists, geologists, and soil scientists,* New York, Wiley.

van Paassen, L. A. 2004. *The influence of pore fluid salinity on consolidation behaviour and undrained shear strength development of clayey soils.* MSc Thesis, TU Delft.

Verhoef, P. N. W. 1992. *The methylene blue adsorption test applied to geomaterials,* Delft :, TU Delft, Faculteit der Mijnbouwkunde en Petroleumwinning Sectie Ingenieursgeologie.

Verruijt, A. & van Baars, S. 2007. *Soil mechanics,* Delft, VSSD.

Verwey, E. J. W., Overbeek, J. T. G. & Nes, K. v. 1948. *Theory of the stability of lyophobic colloids; the interaction of sol particles having an electric double layer,* New York, Elsevier Pub. Co.

Weaver, C. E. 1989. *Clays, muds, and shales,* Amsterdam; New York, Elsevier.

Wieland, E. & Stumm, W. 1992. Dissolution kinetics of kaolinite in acidic aqueous solutions at 25°C. *Geochimica et Cosmochimica Acta,* 56**,** 3339-3355.

Williams, P. R. & Williams, D. J. A. 1989. Rheometry for Concentrated Cohesive Suspensions. *Journal of Coastal Research***,** 151-164.

Winterwerp, J. C. 1998. A simple model for turbulence induced flocculation of cohesive sediment. *Journal of Hydraulic Research,* 36**,** 309-326.

Winterwerp, J. C. 2002. On the flocculation and settling velocity of estuarine mud. *Continental Shelf Research,* 22**,** 1339-1360.

Winterwerp, J. C. 2014. *RE: Lecture notes CIE4308: Sediment Dynamics.*

Winterwerp, J. C. & van Kesteren, W. G. M. 2004. Introduction to the physics of cohesive sediment in the marine environment.